

MARSHALL GRANT  
IN-20-CR  
154091  
1258

**EVALUATION AND IMPROVEMENT OF LIQUID PROPELLANT  
ROCKET CHUGGING ANALYSIS TECHNIQUES: FINAL REPORT PART I**

**A ONE-DIMENSIONAL ANALYSIS OF LOW FREQUENCY  
COMBUSTION INSTABILITY IN THE FUEL PREBURNER  
OF THE SPACE SHUTTLE MAIN ENGINE**

(NASA-CR-183106) EVALUATION AND IMPROVEMENT N88-27224  
OF LIQUID PROPELLANT ROCKET CHUGGING  
ANALYSIS TECHNIQUES. PART 1: A  
ONE-DIMENSIONAL ANALYSIS OF LOW FREQUENCY Unclas  
COMBUSTION INSTABILITY IN THE FUEL PREBURNER G3/20 0154091

**PREPARED BY**

**KAIR CHUAN LIM**

**and presented as a thesis for the Master of Science Degree  
The University of Tennessee, Knoxville  
August, 1986**

**Work supported by NASA GRANT NAG8-542  
Principal Investigator: Paul E. George, II**

**EVALUATION AND IMPROVEMENT OF LIQUID PROPELLANT  
ROCKET CHUGGING ANALYSIS TECHNIQUES: FINAL REPORT PART I**

**A ONE-DIMENSIONAL ANALYSIS OF LOW FREQUENCY  
COMBUSTION INSTABILITY IN THE FUEL PREBURNER  
OF THE SPACE SHUTTLE MAIN ENGINE**

**PREPARED BY**

**KAIR CHUAN LIM**

**and presented as a thesis for the Master of Science Degree  
The University of Tennessee, Knoxville  
August, 1986**

**Work supported by NASA GRANT NAG8-542  
Principal Investigator: Paul E. George, II**

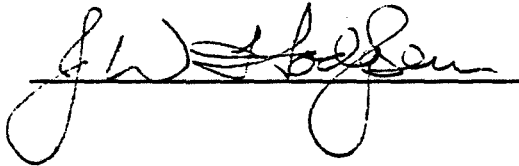
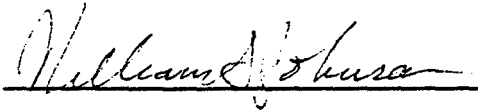
To the Graduate Council:

I am submitting herewith a thesis written by Kair Chuan Lim entitled "A One-Dimensional Analysis of Low Frequency Combustion Instability In the Fuel Preburner Of The Space Shuttle Main Engines." I have examined the final copy of this thesis for form and content and recommend that it be accepted in partial fulfillment of the requirements for the degree of Master of Science, with a major in Aerospace Engineering.

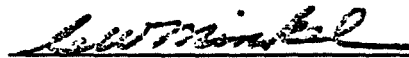


P. E. George II, Major Professor

We have read this thesis and  
recommend its acceptance:



Accepted for the Council:



Vice Provost  
and Dean of the Graduate School

A ONE-DIMENSIONAL ANALYSIS OF LOW FREQUENCY COMBUSTION INSTABILITY  
IN THE FUEL PREBURNER OF THE SPACE SHUTTLE MAIN ENGINES

A Thesis  
Presented for the  
Master of Science  
Degree  
The University of Tennessee, Knoxville

Kair Chuan Lim

August 1986

## ACKNOWLEDGMENTS

The author wishes to acknowledge his major professor, Dr. Paul E. George II, without whom this research would not have been performed. His constant encouragement and willingness in answering my many questions is most gratefully acknowledged. The friendly attitude he possesses and his openness in discussing technical and non-technical matters made this research experience an educational and enjoyable one. The invaluable knowledge and confidence he has shown in me cannot be appreciated enough.

My gratitude is extended to my other members of the committee; Dr. J. W. Hodgson and Dr. W. S. Johnson for their support. Their valuable time and expertise contributed greatly to this research is most sincerely appreciated.

The author would like to thank his expectant wife, Mrs. Josephine Lim, whose constant patience, understanding and willingness to help in any way made this endeavor possible. My deepest gratitude is also extended to my parents, brother and sisters for their support and encouragement.

Finally, the author would like to thank National Aeronautics and Space Administration (NASA) for providing the financial support for this research.

## ABSTRACT

Low frequency combustion instability, known as chugging, is consistently experienced during shutdown in the fuel and oxidizer preburners of the Space Shuttle Main Engines. Such problems always occur during the helium purge of the residual oxidizer from the preburner manifolds during the shutdown sequence. Possible causes and triggering mechanisms are analyzed and details in modeling the fuel preburner chug are presented in this thesis. A linearized chugging model, based on the foundation of previous models, capable of predicting the chug occurrence is discussed and the predicted results are presented and compared to experimental work performed by NASA. Sensitivity parameters such as chamber pressure, fuel and oxidizer temperatures and the effective bulk modulus of the liquid oxidizer are considered in analyzing the fuel preburner chug. The computer program CHUGTEST is utilized to generate the stability boundary for each sensitivity study and the region for stable operation is identified.

# TABLE OF CONTENTS

CHAPTER	PAGE
I. INTRODUCTION . . . . .	1
Space Shuttle Main Engines Description . . . . .	3
Problem Description and Method of Solution . . . . .	8
II. LITERATURE REVIEW . . . . .	13
III. FUEL PREBURNER CHUG MODELING . . . . .	33
Analysis . . . . .	33
Derivation of Characteristic Equation . . . . .	34
Solution of Characteristic Equation . . . . .	44
System Parameters Computation . . . . .	47
Calculation of Stability Boundary . . . . .	59
IV. MODEL APPLICATIONS AND RESULTS . . . . .	61
Verification of Numerical Analysis . . . . .	61
Results of Sensitivity Study . . . . .	69
V. CONCLUSIONS AND RECOMMENDATIONS . . . . .	84
REFERENCES . . . . .	88
APPENDIXES . . . . .	91
A. DERIVATION OF EQUATIONS . . . . .	92
B. LISTING OF PROGRAM CHUGTEST . . . . .	97
VITA . . . . .	112

## LIST OF FIGURES

FIGURE	PAGE
1.1. Space Transportation System Schematic . . . . .	2
1.2 Schematic of propellant flow in the Space Shuttle Main Engine . . . . .	4
1.3 Typical SSME shutdown valve sequence . . . . .	6
1.4 Schematic of Fuel Preburner and Purge System on the SSME . . . . .	7
1.5 SSME fuel and oxidizer preburner showing area of interest . . . . .	9
2.1 Schematic of mono-propellant rocket system . . . . .	14
2.2 Approximate representation of equations (2.3 and 2.4) . .	16
2.3 Nyquist diagram for unstable rocket system . . . . .	19
2.4 Nyquist diagram for stable rocket system . . . . .	19
2.5 Variation in chamber pressure during chugging . . . . .	23
2.6 Variation in fuel flow rate during chugging . . . . .	23
2.7 Block diagram for single vaporization rate model . . . .	25
2.8 Block diagram for proposed model using different vaporization rates . . . . .	25
2.9 Effect of vaporization time on stability boundary . . .	26
2.10 Schematic diagram for Rocket System . . . . .	28
2.11 Block diagram for Rocket System . . . . .	28
2.12 Proposed stabilizers--Flow-Rate Actuated Type . . . . .	30
2.13 Proposed stabilizers--Flow Acceleration Type . . . . .	30
2.14 Stability boundary generated by analog and digital computers . . . . .	32
3.1 Schematic of Fuel Preburner Combustion . . . . .	35



FIGURE	PAGE
3.2 Stability Boundary for Fuel Preburner . . . . .	44
3.3 Fuel Preburner injector element . . . . .	51
3.4 Gas-Phase mixing delay based on experimentally observed chugging frequencies . . . . .	53
3.5 Impedance representation of the oxidizer system . . . . .	55
4.1 Stable operation at full power level (FPL) . . . . .	62
4.2 Fuel Preburner Chug Trace . . . . .	64
4.3 Fuel Preburner chamber pressure variation . . . . .	65
4.4 Instability of preburner $P_c = 4.4815E6$ , $T_o = T_f = 120$ K . . . . .	66
4.5 Stability of preburner with high oxidizer and fuel temperatures at maximum allowable pressure $P_c = 3.7902E6$ Pa, $T_o = T_f = 120$ K . . . . .	67
4.6 Unstable operation with low fuel and oxidizer temperatures at low chamber pressure $T_o = T_f = 40$ K, $P_c = 3.7902E6$ Pa . . . . .	71
4.7 Unstable operation in preburner with low oxidizer and fuel temperatures at mean chugging pressure $T_o = T_f = 40$ K, $P_c = 4.4815E6$ Pa . . . . .	72
4.8 Unstable operation in preburner with low fuel and high oxidizer temperatures at mean chugging pressure $T_o = 40$ K, $T_f = 120$ K, $P_c = 4.4815E6$ Pa . . . . .	74
4.9 Stable operation in preburner with high fuel and high oxidizer temperatures at mean chugging pressure $T_o = 100$ K, $T_f = 120$ K, $P_c = 4.4815E6$ Pa . . . . .	75
4.10 Stable operation in preburner with increasing fuel temperature and lower oxidizer temperature at mean chugging pressure $T_o = 85.7$ K, $T_f = 150$ K, $P_c = 4.4815E6$ Pa . . . . .	76
4.11 Unstable operation in preburner with low fuel flow rate at mean chugging pressure $m_f = 5$ Kg/sec, $P_c = 4.4815E6$ Pa . . . . .	78

FIGURE	PAGE
4.12 Unstable operation in preburner with low fuel flow rate at mean chugging pressure $m_f = 21 \text{ Kg/sec}$ , $P_c = 4.4815\text{E}6 \text{ Pa}$ . . . . .	79
4.13 Variation of chugging frequency with oxidizer temperature . . . . .	81
4.14 Variation of chugging frequency with fuel flow rate $T_o = 100 \text{ K}$ , $T_f = 120 \text{ K}$ , $P_c = 4.4518\text{E}6 \text{ Pa}$ . . . . .	82
4.15 Variation of chugging frequency with chamber pressure . . . . .	83

# LIST OF SYMBOLS

A	:	cross-sectional area	[m <sup>2</sup> ]
a	:	oxidizer injection orifice resistance	[N sec/m <sup>2</sup> kg]
B	:	bulk modulus	[N/m <sup>2</sup> ]
c <sup>*</sup>	:	characteristic velocity of propellant	[m/sec]
C <sub>f</sub>	:	flow discharge coefficient	
D <sub>m</sub> , d	:	mean diameter	[m]
H	:	heat of vaporization	[J/kg]
K	:	pressure ratio defined in eq. (3.22)	
l <sub>50</sub>	:	evaporation length	[m]
l, L	:	length of feed lines	[m]
L <sup>*</sup>	:	characteristic length; ratio of chamber volume to throat area	[m]
$\dot{m}$	:	propellant flow rate	[kg/sec]
$\dot{M}$	:	rate of droplet evaporation	
M	:	molecular weight	[kg/kg mole]
Nu	:	Nusselt No.	
P	:	total pressure	[Pa]
p	:	static pressure	[Pa]
q	:	volumetric flow rate	[m <sup>3</sup> /sec]
R <sub>g</sub>	:	gas constant	[J/kg K]
R <sub>O</sub>	:	real part of oxidizer feed system	[N sec/m <sup>2</sup> kg]
R <sub>f</sub>	:	real part of fuel feed system	[N sec/m <sup>2</sup> kg]
r	:	droplet radius	[m]
s	:	Laplace operator	

T	:	temperature	[K]
t	:	time	[sec]
V	:	volume	[m <sup>3</sup> ]
v	:	velocity	[m/sec]
Z	:	complex flow impedance	[N sec/m <sup>2</sup> kg]
R	:	real part of general system	[N sec/m <sup>2</sup> kg]
I	:	imaginary part of general system	[N sec/m <sup>2</sup> kg]
Y	:	specific heat ratio	
$\Delta P$	:	total pressure drop	[Pa]
$\delta$	:	surface tension	[N/m]
$\theta_g$	:	gas residence time	[sec]
$\rho$	:	density	[kg/m <sup>3</sup> ]
$\mu$	:	viscosity of oxidizer	[N sec/m <sup>2</sup> ]
$\sigma$	:	time delay	[sec]
$\tau$	:	combustion time delay	[sec]
$\phi$	:	equivalence ratio	
$\omega$	:	angular frequency	[rad]

### Subscripts

1	:	propellant tank
2	:	feed line
3	:	injector orifice exit
b	:	burned
c	:	chamber
ci	:	injector face of chamber
e	:	exit

f	:	fuel
fb	:	fuel burned
fi	:	fuel injected
g	:	product gas
hg	:	hot gas manifold
j	:	jet
m	:	gas phase mixing and reaction
man	:	manifold
o	:	oxidizer
ob	:	oxidizer burned
oi	:	oxidizer injected
o2	:	liquid oxygen
s	:	suction feed line
t	:	total
v	:	vaporized
vf	:	vaporized fuel
vo	:	vaporized oxidizer
50	:	vaporized 50 percent

### Superscripts

-	:	mean or steady-state value of variable
~	:	perturbation quantity
'	:	critical value

## CHAPTER I

### INTRODUCTION

The Space Transportation System (STS), better known as the Space Shuttle, is propelled into orbit by two solid rocket boosters and three main engines (Fig. 1.1). The Space Shuttle Main Engines (SSME) have successfully completed twenty-four flights and several hundred test stand firings. The propellants utilized by these engines are cryogenic liquid hydrogen and liquid oxygen. The engines are stable for steady-state operation as well as programmed load changes from minimum power level (MPL) to full power level (FPL). There have, however, been some problems associated with the SSME during shutdown both in flight and on the test stand. In the shutdown sequence, the engine oxidizer system is purged by helium prior to fuel cutoff. During the helium purge, the engines experience a low amplitude low frequency pressure pulsation (chugging) due to combustion instability in the fuel and oxidizer preburners. Since the thrust is essentially reduced to zero there have been no significant effects on the engine's performance. These pulsations have been linked to undesirable bearing loads and damage to the augmented spark ignitor (ASI) line. This problem may require frequent replacement of engine components and can potentially make the STS less cost effective. Therefore, to reduce cost, NASA is sponsoring this research in an effort to reduce the maintenance costs of future SSME designs.

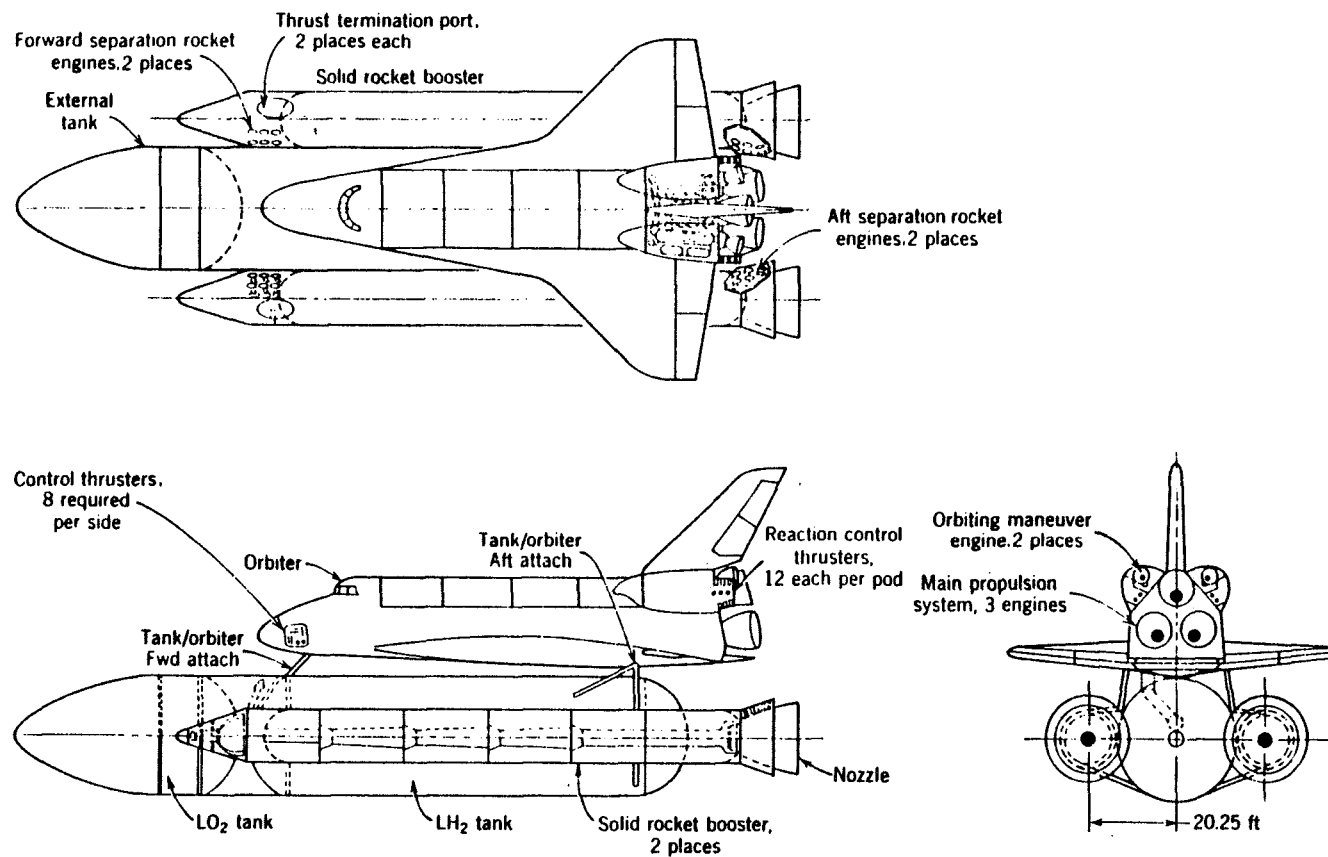


Figure 1.1 Space Transportation System Schematic.

Source: Sutton G. P., Rocket Propulsion Elements, John Wiley and Sons, New York, 1986.

## Space Shuttle Main Engines Description

Fig. 1.2 is a schematic of the propellant flow in the SSME showing the major equipment. Two preburners are used on each engine to preheat the hydrogen and supply power for the fuel and oxidizer pumps.

Cryogenic liquid hydrogen enters the engine from the external tank via a low pressure pump which supplies enough head to prevent cavitation of the three stage high pressure fuel pump. Following the high pressure fuel pump the hydrogen leaves at approximately 7000 psia, at full power level, and is used to cool the nozzle, throat and main combustion chamber before entering the preburner at a temperature of 1027 K. The majority of the fuel flows through the preburners and is partially burned before entering the main combustion chamber.

The oxidizer (liquid oxygen) follows a similar path but is not used for cooling purposes and enters the main combustion chamber directly. The pressure at the outlet of the single stage pump of the oxidizer preburner is approximately 4400 psia and is fed directly into the main combustion chamber operating at 3277 psia. A portion of the oxidizer is supplied to the preburner pump which supplies oxygen at 6850 psia to the fuel and oxidizer preburners.

The main engines supply a nominal thrust of 470,000 lbf at rated power level. Engine power is controlled by throttling the oxidizer flow to the two preburners via the fuel and oxidizer preburner oxidizer valves (FPOV and OPOV). The power available to the turbopumps and hence reactant flow rate is controlled by the supply of oxygen to preburners



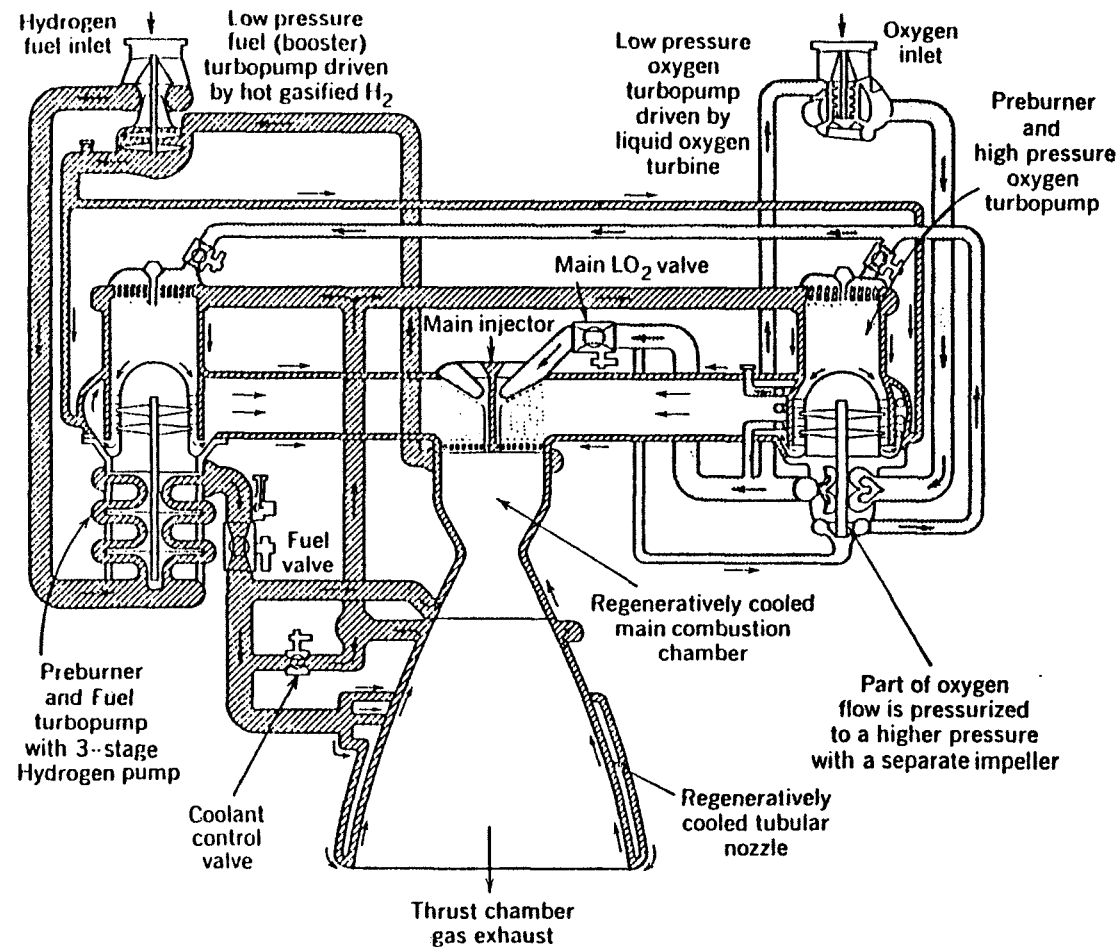


Figure 1.2 Schematic of propellant flow in the Space Shuttle Main Engine.

Source: Sutton G. P., Rocket Propulsion Elements, John Wiley and Sons, New York, 1986.

Under steady-state conditions the preburners are operating at very fuel rich conditions with an approximate equivalence ratio of six. Combustion is extinguished in the preburner and in the main combustion chamber by closing the OPOV in the oxidizer line. The closing of the OPOV causes the suspension of the oxidizer flow to the combustion chamber thus extinguishing combustion prior to fuel cutoff.

The engines are throttled back prior to shutdown in flight operations due to maximum acceleration limitations of the shuttle. The ground test firings on the SSME are frequently shutdown from one hundred percent rated power level. Fig. 1.3 shows the shutdown sequence for a typical engine operation near one hundred percent of rated power level. The oxidizer preburner oxidizer valve (OPOV) is closed first. Shortly after the closure of the OPOV; the fuel preburner oxidizer valve (FPOV) closes. The preburners are isolated from the oxidizer system once the two preburner oxidizer valves are closed. The only oxidizer available to the preburners is the residual trapped in the line and manifold volume between the valve and combustion chamber. This residual oxygen is cleared into the preburners by a helium purge.

Fig. 1.4 shows the purge and the augmented spark ignitor piping for the fuel preburner. A similar arrangement exists for the oxidizer preburner. The check valve in the helium purge supply shown in Fig. 1.4 remains closed until the pressure downstream of the valve drops to about 750 psia. The residual oxidizer is cleared from the ASI line, the oxidizer valve and line and the oxidizer manifold into

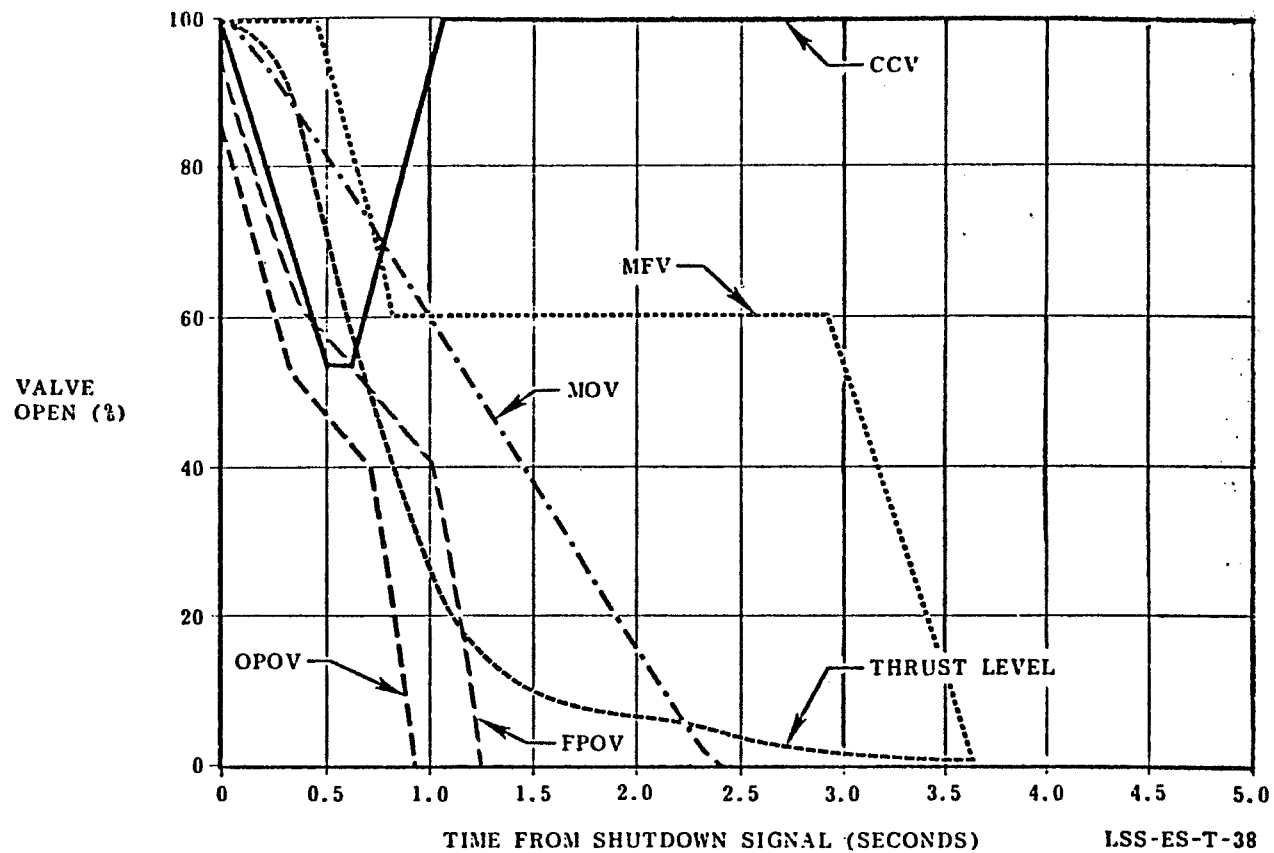


Figure 1.3 Typical SSME shutdown valve sequence,

Source: Space Transportation System--SSME Orientation, Rocketdyne Division, Rockwell International Corporation, 1982.

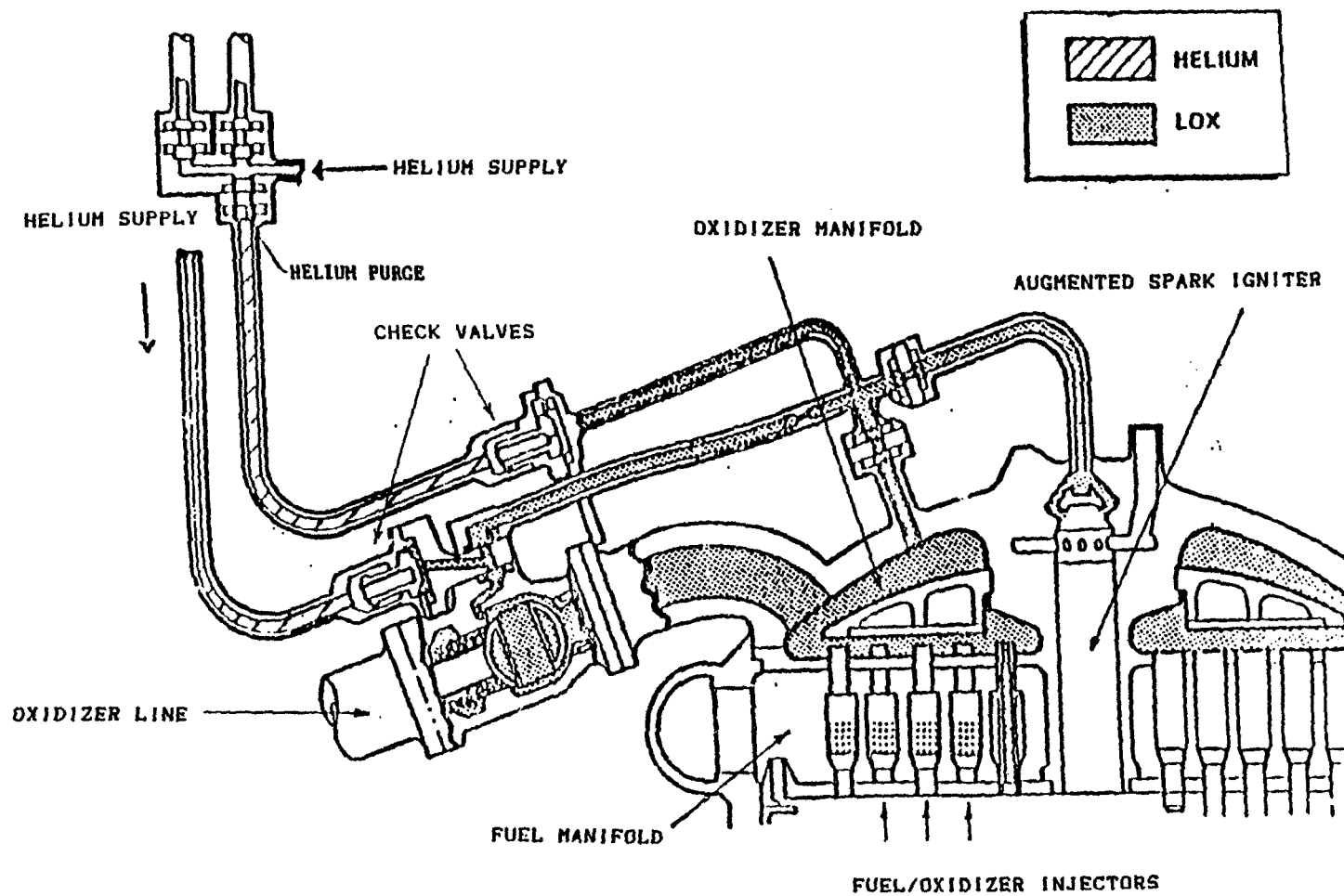


Figure 1.4 Schematic of Fuel Preburner and Purge System on the SSME.

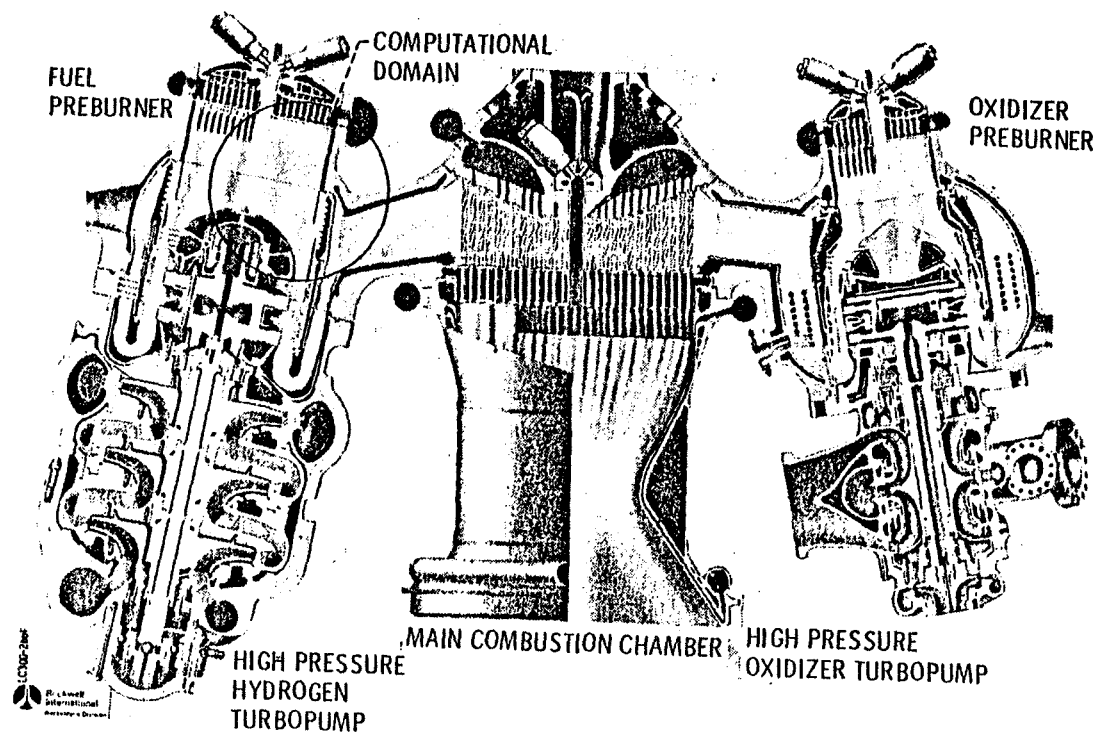
Source: Space Transportation System--SSME Orientation, Rocketdyne Division, Rockwell International Corporation, 1982.

the preburner combustion chamber where combustion with the fuel takes place. Although the fuel flow rate varies due to pump speed variation, substantial fuel flow is maintained until after the purge is completed.

The pressure pulsation experienced during the helium purge of the oxidizer in the fuel preburner is called chugging based on the relatively low frequency (75--200 Hz) and its apparent cause which is a coupling between propellant feed rate and combustion generated pressure in the preburner. Chugging usually begins about 2.3 to 2.5 seconds after the cutoff command is given on ground test. The conditions for flight test data are not available; however, the situation should be similar to ground testing except that in flight cut-off usually occurs at lower power levels. It may appear from Fig. 1.3 that the chug start correspond to the main oxidizer valve (MOV) closing, however, the preburners are completely isolated from the oxidizer system by the time MOV closes.

#### Problem Description and Method of Solution

The SSME consistently experience a low frequency pressure pulsation, called chugging, in both the fuel and oxidizer preburner combustion chambers during the helium purge following cut-off. The area of interest is shown in Fig. 1.5. The amplitude, frequency and duration of the instability appear to be dependent on shutdown conditions particularly the helium compressibility and fuel temperatures. The chug occurs, only on shutdown of the SSME, during the helium purge



ORIGINAL PAGE IS  
OF POOR QUALITY

Figure 1.5 SSME fuel and oxidizer preburner showing area of interest.

Source: Space Transportation System--SSME Orientation, Rocketdyne Division, Rockwell International Corporation, 1982.

of the fuel preburner oxidizer manifold.

Since the chug occurs on shutdown, loss of performance on the SSME is of no major concern. The chug peak pressure never exceeds 1000 psia in the combustion chamber designed for pressures in excess of 6000 psia. Because of this fact, chugging has received very little attention. However, failure of the augmented spark ignitor line and turbopump bearings has been linked to the chug.

The primary objective of this research is to improve on analysis techniques for liquid propellant rocket instability in the fuel preburner of the SSME. The triggering mechanism and the possibilities of elimination were also studied. System variables such as chamber pressure, fuel flow rate, oxidizer flow rate, and fuel and oxidizer temperatures were varied and their effect on the fuel preburner chug is presented in the following chapters.

Combustion instabilities, particularly in rocket engines, have been the subject of several previous investigations. The analysis presented by Crocco and Cheng [14] and Harrje and Reardon [7] are more extensive in the analysis of combustion instabilities compared to earlier models. Their models concentrated on design criteria that should be avoided during engine construction. The early developments of combustion instability analysis were linearized models based upon the work done by Crocco and Cheng. These models have shown that chugging is critically sensitive to combustion time delay and low injector pressure drops. The compressibility of the feed system was also considered as a principal contributor to the chug. A literature

search by the author showed that most chugging problems are analyzed using the one-dimensional lumped parameter model. The approach taken by J. R. Szuch [12] in analyzing main combustion chamber chugging instabilities appeared to be the most effective of the techniques available. The computer program written by Szuch was used as a foundation for this work. The method was adapted to the SSME propellant flow arrangement including the unchoked exit flow in the SSME fuel preburner.

Following the analysis performed by Szuch [12] the characteristic equation, derived from the non-linear differential equation modeling the propellant flow, describing the stability of a bipropellant rocket system is reduced to a quadratic equation. The quadratic formula, which is a closed-form solution, is used to solve the characteristic equation. A high accuracy solution is obtained as no iterative process is required. The two roots obtained are either real and distinct, equal or complex conjugates. The solution of the characteristic equation, utilizing critical system values, will result in the generation of a critical stability boundary. It is therefore possible to predict if the operating point of the fuel preburner is in the stable or unstable region. Only the complex roots with positive real parts are sought. Complex roots with positive real parts indicate that the system is unstable; the imaginary part obtained provides the frequency of interest at the critical operating point.

A chug analysis program was written for the fuel preburner of the SSME and implemented on the VAX 11/780 computer at the University of



Tennessee. The program provides insight into the critical parameters affecting chugging and suggests ways to avoid operating conditions conducive to chugging. The code was verified by comparison to several experimental test cases which are discussed below. Program results in the form of stability diagrams will be analyzed and compared to data obtained from static firings performed under the direction of NASA engineers at Rocketdyne and National Space Technology Laboratory.

## CHAPTER II

### LITERATURE REVIEW

A literature review of liquid propellant rocket instability was conducted by the author to gain some insight into the problems and work associated with combustion instabilities. Although the majority of this research is devoted to low frequency instability analysis, a brief discussion on the different types of rocket instability is presented.

Instability refers to an uncontrolled pressure oscillation in the rocket combustion chamber. In extreme cases, characterized by an increase in amplitude with time, the combustion chamber may rupture or be severely damaged. Rocket instabilities are characterized by the frequency of the pressure oscillation. There are basically three types of rocket instabilities; low, intermediate and high frequency referred to as chug, buzz and scream respectively. These instabilities result from the coupling between the combustion of the propellant and the fluid dynamics of the system. Low frequency instability involves a coupling between the combustion chamber pressure and the propellant flow rate. Intermediate frequency instability involves standing pressure waves in the feed line system. High frequency instability involves the occurrence of pressure waves in the combustion chamber.

One such type of instability, low frequency instability, which occurs during shutdown of the Space Shuttle Main Engines (SSME) is the principal focus to be discussed in this thesis. Chugging is characterized by the constructive coupling between the combustion energy release and the propellant feed process. The chugging frequency is generally less than 200 Hz, although there is no clear distinction in the cutoff frequency range between low and intermediate combustion instabilities.

Fig. 2.1 shows the schematic of a mono-propellant rocket system.

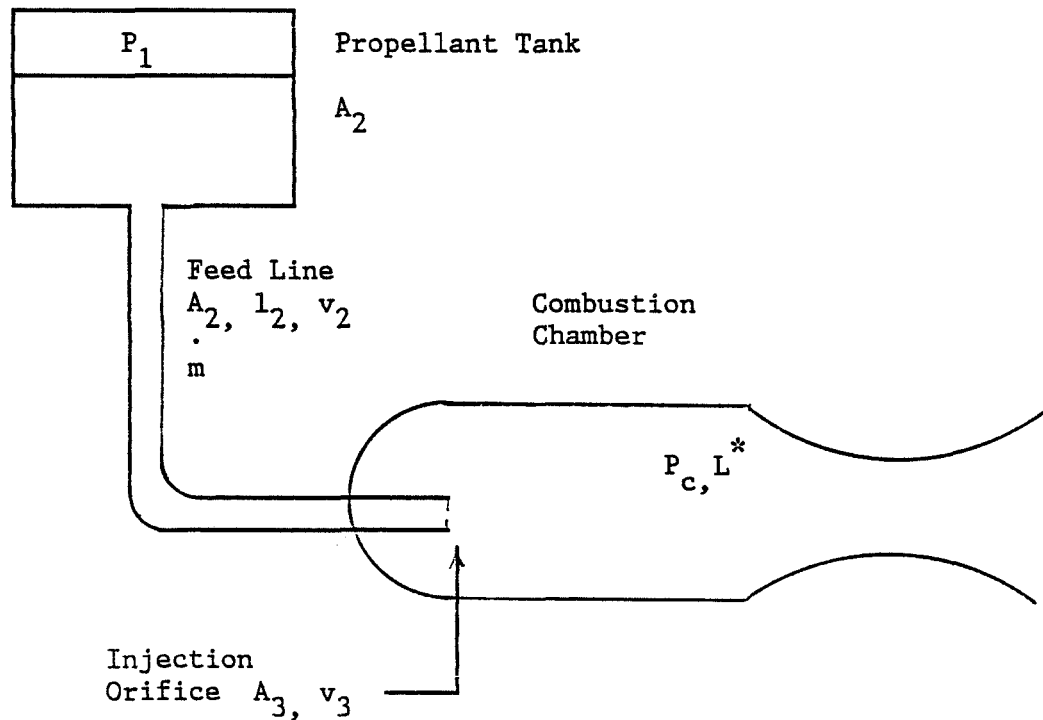


Figure 2.1 Schematic of mono-propellant rocket system.

Assuming that the injector flow velocity ( $v_3$ ) decreases by a small amount, this will cause a decrease in the chamber pressure ( $P_c$ ) which

will increase the flow velocity. Shortly after the input flow increases,  $P_c$  will also increase thereby decreasing  $v_3$ . This process continues and the pressure oscillation is known as chugging. The amplitude could increase or decrease with time. If the amplitude increases with time, the system is unstable and continued chugging will cause severe damage and undesirable irregularity in the thrust of the rocket motor.

Most of the research on chugging was done in the early 1950's with the birth of the space program. The chugging phenomenon was observed by Summerfield [1] during a series of tests on a 1000 lbf thrust rocket motor. For mathematical simplicity, Summerfield analyzed the mono-propellant rocket system neglecting the inertia of the liquid propellant. Utilizing the concept of Crocco's [2] time lag theory, the governing equation was derived from the conservation of momentum and energy. The resulting non-linear differential equation was linearized by perturbation methods and expressed as:

$$v'' + Av' + Bv + Cv(t - \tau) = 0 \quad (2.1)$$

where  $v$  is the flow acceleration of the propellant,  $\tau$  is the combustion time lag and  $A$ ,  $B$  and  $C$  are parameters evaluated at the operating conditions. The general solution of eq. (2.1) can be represented as a linear sum of the particular solutions as:

$$v = \sum_{n=0}^{\infty} v_n e^{(\lambda_n + i\omega_n)t} \quad (2.2)$$

The roots of the characteristic equation (  $\lambda$  ,  $\omega_n$  ) are obtained by substituting eq. (2.2) into eq. (2.1), grouping real and imaginary terms, and transforming into:

$$x^2 + ax + b - \psi^2 + ce^{-x} \cos \psi = 0 \quad (\text{Real}) \quad (2.3)$$

$$(2x + a)\psi - ce^{-x} \sin \psi = 0 \quad (\text{Imaginary}) \quad (2.4)$$

where  $a$ ,  $b$ ,  $c$ ,  $x$  and  $\psi$ , are system parameters expressed in terms of the combustion time lag.

Plotting these equations on the  $x$  and  $\psi$  plane, shown in Fig. 2.2, it is possible to locate the intersections of equations (2.3 and 2.4). The behavior of the the rocket system can be determined for any given values of  $A$ ,  $B$ ,  $C$  and  $\psi$ . The solutions involving positive values of  $x$  lead to instability; while negative values of  $x$  represent stability.

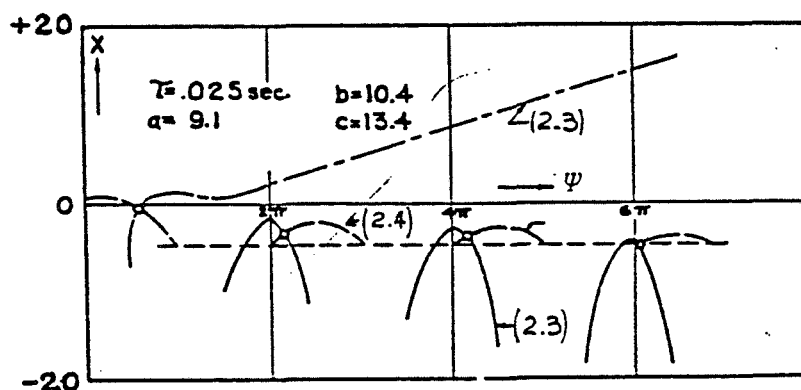


Figure 2.2 Approximate representation of equations (2.3 and 2.4).

Source: Summerfield, M., "A Theory of Unstable Combustion in Liquid Propellant," ARS 21, 1951, pp. 108-114.

It is the objective of the designer to select appropriate values of A, B, and C such that these values are damped out. Therefore, it is possible to manipulate values of A, B, and C such that solutions with positive values of x are impossible. This leads to a sufficient condition for stability defined by Summerfield [1] as:

$$\frac{l_2 \dot{m}}{P_c A_2} + \frac{C^* L^*}{R_g T_c} \cdot \frac{2\Delta P}{P_c} > \tau \quad (2.5)$$

where  $C^*$  and  $L^*$  are the characteristic velocity and length respectively,  $l_2$  and  $\dot{m}$  are the length of the feed line and propellant flow and  $\Delta P$  is the pressure drop across the injector.

From eq. (2.5) the following actions may be inferred for overcoming instability:

1. increase the pressure difference between the supply tank and combustion chamber either by reducing the area of injector orifices or inserting resistance elements in feed lines
2. increase  $L^*$ , which is the ratio of combustion chamber volume to throat area
3. increase the length of the feed lines to the combustion chamber
4. reduce the cross-sectional area of the propellant feed line
5. reduce the combustion time lag ( $\tau$ ) of the propellant either by changing to a more reactive propellant or adding a catalyst to the propellant

Summerfield [1] noted that changing the propellant from nitric acid--gasoline to nitric acid--aniline removed the instability. The aniline, being self-igniting reduces the combustion time delay, confirms that different propellants should be examined.

The analysis performed by Gunder and Friant [6] suggests ways to eliminate the chugging instability of a bipropellant rocket motor. The governing differential equation was derived from the equation of motion of the propellants. Four different methods of solving the characteristic equation were proposed. The Nyquist stability method, which involves a conformal transformation, was chosen.

Gunder and Friant [6] showed the instability could be determined, by plotting the transformation of the governing differential equation in the  $f(z)$ -plane. If the plot encircles the origin the system is unstable. In the plots shown below, Fig. 2.3 shows an unstable system, while the system shown in Fig. 2.4 is stable. The system represented in Fig. 2.4 is similar to that in Fig. 2.3 but was stabilized by changing certain parameters in the system, such as, decreasing the area of feed lines or increasing the pressure drop across the tank and chamber for the oxidizer and fuel.

Several authors including Summerfield and Gunder and Friant have approached the chugging instability of liquid propellant rocket with a simplified mathematical description of the combustion process to obtain a closed-form solution or a simplified differential equation for analog and digital computers. Webber [4] presents a method of calculating low frequency unsteady combustor behavior based upon the

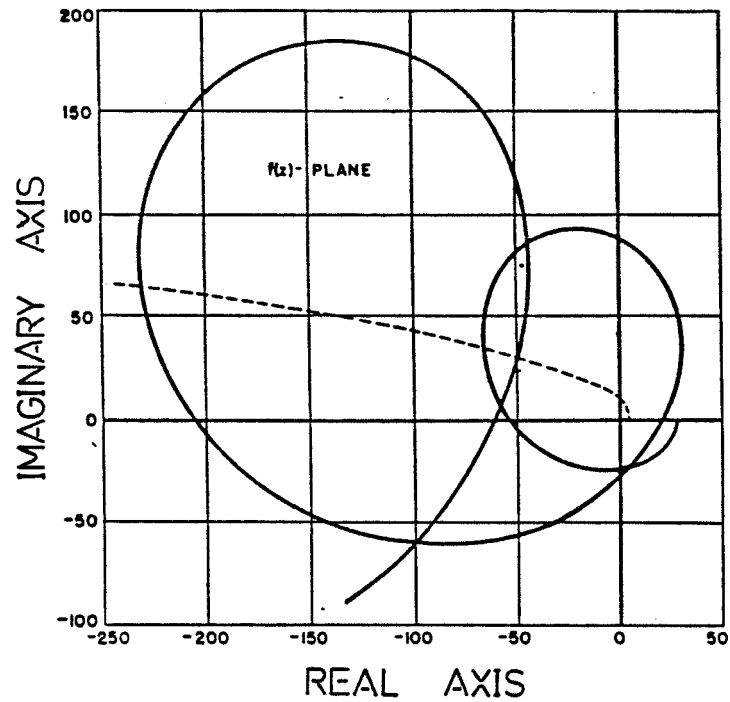


Figure 2.3 Nyquist diagram for unstable rocket system.

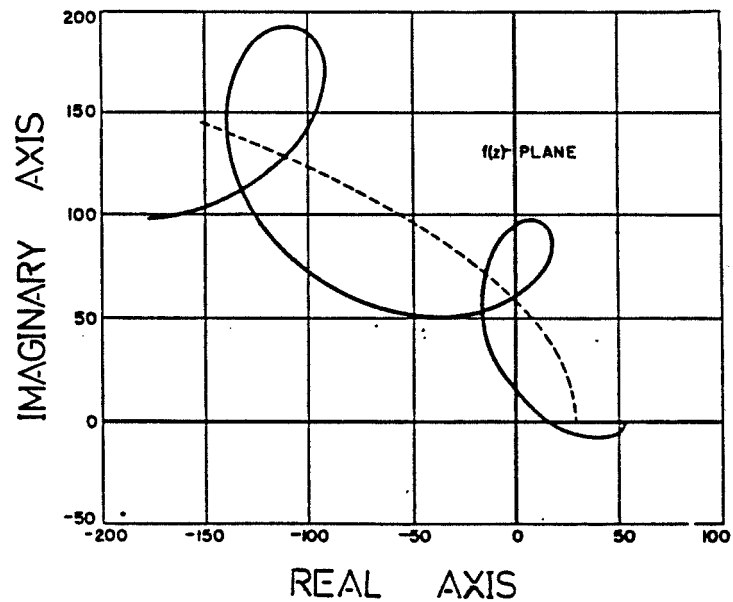


Figure 2.4 Nyquist diagram for stable rocket system.

Source: Gunder, D. F., and Friant, D. R., "Stability of Flow in A Rocket Motor," Journal of Applied Mechanics, 17, 1950, pp. 327-333.



simultaneous integration of the differential equations describing:

1. the propellant flow in the feed system and the injectors and
2. the evaporation and combustion rates of propellant droplets

The model included a fuel and oxidizer supply system, an injector, a combustion chamber and a nozzle. The calculations are based upon the Euler marching technique for the calculated rate of change of the system variables and the integrating time interval.

In Webber's model, the time-varying injection rate of each propellant component is expressed as a function of chamber pressure. The lumped parameter approximation approach is used to obtain:

$$\frac{dq}{dt} = \frac{\left[ \Delta P - \frac{1}{2} R \rho q^2 \right]}{\rho \Sigma l / A} \quad (2.6)$$

for the liquid propellant flow incorporating only resistance and inertia terms, where  $l$  and  $A$  are the length and cross-sectional area of the feed lines,  $R$  is a constant to approximate line losses and  $q$  is the volumetric flow rate. The summation is performed only if the feed line has varying cross-sectional area or multiple feed lines are used. The initial axial velocity of the droplet produced by the injected stream is:

$$v_x = K2 v_j \quad (2.7)$$

where the constant  $K2$  includes the velocity losses due to atomization

process and  $v_j$  is the velocity of the jet spray expressed as:

$$v_j = \frac{\dot{m}}{\rho A} \quad (2.8)$$

The atomization process is approximated by computing the time-varying mean diameter as a function of physical propellant properties and system geometry. Webber calculates the mean diameter of the droplet ( $\bar{D}_m$ ) empirically from:

$$\bar{D}_m = \frac{7.99 [\delta\mu/\rho]^{\frac{1}{3}} D_j}{39.37 \{ [D_j v_j]^{\frac{1}{3}} + 195 D_j \}} \quad (2.9)$$

where  $D_j$  is the injector orifice diameter in meters,  $\mu$ ,  $\delta$  and  $\rho$  are viscosity, surface tension and density respectively. The respective units are defined in the list of symbols.

The evaporation rate of a stable propellant is dependent upon the heat transfer mechanism to the surface of the droplet and the molecular diffusion away from it. The heat transfer mechanism from the surface to the interior of the droplet is significant, however, the assumption that heat transfer to the interior of the droplet is infinitely fast, due to small droplet size, simplifies the analysis. From this assumption the rate of evaporation of the propellant droplet is:

$$\dot{M} = Nu \pi k \bar{D}_m \Delta T / \Delta H \quad (2.10)$$

where  $Nu$  is the Nusselt number and  $\Delta H$  is the sum of sensible heat

and latent heat required to raise the droplet temperature from the injected temperature to the boiling point, and  $k$  is the thermal conductivity of the gas. The rate of efflux of gas from the chamber is expressed in terms of time-varying pressure, temperature and thermal properties in the combustion chamber. The exhaust gases are assumed to be ideal, well mixed and in thermochemical equilibrium.

Two interesting results reported by Webber [4] are shown in Figures 2.5 and 2.6 below. Both plots were calculated for a 100 msec sequence of high-amplitude, 66 Hz, chugging instability. The integrating time interval used was 0.25 msec. Webber discovered that the numerical calculations appear to be negligibly influenced by the integrating time interval for the nominal values used. When a double time interval of 0.5 msec was used the amplitude changed by only 2 percent and the frequency changed by less than 3 percent. The program was tested in comparison with an experimental engine producing low frequency instability. The experimental and calculated frequencies were found to differ by not more than 7 percent with a 5 percent agreement in amplitude.

Few researchers have analyzed chugging instability using different vaporization rates for the propellant. Wenzel and Szuch [8] postulated a model with different delay times (vaporization times) applied to the respective propellants. The difference between this model and previous models lies in the feed system. In the previous analysis, the dead times for all the process were lumped together and applied equally to both propellants. While it is true that mixing

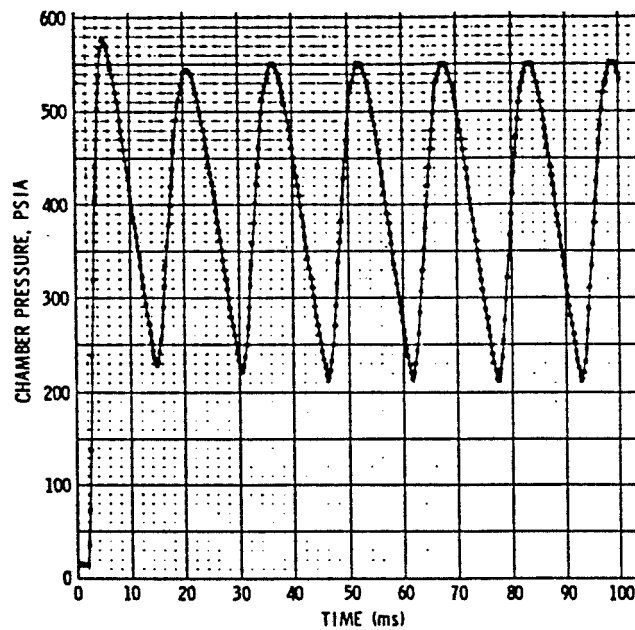


Figure 2.5 Variation in chamber pressure during chugging.

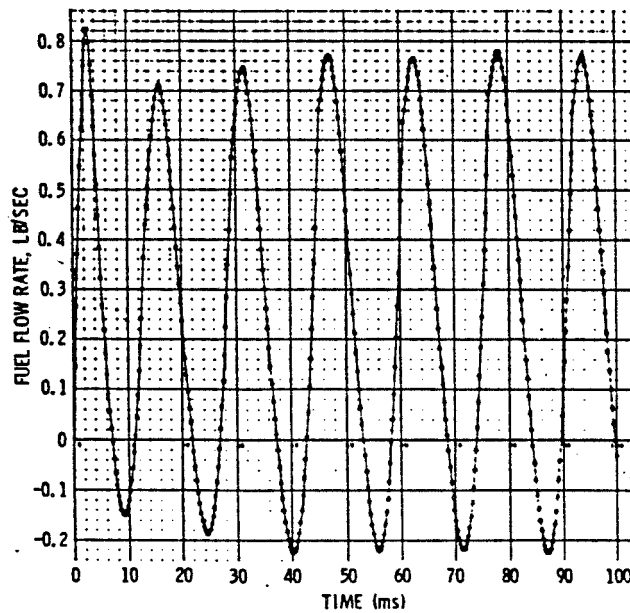


Figure 2.6 Variation in fuel flow rate during chugging.

Source: Webber, W. T., "Calculation of Low Frequency Unsteady Behavior of Liquid Rocket from Droplet Combustion Parameters," ARS 26, 1956, pp. 26-39.

and reaction times are common, vaporization times associated with the individual propellants should be treated separately. The feed system in this model is assumed to be completely decoupled from the combustion chamber. Figures 2.7 and 2.8 show the comparison between the two models.

The governing equation is derived from the conservation of mass and the Laplace transformation is used to obtain:

$$0 = 1 + \frac{e^{-\sigma_m s}}{\theta_g s + 1} \left[ \frac{\partial P_c}{\partial m_o} \cdot \frac{\partial m_o}{\partial \Delta P_{oi}} e^{-\sigma_{vo} s} + \frac{\partial P_c}{\partial m_f} \cdot \frac{\partial m_f}{\partial \Delta P_{fi}} e^{-\sigma_{vf} s} \right] \quad (2.11)$$

Assuming that the burned gas behaves ideally with constant gas residence time ( $\theta_g$ ) and incorporating further mathematical reductions, the characteristic equation is reduced to:

$$-1 = \frac{e^{-\sigma_m s}}{\theta_g s + 1} \left[ e^{-\sigma_{vo} s} \cdot \frac{a1}{\frac{\Delta P_{oi}}{P_c}} \left\{ \frac{\epsilon_g}{\epsilon_g + 1} + \epsilon_g \frac{\left( \frac{\partial C^*}{\partial \epsilon_g} \right)}{C^*} \right\} + e^{-\sigma_{vf} s} \cdot \frac{b1}{\frac{\Delta P_{fi}}{P_c}} \left\{ \frac{1}{\epsilon_g + 1} - \epsilon_g \frac{\left( \frac{\partial C^*}{\partial \epsilon_g} \right)}{C^*} \right\} \right] \quad (2.12)$$

for implementation on a digital computer solving for engine stability. Here  $\sigma_m$  is the gas mixing time,  $\sigma_{vo}$  and  $\sigma_{vf}$  are the vaporization time of the respective propellants,  $\epsilon_g$  is the mixture ratio and a1 and b1 are constants evaluated from steady (mean) operating conditions.

This model indicates that stability may be achieved by manipulating the vaporization time, shown in Fig. 2.9, from 0.5 to 2.0

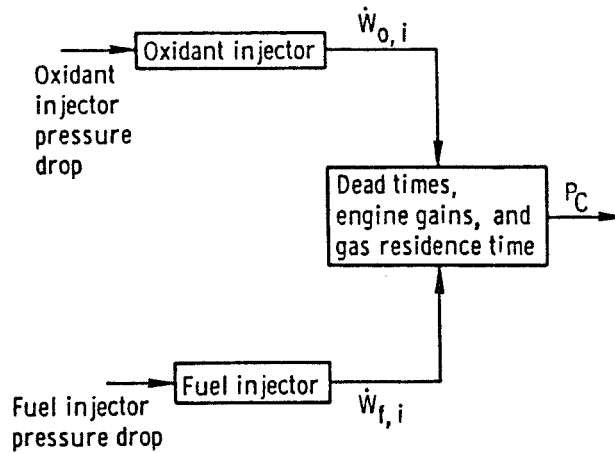


Figure 2.7 Block diagram for single vaporization rate model.

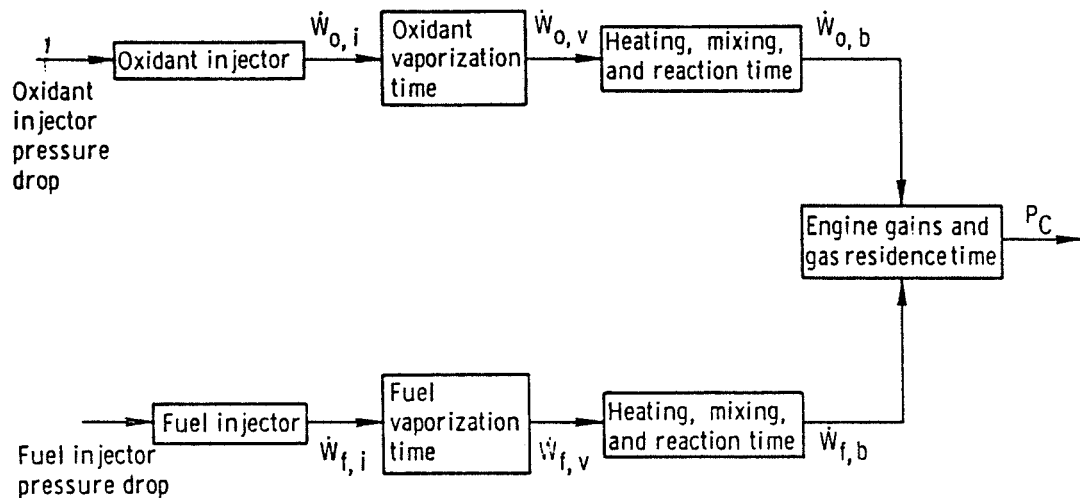


Figure 2.8 Block diagram for proposed model using different vaporization rates.

Source: Wenzel, L. M., and Szuch, J. R., "Analysis of Chugging in Liquid Bipropellant Rocket Engines using Propellants with different Vaporization Rates," NASA TN--D--3080, 1965.

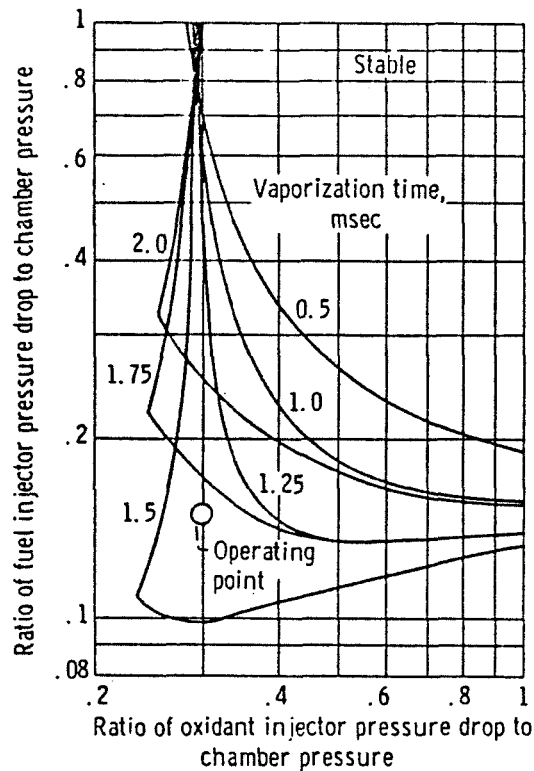


Figure 2.9 Effect of vaporization time on stability boundary.

Source: Wenzel, L. M., and Szuch, J. R., "Analysis of Chugging in Liquid Bipropellant Rocket Engines using Propellants with different Vaporization Rates," NASA TN--D--3080, 1965.

msec at a constant mixing time of 1.0 msec. If the operating condition is as indicated, then increasing the oxidant vaporization time from some lower value up to 1.5 msec improved the stability. This behavior is contrary to that predicted by the single delay time model, since an increase in vaporization time is destabilizing. Further increase in vaporization time, however, shifts the curve upward resulting in unstable behavior. The stability was achieved due to the relatively short mixing time. As the mixing time was increased to

4.0 msec, increasing the oxidant vaporization time was destabilizing. There are limited experimental data to substantiate the behavior predicted by this model, however, this model should not be abandoned as more experimental data will become available.

Barrere and Moutet [3] did experimental analyses on low frequency combustion instability with two objectives in mind:

1. experimental determination of the influence of various parameters on an engine with low frequency instability, and

2. comparison of theoretical and experimental results

They performed a series of experiments involving both a rectangular and a circular combustion chamber. Their analysis showed that the nature of the propellant, characteristic length of the combustion chamber and the mean pressure of the flame body are important parameters in influencing the chugging instability. High injection pressure, mixture ratio or length of combustion chamber did not influence the instability significantly. The experimental results obtained were consistent with Crocco's [2] theory, as long as the chamber pressure takes on the same value as Crocco's theory. The results were inconsistent with Crocco's theory as soon as the chamber pressure was altered.

Another attempt at eliminating combustion instability lies in the modification of the fuel supply line proposed by Li [5]. A suitable servo-mechanism is designed to control the fuel flow which is controlled by the pressure oscillation in the combustion chamber. In his analysis, Li treats the dynamic performance of the fuel supply system



as a first order system assuming an incompressible fuel supply. The purpose of using the feedback system is to associate familiar techniques to stabilize the feedback system such as that shown in Figures 2.10 and 2.11.

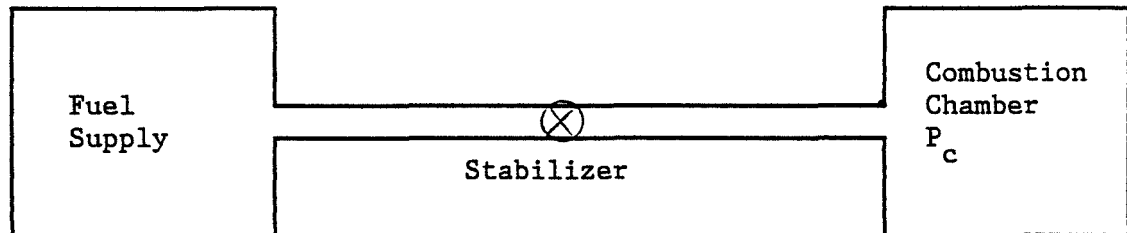


Figure 2.10 Schematic diagram for Rocket System

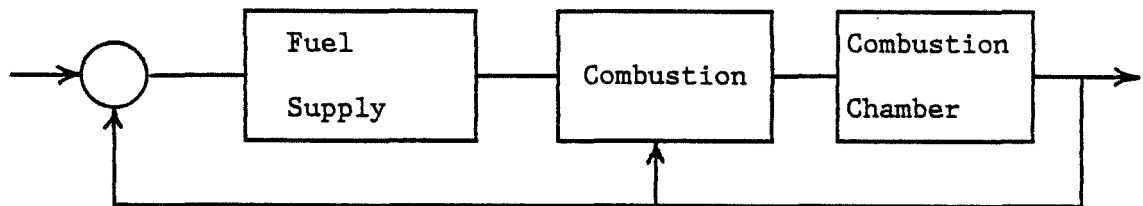


Figure 2.11 Block diagram for Rocket System

Two methods are presented to improve the stability of the first order system. The first is to decrease the time constant so that at the unstable frequency the phase lag was reduced. The other method is to increase the time constant so that at the unstable frequency the amplitude ratio will be reduced. There is an undesirable increasing phase lag associated with the second approach due to the increase in time constant.

Two types of stabilizers were proposed:

1. flow rate actuated-type stabilizer, and

## 2. flow acceleration actuated stabilizer

The construction of the flow rate actuated stabilizer, shown in Fig. 2.12, uses a spring-loaded piston valve and a sensing nozzle to regulate the propellant flow. A pressure drop across the nozzle will produce a force, on the piston valve, that will open or close the valve port. The flow acceleration actuated stabilizer, shown in Fig. 2.13, uses a spring-loaded piston valve to control two sets of ports. The piston has an annular cavity which allows the entire propellant flow to pass through. The inlet and outlet ports are arranged such that the propellant flows perpendicular to the axial motion of the piston. The movement of the piston is thus due to the change in momentum of the propellant in the annular cavity.

The solution to the chugging instabilities with this approach is not as simple as it seems. There are problems associated with the operation of both stabilizers at the chugging frequency. Furthermore, this theory has not been verified experimentally.

Some of the ideas presented by Harrje and Reardon [7] to eliminate low frequency instabilities include:

1. increasing the pressure drop in the injector
2. increasing the fluid inertance (i.e. longer  $l/d$  ratio in the injector or feed system)
3. decreasing chamber volume
4. changes in the time delay in the combustion of the fuel, such as vigorously mixing the recirculated hot gases with the incoming propellant to preheat the fuel, and

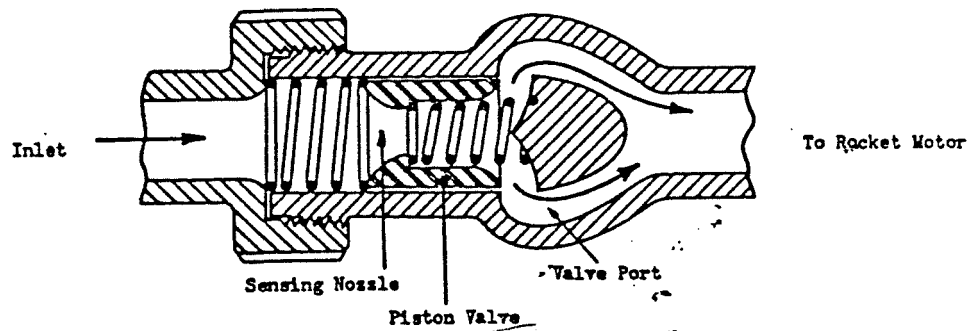


Figure 2.12 Proposed stabilizers -- Flow-Rate Actuated Type.

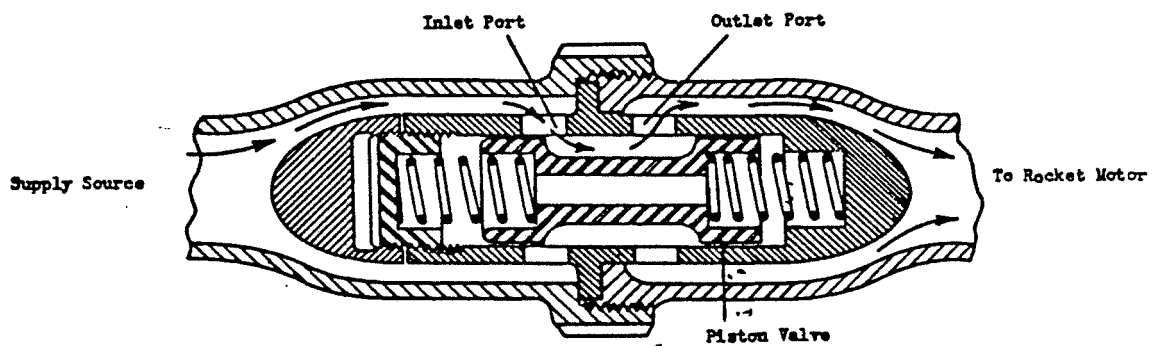


Figure 2.13 Proposed stabilizers -- Flow Acceleration Type.

Source: Li, Y. T., "Stabilization of Low Frequency Oscillations of Liquid Propellant Rocket with Fuel Line Stabilizer," ARS 26, Jan. 1956, pp. 26-39.

5. increasing the damping process to dissipate the oscillatory energy in the combustion chamber or decreasing the coupling between the driving forces.

The idea of decreasing the chamber volume, which seems to contradict Summerfield's work, is because Harrje and Reardon define the combustion time delay of the fuel as:

$$\tau = \frac{1}{\tau_r} \quad (2.13)$$

where

$$\tau_r = L^* \left( \gamma R_g T \right)^{-\frac{1}{2}} \left( \frac{\gamma + 1}{2} \right)^{\frac{\gamma + 1}{2(\gamma - 1)}} \quad (2.14)$$

Therefore decreasing the chamber volume is similar to decreasing  $L^*$  and increasing  $\tau$  and in essence agrees with Summerfield's theory.

The model presented by J. R. Szuch [12] showed promise for analyzing the fuel preburner chug with minor modifications. In this model the governing equation is obtained from the conservation of mass applied to the combustion chamber with the ideal gas assumption and sonic nozzle exit. The model was tested with varying fuel injector annulus area, analogous to injector pressure drop changes, and the results obtained were compared to experimental and analog data. The results obtained from the computer model compared very well with the analog data and are presented in Fig. 2.14 below.

In the literature review the author has discovered that most of the work and research done on rocket instability analysis involved

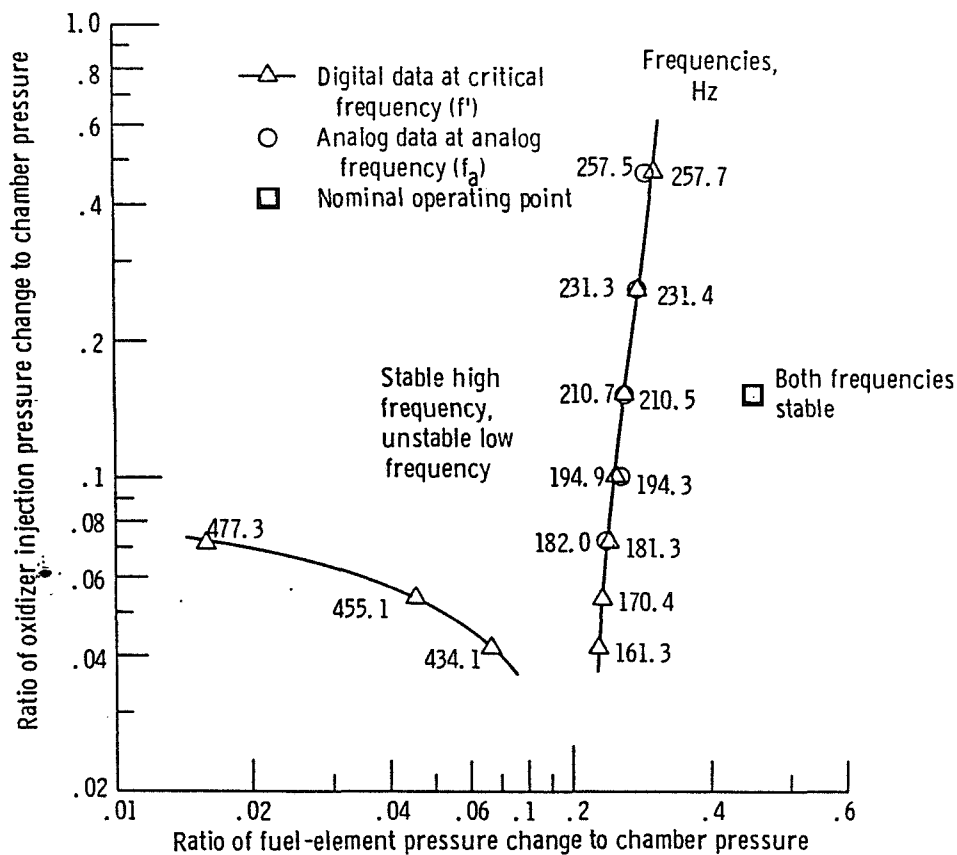


Figure 2.14 Stability boundary generated by analog and digital computers.

Source: Szuch, J. R., "Digital Computer Program for Analysis of Chugging Instabilities," NASA TN--D--7026, Dec. 1970.

linearized steady-state models. This approach is applicable to the SSME fuel preburner chug, however, it does not give any information on the magnitude of the chug amplitude which are transient and non-linear. The model presented by Szuch [12] was selected and applicable for the SSME fuel preburner analysis. The mathematical formulation and details of the analysis are presented in the following chapter.

## CHAPTER III

### FUEL PREBURNER CHUG MODELING

#### Analysis

The model presented by Szuch [12] for the analysis of combustion instabilities has been modified and is now capable of analyzing chugging instabilities in the fuel preburner of the Space Shuttle Main Engines (SSME). This chapter is thus devoted to the mathematical formulation used for modeling the fuel preburner chug. A satisfactory working model, capable of predicting fuel preburner pressure excursion, is presented in this chapter. Although this model analyzes the fuel preburner chug, it could also be applied to the oxidizer preburner with minor modifications.

Although detailed analysis of the actual combustion process taking place in the fuel preburner is beyond the scope of the present work a few elementary assumptions allow analytical treatment. The burnt gases in the fuel preburner can be considered as an ideal gas, and the flow is determined by the conservation laws of mass, momentum and energy. In the range of low frequencies pertaining to chugging, the propagation of the pressure waves is assumed to be instantaneous, thus, the following fundamental assumptions for chugging can be stated:

1. the gas pressure is uniform throughout the combustion chamber and oscillates about a mean or steady-state value

2. the temperature of the gases is constant and uniform regardless of the pressure oscillations, but depends on stoichiometry
3. the time lag (or delay) is uniform, that is, it has the same value for all the propellant elements, and
4. the combustion of the propellant is infinitely fast once the droplet has evaporated and mixed, therefore chemical kinetics may be neglected.

These four assumptions greatly simplify the analytical treatment of the combustion process; the introduction of assumptions (1) and (2) replace the momentum and energy equations which therefore need not be considered. The introduction of assumptions (3) and (4) allow the finite droplet evaporation time to collapse to a single characteristic time. With the combustion proceeding infinitely fast, a quasi-steady state process is assumed.

These assumptions reduce the formulation for the dynamics of the combustion process in the fuel preburner to be essentially governed by the balance of mass, that is, the rate of burned gas produced must be equal to the sum of the rate of ejection of gas out of the fuel preburner through the high pressure fuel turbine and the rate of mass accumulated in the preburner.

#### Derivation of the Characteristic Equation

The combustion process of the fuel preburner during shutdown in the SSME is shown schematically in Fig. 3.1. Following shutdown, the oxidizer line is closed by a ball valve and the residual oxidizer is

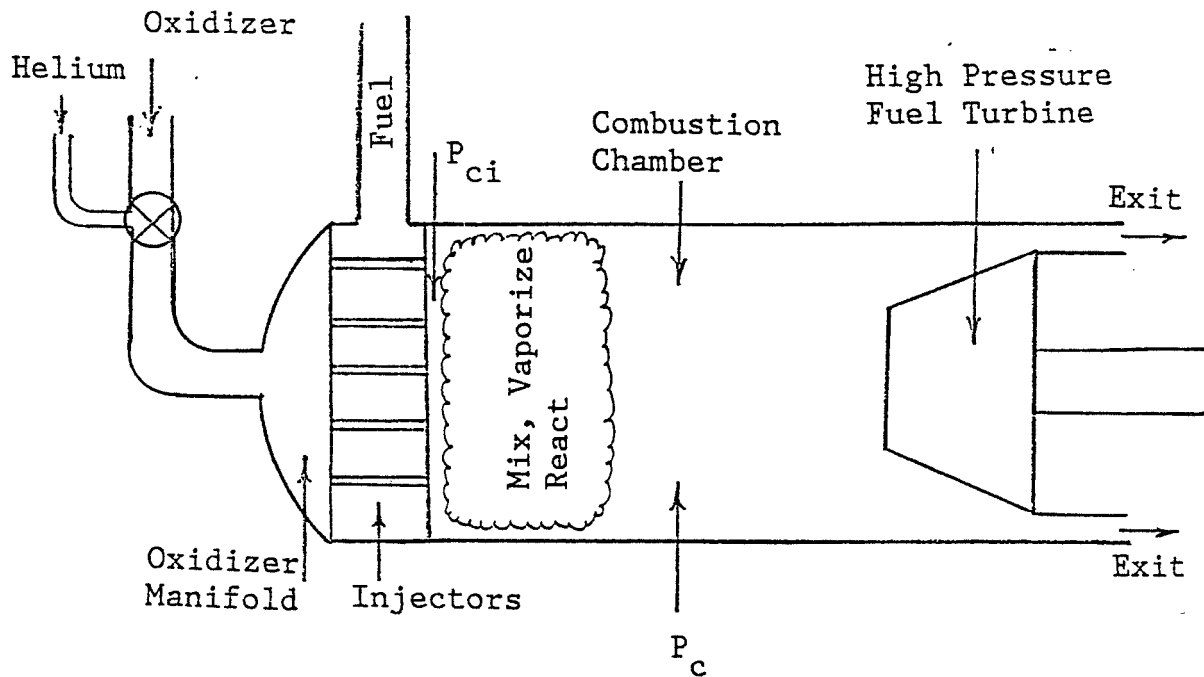


Fig. 3.1 Schematic of Fuel Preburner Combustion

purged by the helium flow. The fuel and helium flow rates are determined by conditions upstream and downstream of the injector elements. The oxidizer vaporizes, mixes and reacts with a small fraction of the fuel to produce a hot gas consisting primarily of  $H_2$  and  $H_2O$ . The time interval that exists between liquid propellant injection and conversion to vaporized propellant is referred to as the vaporization time delay. The characteristic vaporization time delay ( $\sigma_v$ ), used in this model, is the time required for the conversion of 50 percent of the liquid propellant to the vaporized state. The gas



phase mixing time delay ( $\sigma_m$ ) is the time interval required for conversion of vaporized propellant to burned gases. These time delays ( $\sigma_m$  and  $\sigma_v$ ), which are functions of time, are assumed to be combined into a single characteristic time. The following equations, therefore, relate the rate of change of burned products to the injected propellant flow rates.

$$\dot{m}_{ob}(t) = \dot{m}_{oi}(t - \sigma_{vo} - \sigma_m) \quad (3.1)$$

$$\dot{m}_{fb}(t) = \dot{m}_{fi}(t - \sigma_{vf} - \sigma_m) \quad (3.2)$$

where  $\dot{m}$  is the mass flow rate, and subscripts ob, fb, oi, and fi represent oxidizer burned, fuel burned, oxidizer injected and fuel injected respectively.

Using a one-dimensional lumped parameter approach, Harrje and Reardon [7] state that the basic governing equation is obtained from the conservation of mass. The conservation of mass written for the fuel preburner assuming that all the reactants are burned yields:

$$\frac{\partial}{\partial t} \left[ \rho V_c \right] = \dot{m}_{fb}(t) + \dot{m}_{ob}(t) - \dot{m}_e(t) \quad (3.3)$$

where  $\rho$  is the gas density,  $V_c$  is the volume of the fuel preburner combustion chamber; subscript e represents the exit flow. The helium purge is included in the  $\dot{m}_{ob}$  term. Eq. (3.3) is based on the assump-

tion that the volume occupied by the liquid is very small compared to the total chamber volume, and is valid only for low frequencies [7]. The exit mass flow is given by [9]:

$$\dot{m}_e = CP_c^{\frac{1}{2}} T^{-\frac{1}{2}} \left[ \left\{ \frac{P_{hg}}{P_c} \right\}^{1.4286} - \left\{ \frac{P_{hg}}{P_c} \right\}^{1.7143} \right]^{\frac{1}{2}} \quad (3.4)$$

where C is an empirically determined coefficient which is a function of turbine speed; P and T are the pressure and temperature respectively. Subscripts c and hg represent the combustion chamber and hot gas manifold respectively.

Since the gas density is a function of pressure and temperature, eq. (3.3) is non-linear and must be linearized to obtain the desired solution. Linearization of eq. (3.3) is performed by assuming a small perturbation in the system variables about a steady-state operating point. Neglecting the products of perturbations yields the following equation:

$$\theta_g \frac{\partial}{\partial t} \left[ \frac{\tilde{p}}{\bar{p}} \right] + \frac{\tilde{m}_e(t)}{\bar{m}_t} = \frac{\tilde{m}_{fb}(t) + \tilde{m}_{ob}(t)}{\bar{m}_t} \quad (3.5)$$

where the curl superscripts are the perturbation quantities,

$$\theta_g = \frac{\bar{p} V_c}{\bar{m}_t} \quad (3.6)$$

is the gas residence time, and

$$\bar{m}_t = \bar{m}_{fb} + \bar{m}_{ob} = \bar{m}_e \quad (3.7)$$

is the total mean mass flow of the exhaust gases. The process involved in acquiring eq. (3.5) from eq. (3.3) is found in Appendix A. Assuming that the gas behaves as an ideal gas, the first term on the left hand side of eq. (3.5) can be shown to be:

$$\theta_g \frac{\partial}{\partial t} \left[ \frac{\tilde{p}}{\rho} \right] = \theta_g \frac{\partial}{\partial t} \left[ \frac{\tilde{P}_c}{P_c} \right] - \theta_g \frac{\partial}{\partial t} \left[ \frac{\tilde{T}_c}{T_c} \right] \quad (3.8)$$

Since the temperature perturbation varies, that is, the perturbation at the combustion front and the exit of the preburner is not the same, the mean temperature perturbation should be integrated over the entire preburner combustion chamber. However, with assumption (2) stated earlier the average chamber temperature remains relatively constant. Thus, the second term on the right hand side of eq. (3.8) goes to zero.

Utilizing the ideal gas law in eq. (3.4), the second term on the left hand side of eq. (3.5) may be expressed as:

$$\frac{\tilde{m}_e(t)}{\dot{m}_t} = C1 \left[ \frac{\tilde{P}_c}{P_c} \right] - \frac{1}{2} \left[ \frac{\tilde{T}_c}{T_c} \right] \quad (3.9)$$

where C1 is determined from input parameters, and is a function of the specific heat ratio of the combustion products and pressure ratio found in eq. (3.4).

Equations (3.5), (3.8), and (3.9) are combined to yield the following equation:

$$\theta_g \frac{\partial}{\partial t} \left[ \frac{\tilde{P}_c}{\bar{P}_c} \right] + C1 \left[ \frac{\tilde{P}_c}{\bar{P}_c} \right] = \frac{\tilde{m}_{fb} + \tilde{m}_{ob}}{\bar{m}_t} + \frac{1}{2} \left[ \frac{\tilde{T}_c}{\bar{T}_c} \right] \quad (3.10)$$

Assuming that  $T_c$  is the adiabatic flame temperature then clearly,

$$T_c = F(\phi, P_c) \quad (3.11)$$

for any given set of reactants where  $\phi$  is the equivalence ratio.

Therefore, the last term in eq. (3.10) becomes:

$$\frac{\tilde{T}_c}{\bar{T}_c} = \frac{\bar{\phi}}{\bar{T}_c} \left[ \frac{\partial \bar{T}_c}{\partial \phi} \right]_P \frac{\tilde{\phi}}{\bar{\phi}} + \frac{\bar{P}_c}{\bar{T}_c} \left[ \frac{\partial \bar{T}_c}{\partial P_c} \right]_{\phi} \frac{\tilde{P}_c}{\bar{P}_c} \quad (3.12)$$

since the temperature is a weak function of chamber pressure, the last term in eq. (3.12) is neglected. The equivalence ratio perturbation may be expressed in terms of the oxidizer and fuel mass flux perturbations as:

$$\frac{\tilde{\phi}}{\bar{\phi}} \approx \frac{(1 + \bar{\phi}) \tilde{m}_{ob}}{\bar{\phi} \bar{m}_t} - \frac{(1 + \bar{\phi}) \tilde{m}_{fb}}{\bar{m}_t} \quad (3.13)$$

which is analogous to eq. (5.2.1-7) in Harrje and Reardon [7].

Equations (3.1), (3.2), (3.10), (3.12) and (3.13) are combined yielding the following equation which relates the chamber pressure to the injected propellant flow rate.

$$\theta_g \frac{\partial}{\partial t} \left[ \frac{\tilde{P}_c}{\bar{P}_c} \right] + C1 \left[ \frac{\tilde{P}_c}{\bar{P}_c} \right] = X \tilde{m}_{oi}(t - \tau_o) + Y \tilde{m}_{fi}(t - \tau_f) \quad (3.14)$$

where  $\tau = (\sigma_v + \sigma_m)$ , is the combustion time delay, and

$$X = \frac{1}{\bar{m}_t} \left[ 1 + \frac{1}{2} \frac{(1 + \bar{\Phi})}{\bar{T}_c} \left\{ \frac{\partial \bar{T}_c}{\partial \bar{\Phi}} \right\} \right] \quad (3.15)$$

$$Y = \frac{1}{\bar{m}_t} \left[ 1 - \frac{1}{2} \frac{\bar{\Phi}(1 + \bar{\Phi})}{\bar{T}_c} \left\{ \frac{\partial \bar{T}_c}{\partial \bar{\Phi}} \right\} \right] \quad (3.16)$$

o and f refer to oxidizer and fuel respectively. The Laplace transformation of eq. (3.14) is:

$$\left[ \theta_g s + C1 \right] \tilde{P}_c(s) = \bar{P}_c X \tilde{m}_{oi}(s) e^{-\tau_o s} + \bar{P}_c Y \tilde{m}_{fi}(s) e^{-\tau_f s} \quad (3.17)$$

The perturbation in the injected propellant flow rate is related to the perturbation in the chamber pressure at the injector face by:

$$\dot{\tilde{m}}_{oi} = - \frac{\tilde{P}_{ci}(s)}{Z_o(s)} \quad (3.18)$$

$$\dot{\tilde{m}}_{fi} = - \frac{\tilde{P}_{ci}(s)}{Z_f(s)} \quad (3.19)$$

where  $Z_o(s)$  and  $Z_f(s)$  are defined as the linearized output impedance of the oxidizer and fuel feed system respectively, and  $\tilde{P}_{ci}$  is the chamber pressure at the injector face. The determination of  $Z_o(s)$  and  $Z_f(s)$  will be presented in the next section.

The total and static chamber pressure at the injector face are related by their definition as:

$$P_{ct} = p_{cs} \left[ 1 + \frac{(\gamma - 1)}{2} M^2 \right]^{\frac{\gamma}{\gamma - 1}} \quad (3.20)$$

where  $M$  is the Mach number and  $\gamma$  is the specific heat ratio. Subscripts  $t$  and  $s$  represent the total and static pressures respectively.

The static pressure in the combustion chamber and at the injector face are written in terms of the Mach number as:

$$\frac{p_{ci}}{p_c} = \frac{1 + \gamma M_c^2}{1 + \gamma M_{ci}^2} \quad (3.21)$$

Assuming that  $M_{ci}$  is small, (i.e. a large chamber), equations (3.20) and (3.21) can be combined to yield the following pressure ratio (K).

$$\frac{P_{ci}}{P_c} = \frac{1 + \gamma M_c^2}{\left[1 + \frac{(\gamma-1)}{2} M_c^2\right]^{\gamma(\gamma-1)}} = K \quad (3.22)$$

Assuming that there is no loss in the total chamber pressure, equations (3.17), (3.18), (3.19) and (3.22) are combined to yield the following result:

$$\tilde{P}_c = \frac{\bar{P}_c}{\theta_g s + C1 + \frac{P_c X K}{Z_o(s)} e^{-\tau_o s} + \frac{P_c Y K}{Z_f(s)} e^{-\tau_f s}} \quad (3.23)$$

The above equation relates the steady-state average chamber pressure to the perturbed chamber pressure in the system. The existence of the chug is inferred by an unbounded pressure perturbation, that is,  $\tilde{P}_c(s)$  approaches infinity. This condition is obtained by setting the denominator of eq. (3.23) to zero resulting in:

$$-1 = \frac{\frac{P_c X K}{Z_o(s)} e^{-\tau_o s} + \frac{P_c Y K}{Z_f(s)} e^{-\tau_f s}}{\theta_g s + C1} \quad (3.24)$$

Eq. (3.24) is, therefore, the characteristic equation describing the stability of the bipropellant rocket system. Eq. 3.24 applies to the fuel preburner system when the proper choice of  $K$ ,  $P_c$ ,  $X$ ,  $Y$ ,  $Z$ , and  $C_1$  are made.

Eq. (3.24) is solved only for complex roots having positive real parts (exponential growth). Appearance of these roots indicates that chugging is present and defines the stability boundary. The appearance of a negative root signifies that the system is stable. The imaginary root defines the frequency at which the chug occurs. The stability boundary (Fig. 3.2) generated for  $P_c = 4.4815E6$  Pa (650 psia) with  $T_o = T_f = 40$  K (72 R) shows the operating point in the unstable region at a frequency of 121 Hz. A minimum frequency of 75 Hz was selected and the stability program solved the characteristic equation for positive real complex roots. If no non-negative roots are found, the procedure is repeated with another selected frequency. The positive real part of the complex root obtained is related to the respective pressure drops ( $\Delta P_{fi}/P_c$  and  $\Delta P_{oi}/P_c$ ). The curve, therefore, signifies the boundary at which the positive real part exists. The region to the right of the boundary, outside the envelope, corresponds to stable operation, while the region within the envelope is unstable. The shape of the stability boundary is such that an increase in oxidizer or fuel pressure drop stabilizes the preburner. This type of modeling provides insights into the probability of instabilities, but provides no information on the limits of the chug amplitude.



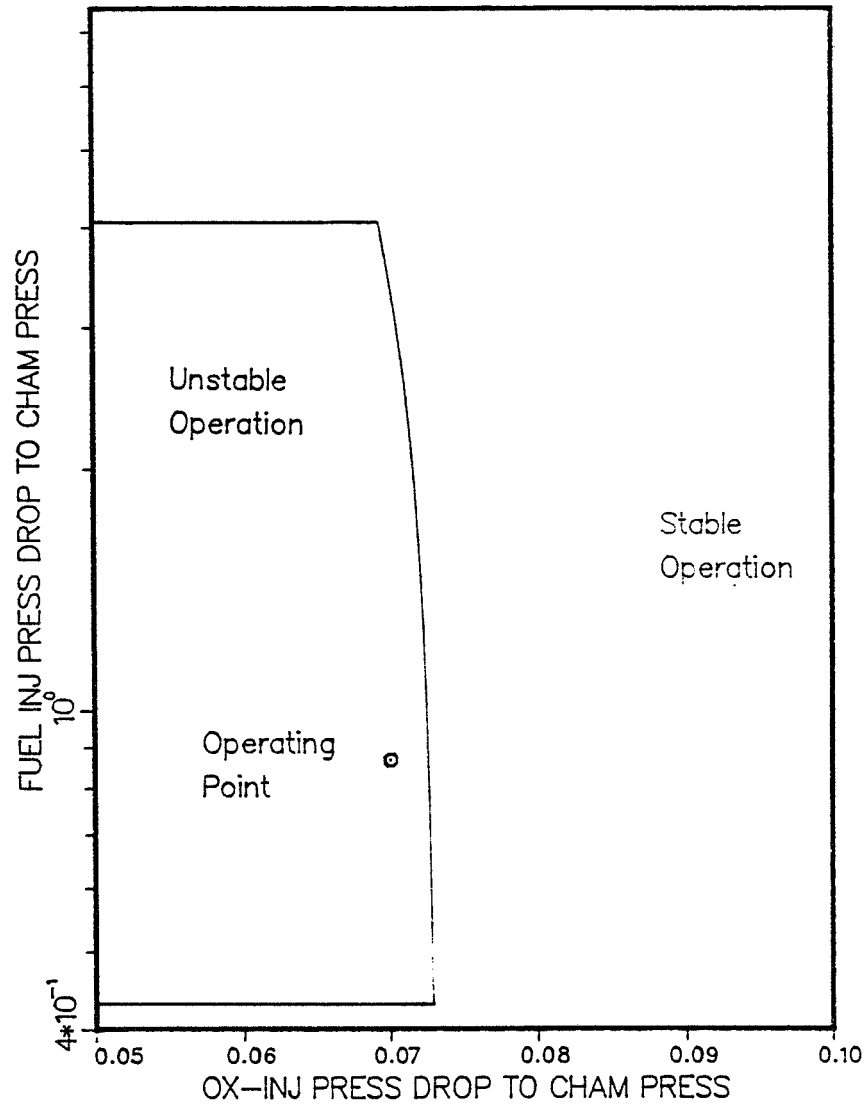


Fig. 3.2 Stability Boundary for Fuel Preburner.

#### Solution of Characteristic Equation

The solution of the characteristic equation is performed by separating the output impedances  $Z_o(s)$  and  $Z_f(s)$  into their real and imaginary parts. Letting  $s = j\omega$ , the characteristic equation is

separated, resulting in the following real and imaginary equations  
(3.25 and 3.26) respectively.

$$-C1 = \frac{P_c XKR_o \cos(\omega\tau_o) - P_c XKI_o \sin(\omega\tau_o)}{R_o^2 + I_o^2} +$$

$$\frac{P_c YKR_f \cos(\omega\tau_f) - P_c YKI_f \sin(\omega\tau_f)}{R_f^2 + I_f^2} \quad (3.25)$$

$$\omega\theta_g = \frac{P_c XKI_o \cos(\omega\tau_o) + P_c XKR_o \sin(\omega\tau_o)}{R_o^2 + I_o^2} +$$

$$\frac{P_c YKI_f \cos(\omega\tau_f) - P_c YKR_f \sin(\omega\tau_f)}{R_f^2 + I_f^2} \quad (3.26)$$

where

$$Z_o(j\omega) = R_o + jI_o \quad (3.27)$$

$$Z_f(j\omega) = R_f + jI_f \quad (3.28)$$

For the frequency range of interest, equations (3.25) and (3.26) are solved for two critical parameters  $R_o$  and  $R_f$ . The real parts of  $R_o$  and

$R_f$  are selected because they can be related to the injector flow resistances  $2\Delta P/m$ , which are independent of the frequency.

It can be shown that equations (3.25) and (3.26) reduce to a quadratic equation relating the critical value of the real part of the oxidizer impedance  $R_o'$ , for a specified critical frequency, to the imaginary feed system impedances  $I_o'$  and  $I_f'$ . The procedure, outlined in Appendix A, for the combination and reduction of equations (3.25) and (3.26), will yield the following quadratic equation:

$$\begin{aligned}
 & R_o'^2 \left[ F - \frac{I_f}{P_c Y K} \left\{ C1^2 + \omega'^2 \theta_g^2 \right\} \right] + \\
 & R_o' \left[ \frac{2XI_f}{Y} \left\{ C1 \cos(\omega' \tau_o) + \omega' \theta_g \sin(\omega' \tau_o) \right\} - P_c X K \sin(\omega' \tau_o - \omega' \tau_f) \right] + \\
 & \left[ I_o'^2 F - I_o' P_c X K \cos(\omega' \tau_o - \omega' \tau_f) - \frac{I_o'^2 I_f}{P_c Y K} (C1^2 + \omega'^2 \theta_g^2) \right. \\
 & \left. - \frac{I_f P_c X^2 K}{Y} - \frac{2XI_o' I_f}{Y} \left\{ C1 \sin(\omega' \tau_o) - \omega' \theta_g \cos(\omega' \tau_o) \right\} \right] = 0 \quad (3.29)
 \end{aligned}$$

where

$$F = \omega' \theta_g \cos(\omega' \tau_f) - C1 \sin(\omega' \tau_f) \quad (3.30)$$

As shown in Appendix A, the solution of eq. (3.29) will be used to compute the critical real part of the fuel impedance  $R_f'$  via:

$$R_f' = \frac{R_o' P_c YK \cos(\omega' \tau_f) + I_o P_c YK \sin(\omega' \tau_f) + I_f P_c XK \sin(\omega' \tau_o) - \omega' \theta_g R_o' I_f + C1 I_o I_f}{\omega' \theta_g I_o + C1 R_o' - P_c XK \cos(\omega' \tau_o)} \quad (3.31)$$

The solution of equations (3.29) and (3.31) will be related physically to the injector element and feed system being studied. The imaginary variables  $I_o$  and  $I_f$  must be computed, at each specified critical frequency, prior to the solution of equations (3.29) and (3.31). The modeling of the feed system, injector element, and other system parameters as well as the computation of the operating point variables will be presented in the next section.

#### System Parameters Computation

A Fortran 77 computer program based on a program for the analysis of chugging instabilities by Szuch [12] was written for the fuel preburner of the SSME. The quadratic formula is applicable for the solution of the characteristic equation. The two roots procured will either be real and distinct, equal, or complex conjugates. Although an iterative solution is not required, the computer program is written to calculate the system variables at each specified frequency of interest. Thus, a critical frequency is selected and the characteristic equation is solved for  $R_o'$  and  $R_f'$ , where the superscripts (') represent critical values. The solutions of  $R_o'$  and  $R_f'$  are then related to the critical oxidizer and fuel pressure drop ratios. The main function of the program is, therefore, to generate

the stability boundary of the chug during the shutdown transient of the SSME for different parametric test cases. Regardless of the type of study, the solutions of equations (3.29) and (3.31) require prior calculations of the system variables at each operating point.

The variables X and Y are computed directly using equations (3.15) and (3.16) respectively. The steady-state value of exit flow rate  $\dot{m}_e$  is the total flow rate of the exhaust gases leaving the fuel preburner. Assuming that complete combustion is taking place in the fuel preburner, the following reaction equation is applicable to the combustion process:



The NASA SP-273 code by Gordon and McBride [10] is used, with an equivalence ratio ( $\phi$ ) of six, to calculate the combustion chamber temperature ( $T_c$ ). The chamber temperature calculated is approximately 1065 K which is too low a temperature to dissociate  $\text{H}_2$  and  $\text{H}_2\text{O}$ ; hence the assumption of complete combustion is valid. The NASA code is also used to obtain a plot of  $T_c$  verses  $\phi$ , with varying equivalence ratio from one to eight at the shutdown condition. A least squares curve fit is utilized to acquire a polynomial relationship between  $T_c$  and  $\phi$ . The slope ( $\partial T_c / \partial \phi$ ) at the specified equivalence ratio can thus be calculated.

The chamber pressure ratio (K) is computed using eq. (3.22). The specific heat at constant pressure ( $\bar{C}_p$ ) for each component of the products is procured from  $\phi$ , and the approximated empirical

polynomial expressed as [11]:

$$C_{p_{H_2O}} = 34.19 - 43.87 \theta^{0.25} + 19.78 \theta^{0.5} - 0.88 \theta \quad (3.33)$$

$$C_{p_{H_2}} = 13.51 - 167.96 \theta^{-0.75} + 278.44 \theta^{-1} - 134.01 \theta^{-1.5} \quad (3.34)$$

Utilizing the mole fraction weighted average the specific heat ratio and the exit Mach number ( $M_c$ ) can be solved from equations (3.35) and (3.36) respectively.

$$\gamma = \frac{C_{p_{avg}}}{C_{p_{avg}} - R_u} \quad (3.35)$$

$$M_c = \frac{\dot{m}_t}{\sqrt{\gamma R_g T_c} \rho A} \quad (3.36)$$

where  $R_u$  is the universal gas constant and the density is obtained from the weighted average.

The gas residence time is computed from its definition (eq. 3.6). The vaporization time delay ( $\sigma_v$ ) for the oxidizer is defined as the time required to vaporize 50 percent of the mass of the injected droplet. The average droplet velocity over this length is approximately equal to the injection velocity of the droplet as reported by Priem and Heidmann [13]. Based on this information, the

vaporization time delay can be calculated from:

$$\sigma_{vo} = \frac{l_{50}}{v_{ip}} \quad (3.37)$$

where  $l_{50}$  is the length required to vaporize 50 percent of the injected mass droplet, and  $v_{ip}$  is the injection velocity of the propellant droplet. The vaporization time delay was computed for the liquid oxidizer only. Since the fuel is already completely vaporized before injection into the combustion chamber, the vaporization is set to zero.

The length required to vaporize 50 percent of the injected mass is computed utilizing:

$$l_{50} = 0.0699 \frac{\left\{ 1 - \frac{\bar{T}_c}{T_{cr}} \right\}^{0.4} \left\{ \frac{r}{7.62 \times 10^{-5}} \right\}^{1.45} \left\{ \frac{v_{ip}}{30.5} \right\}^{0.75} \left\{ \frac{M}{100.} \right\}^{0.35} \left\{ \frac{H}{3.26 \times 10^5} \right\}^{0.8}}{\left\{ \frac{P_c}{2.07 \times 10^6} \right\}^{0.66}} \quad (3.38)$$

where  $r$  is the mean droplet radius in meters,  $M$  and  $H$  are the molecular weight and heat of vaporization with units defined in kg/kg mole and J/kg respectively [12].

The drop radius of the liquid oxidizer is required in computing  $l_{50}$ . Experimental evidence has shown that mean oxidizer drop radius for a concentric element, with gaseous fuel injected through an annulus (shown in Fig 3.3) is proportional to the square-root of the injection momentum ratio with a proportionality constant  $K_r$  of 0.118 [12].

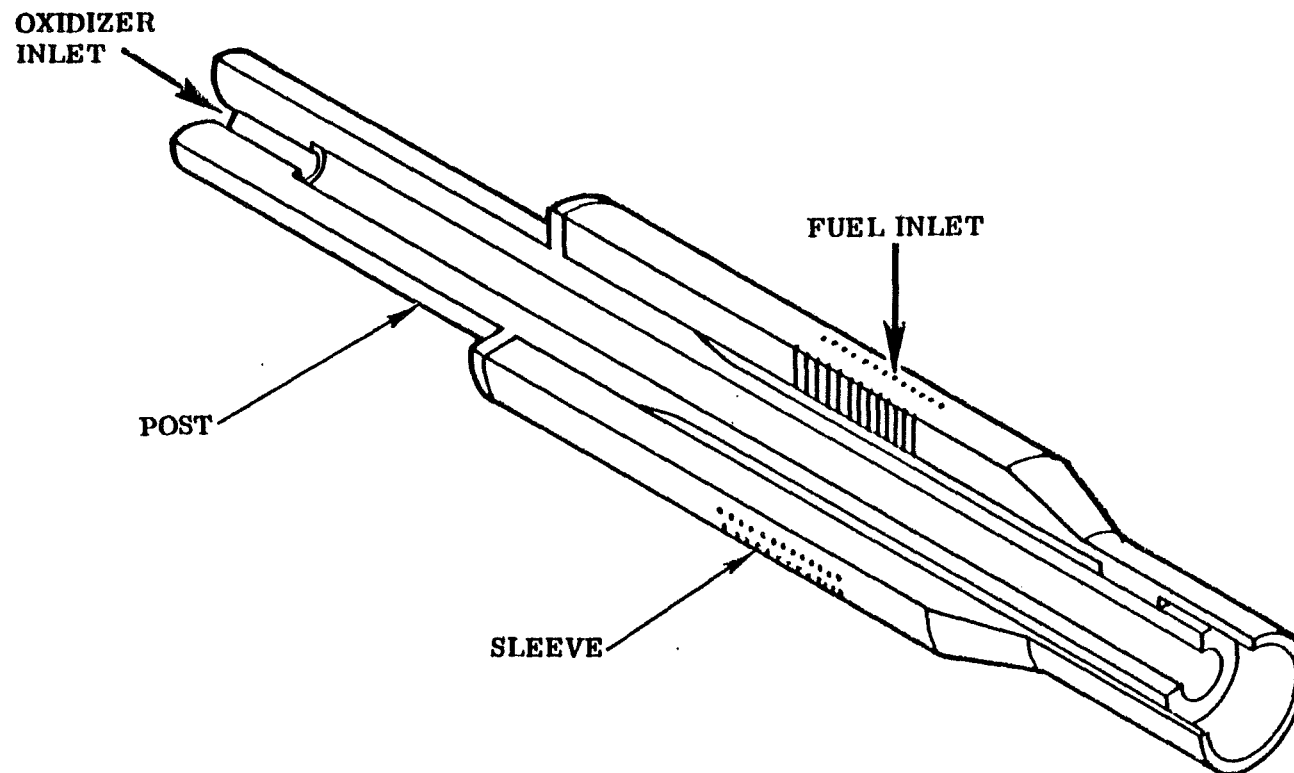


Figure 3.3 Fuel Preburner Injector Element.

Source: Space Transportation System--SSME Orientation, Rocketdyne  
Division, Rockwell International Corporation, 1982.



$$r = K_r d_o \left[ \frac{m_o v_o}{m_f v_f} \right]^{0.5} \quad (3.39)$$

where  $d_o$  is the oxidizer injector diameter. The drop radius is also affected by the properties of the oxidizer at the boiling point temperature (90 K). This effect is represented by:

$$r \propto \left[ \frac{\mu \delta}{\rho} \right]^{0.25} \quad (3.40)$$

where  $\mu$  is the viscosity and  $\delta$  is the surface tension at 1 atm, 90 K. To calculate the drop radius,  $K_r$  must be modified to incorporate this effect. Therefore, with the modified value of  $K_r$ , the resulting expression;

$$r = 0.118 d_o \left[ \frac{\delta_o \mu_o \rho_{o2}}{\delta_{o2} \mu_{o2} \rho_o} \right]^{0.25} \left[ \frac{m_o v_o}{m_f v_f} \right]^{0.5} \quad (3.41)$$

can be used for any liquid oxidizer. The subscripts o2 represent the properties of the liquid oxidizer at the reference condition. The units used for the above expression (eq. 3.41) are defined in the list of symbols.

The injection of the oxidizer, through the injectors which are rifled on the inside, produces a swirling effect which enhances the mixing of the oxidizer with the fuel. Therefore, eq. (3.41) is multiplied by 0.448 as recommended by Szuch.

The gas-phase mixing time delay ( $\sigma_m$ ) is obtained from published experimental data correlated by:

$$\sigma_m = G \left\{ \frac{10^3(l_c + l_n - l_{50})}{v_c} \right\} \quad (3.42)$$

where  $l_c$  and  $l_n$  are the chamber and nozzle lengths. Since there is no nozzle in the preburner,  $l_n$  is neglected resulting in a conservative approach in computing  $\sigma_m$ . The exit gas velocity  $v_c$  is computed from:

$$v_c = M_c \sqrt{\gamma R_g \overline{T}_c} \quad (3.43)$$

and  $G$  is the functional relation plotted in Fig. 3.4 below.

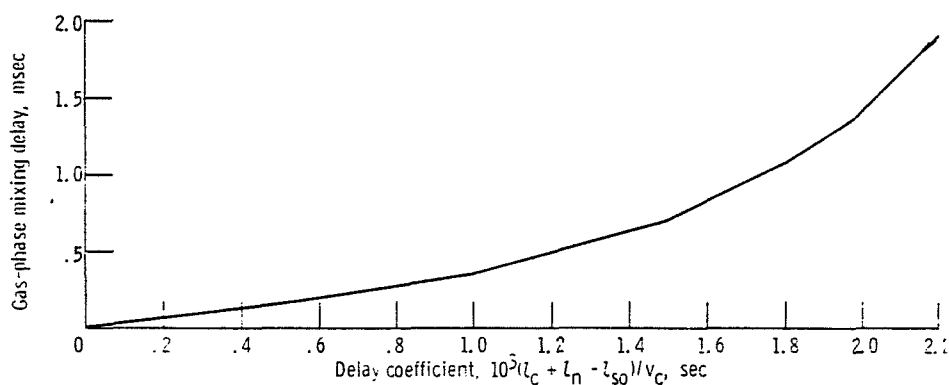


Figure 3.4 Gas-phase mixing delay based on experimentally observed chugging frequencies.

Source: Szuch J. R., "Digital Computer Program for Analysis of Chugging Instabilities," NASA TN--D--7026, Dec. 1970.

The imaginary feed system impedances,  $I_o$  and  $I_f$ , must be computed, as well as the comparison of the critical real values,  $R_o'$  and  $R_f'$ , with the operating point values. The computer program was utilized to calculate  $I_o$  and  $I_f$  at the operating point, solving equations (3.29) and (3.31) to obtain  $R_o'$  and  $R_f'$  at the specified frequency of interest. This calculation involves:

1. breaking the feed system into elements, each having an impedance with real and imaginary parts  $\alpha$  and  $\beta$  respectively.
  2. manipulating these elements into series and parallel combinations, and
  3. reducing the combinations to a single feed system impedance.
- The series combination of  $Z_i$  and  $Z_j$  (i.e.  $Z_k = Z_i + Z_j$ ) produces:

$$\alpha_k = \alpha_i + \alpha_j \quad (3.44)$$

$$\beta_k = \beta_i + \beta_j \quad (3.45)$$

while the parallel combination of  $Z_i + Z_j$  {i.e.  $Z_k = Z_i Z_j / (Z_i + Z_j)$ } produces:

$$\alpha_k = \frac{\alpha_j (\alpha_i^2 + \beta_i^2) + \alpha_i (\alpha_j^2 + \beta_j^2)}{(\alpha_i + \alpha_j)^2 + (\beta_i + \beta_j)^2} \quad (3.46)$$

$$\beta_k = \frac{\beta_j (\alpha_i^2 + \beta_i^2) + \beta_i (\alpha_j^2 + \beta_j^2)}{(\alpha_i + \alpha_j)^2 + (\beta_i + \beta_j)^2} \quad (3.47)$$

Using a lumped parameter approach, the feed system can be divided into the following elements:

1. lines having only inertial pressure drop. The flow impedance therefore consists of  $\alpha = 0$ , and  $\beta = \omega l/A$ , where  $l$  is the line length and  $A$  the cross-sectional area of the line. This is analogous to an electrical inductance
2. orifices having only frictional pressure drop. The flow impedance therefore consists of  $2\Delta P/\dot{m}_o$ , and  $\beta = 0$ , where  $\Delta P$  and  $\dot{m}$  are the steady-state pressure drop across the injector element and mass flow rate respectively. This is analogous to an electrical resistance
3. Storage volumes have an impedance consisting of  $\alpha = 0$ , and  $\beta = -B/\omega \rho V_g$ , where  $B$  is the bulk modulus and  $V_g$  is the manifold volume. This is analogous to an electrical capacitance

Fig. 3.5 shows the impedance representation for the oxidizer system

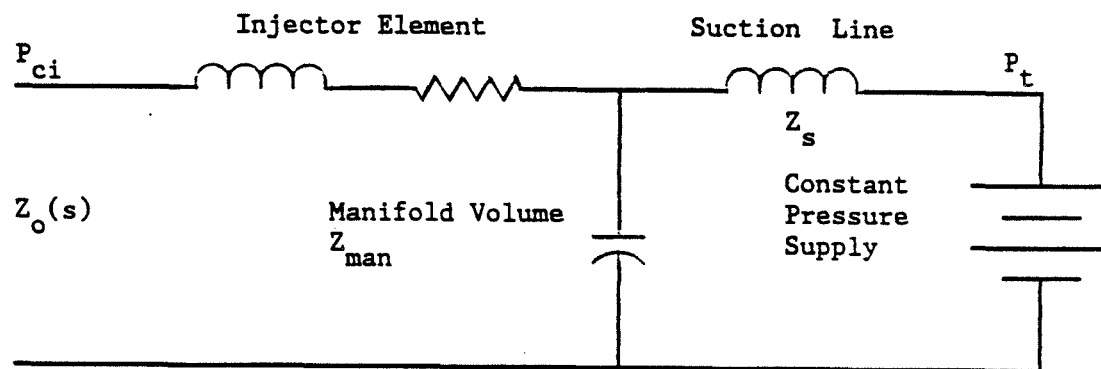


Fig. 3.5 Impedance representation of the oxidizer system.

The above system is collapsed to the following equation utilizing the series and parallel combinations.

$$Z_o(s) = a + j\omega b + \frac{Z_s Z_{man}}{Z_s + Z_{man}} \quad (3.48)$$

where  $a$  is the injector resistance ( $2\Delta p/\dot{m}_o$ ),  $b$  is the injector tube inductance  $\omega l/A$ , and  $Z_s$  and  $Z_{man}$  are the suction line and manifold volume impedance respectively.

The real and imaginary parts of the oxidizer feed system impedance are computed according to the following:

$$R_o = 2\Delta p/\dot{m}_o \quad (3.49)$$

and

$$I_o = \omega b + \frac{\beta_{man}(\beta_s^2) + \beta_s(\beta_{man}^2)}{(\beta_s^2 + \beta_{man}^2)} \quad (3.50)$$

The imaginary part  $I_o$  will be used to solve the characteristic equation and the real part  $R_o$  will be compared to the critical value obtained from the solution of the characteristic equation.

The same procedure holds for the fuel impedance  $Z_f(s)$ , although some simplifying assumptions are required to handle the system conveniently. Assuming steady-state conditions upstream, the fuel injector may be considered to be fed by a constant fuel flow rate. Since the fuel is completely vaporized, the isothermal compressibility must be considered in computing  $Z_f(s)$ . With the above assumptions

the following equation is utilized to compute the fuel flow rate through the injector element.

$$\dot{m}_{fi} = C_f \left[ \frac{P_{fi}^2 - P_{ci}^2}{T_f} \right]^{\frac{1}{2}} \quad (3.51)$$

where  $C_f$  is the flow discharge coefficient. The flow discharge coefficient for the SSME fuel preburner injector is calculated from conditions at rated power level and found to be 0.52.

The steady-state fuel injection velocity  $v_f$ , which is required for the computation of the drop size, is computed from:

$$v_f = \frac{(R_g T_f) \bar{m}_{fi}}{P_{ci} A_f} \quad (3.52)$$

Linearizing and taking the Laplace transformation of eq. (3.51) results in the following equation.

$$\tilde{m}_{fi}(s) = \left[ \frac{P_{fi} \dot{m}_f}{P_{fi}^2 - P_{ci}^2} \right] P_{fi}(s) - \left[ \frac{P_{ci} \dot{m}_f}{P_{fi}^2 - P_{ci}^2} \right] \tilde{P}_{ci}(s) \quad (3.53)$$

The perturbations in the injection manifold pressure may be expressed as:

$$P_{fi}(s) = \left[ \frac{R_g T}{V} \right]_f \frac{\tilde{m}_{fi}(s)}{S} \quad (3.54)$$

where  $V_f$  is the fuel injector manifold volume. Combination of equations (3.52) and (3.53) and letting  $s = j\omega$ , results in:

$$Z_f(j\omega) = \frac{P_{fi}(s) - P_{ci}(s)}{\dot{m}_{fi}(s)} \quad (3.55)$$

where

$$R_f = \frac{P_{fi}^2 - P_{ci}^2}{P_{ci} \dot{m}_f} \quad (3.56)$$

$$I_f = - \frac{P_{fi}}{\omega' P_{ci}} \left[ \frac{R_g T}{V} \right]_f \quad (3.57)$$

The imaginary part,  $I_f$ , is used in the solution of the characteristic equation and the real part,  $R_f$ , will be compared to the critical value obtained from the solution of the characteristic equation.

The critical values of the pressure upstream of the injector element tube and the corresponding ratios of pressure drop to chamber pressure are computed from:

$$\left[ \frac{\Delta P_{oi}}{P_c} \right]_c = \frac{R_o' \dot{m}_o}{2 P_c} \quad (3.58)$$

$$\left[ \frac{\Delta P_{fi}}{P_c} \right]_c = \frac{P_{fi}' - P_{ci}}{P_c} \quad (3.59)$$

### Calculation of Stability Boundary

A computer program capable of generating stability limits over a range of operating conditions has been developed and applied to the fuel preburner of the SSME. The program, drawing extensively from an earlier program by Szuch [12], is written in Fortran 77 and implemented on the VAX 11/780 at the University of Tennessee Computing Center. The program solves the characteristic equation, utilizing the closed-form quadratic formula, for various sensitivity studies. This section will assist the reader in obtaining an overview of the computation of the stability boundary.

A range of possible chugging frequencies must be specified to initiate the program. It was found in the literature that the frequency range for chugging instabilities is between 75 to 200 Hz. Frequencies higher than 200 Hz will be neglected. At the selected operating point and frequency of interest, the following computations are made by the computer program:

1. calculate the steady-state value of imaginary fuel impedance  $I_f$  from eq. (3.47)
2. calculate the real and imaginary oxidizer impedance  $R_o$  and  $I_o$  from equations (3.49 and 3.50)
3. calculate the remaining variables in equations (3.29 and 3.31)
4. solve eq. (3.29) for  $R_o'$ . Negative values of  $R_o'$  are neglected
5. using the result from step (4), calculate  $R_f'$  from eq.



(3.31). Negative values of  $R_f'$  are also neglected

6. convert results of  $R_o'$  and  $R_f'$  to critical values of injection pressure drop from equations (3.58 and 3.59)

7. store results from step (6) including the frequency and repeat steps (1) to (6)

8. write out results from step (7) when frequency is out of specified range

A sorting routine is incorporated into the program to write out the critical pressure drop ratios ( $\Delta P_{oi}/P_c$ ) and ( $\Delta P_{fi}/P_c$ ) in order of increasing ( $\Delta P_{fi}/P_c$ ).

The modified program is capable of producing sensitivity studies for variations in chamber pressure, fuel flow rate, oxidizer flow rate, fuel and oxidizer temperatures, and its affects on the instabilities are studied. The effects of these parameters on instability are presented in the following chapter.

## CHAPTER IV

### MODEL APPLICATIONS AND RESULTS

#### Verification of Numerical Analysis

The computer program, presented in Appendix B, was verified by comparing the results obtained from the numerical procedure to experimental results provided by NASA and Rocketdyne. The required program input values for full power level are presented in Table 4.1. The model was tested with values at full power level (FPL) and predicted stable operation in the fuel preburner of the SSME (Fig 4.1). This prediction conforms with experimental results since it was noted by NASA, during test stand firings and flight conditions, that the SSME is stable at steady-state conditions.

Table 4.1 Input values at FPL obtained from Rocketdyne

Parameters	Values
$P_c$ . . . . .	40.403E6 Pa (5860 psia)
$T_o$ . . . . .	118.8 K (214 R)
$T_f$ . . . . .	157.8 K (284 R)
$\dot{m}_o$ . . . . .	37.72 Kg/sec (83.0 lbm/sec)
$\dot{m}_f$ . . . . .	36.36 Kg/sec (81.0 lbm/sec)
$T_c$ . . . . .	1105.5 K (1990 R)

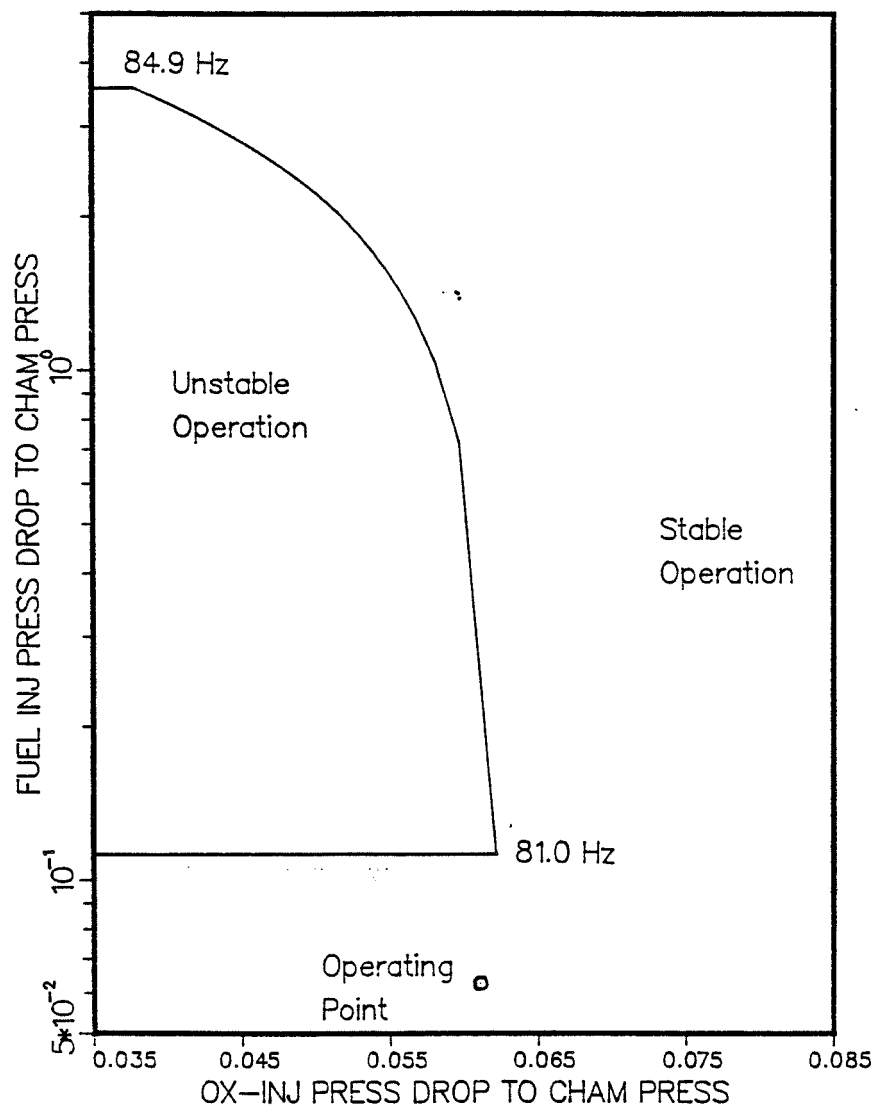


Figure 4.1 Stable operation at full power level (FPL).

The analysis of the SSME fuel preburner chug during shutdown, presented in this thesis, is in agreement with the experimental results supplied. The frequency for the fuel preburner chug (Fig. 4.2) varies from 115 Hz to 145 Hz, as determined by counting the peaks over a selected time segment. The mean frequency of the chug over the entire time interval is 125 Hz. The chug frequency predicted by the model differed by 10 percent from the mean value obtained experimentally. This disagreement was due to the conservative linearized approach taken in the analysis. The predicted frequencies are in good agreement at the two end regions of the chug, since the low amplitude chug is more linear at the start and finish. The frequency at the two end points is approximately 140 Hz. Figures 4.2 and 4.3, which are experimental results performed by NASA, show the chug frequency trace at the mean chugging pressure and the chamber pressure variation in the fuel preburner during shutdown respectively. These results, in conjunction with Figures 4.4 and 4.5, show the comparison between experimental and analytical predictions.

In order to isolate the chug during experimental runs, the analog data were filtered to pass only frequencies on the range  $70 < f < 200$  Hz and scanned visually for an amplitude surge representing the chug. When the surge was noticed the data were electronically plotted with pressure as a function of time. The fuel preburner chug trace presented in Fig. 4.2 shows that at a mean chamber pressure of  $4.4815 \times 10^6$  Pa (650 psia) the chug starts at approximately 2.3

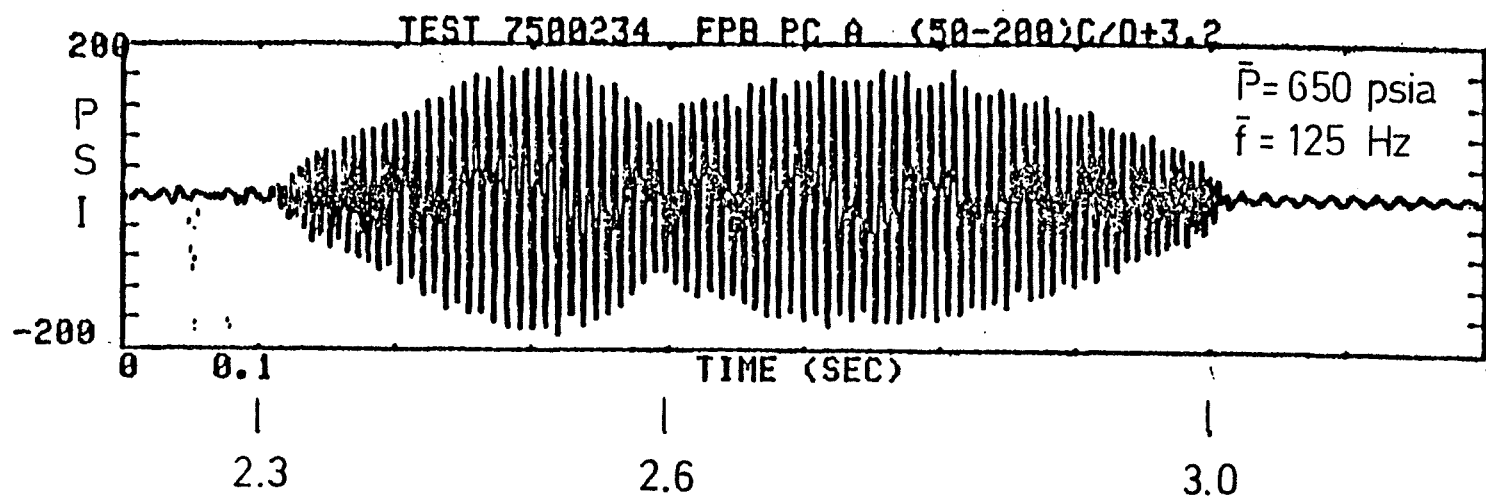


Figure 4.2 Fuel Preburner Chug Trace (Courtesy of NASA Huntsville).

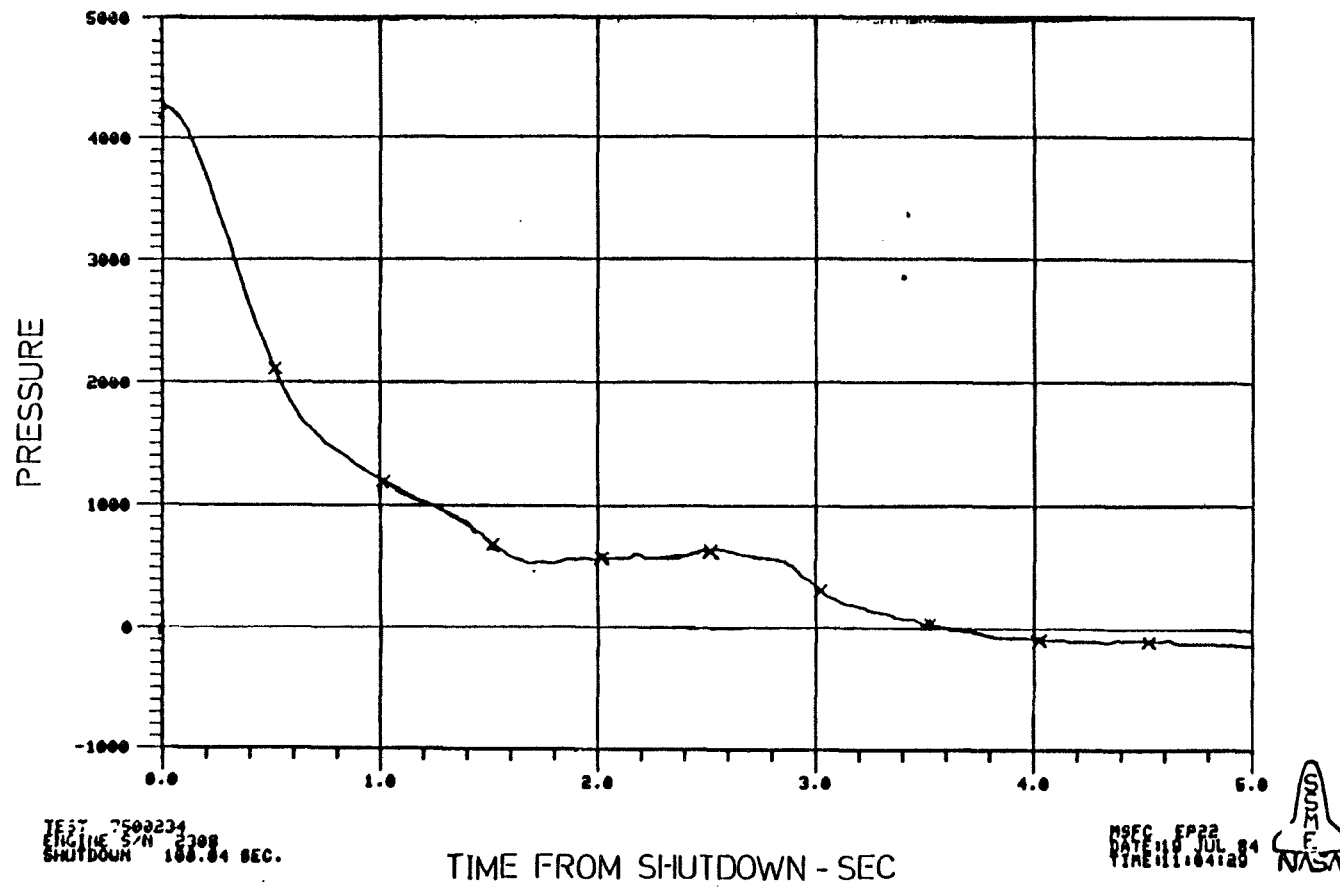


Figure 4.3 Fuel Preburner chamber pressure variation (Coutesy of NASA Huntsville).

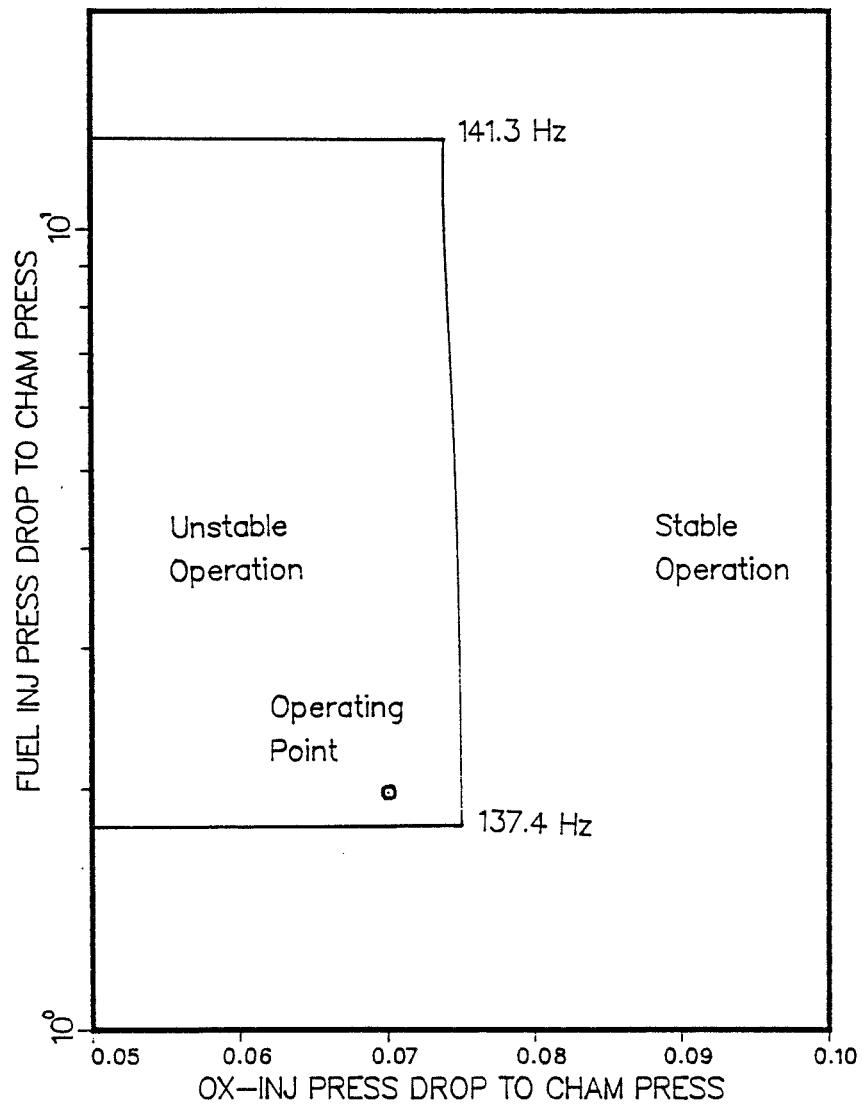


Figure 4.4      Instability of preburner.  
 $P_c = 4.4815E6 \text{ Pa}$ ,  $T_o = T_f = 120 \text{ K}$

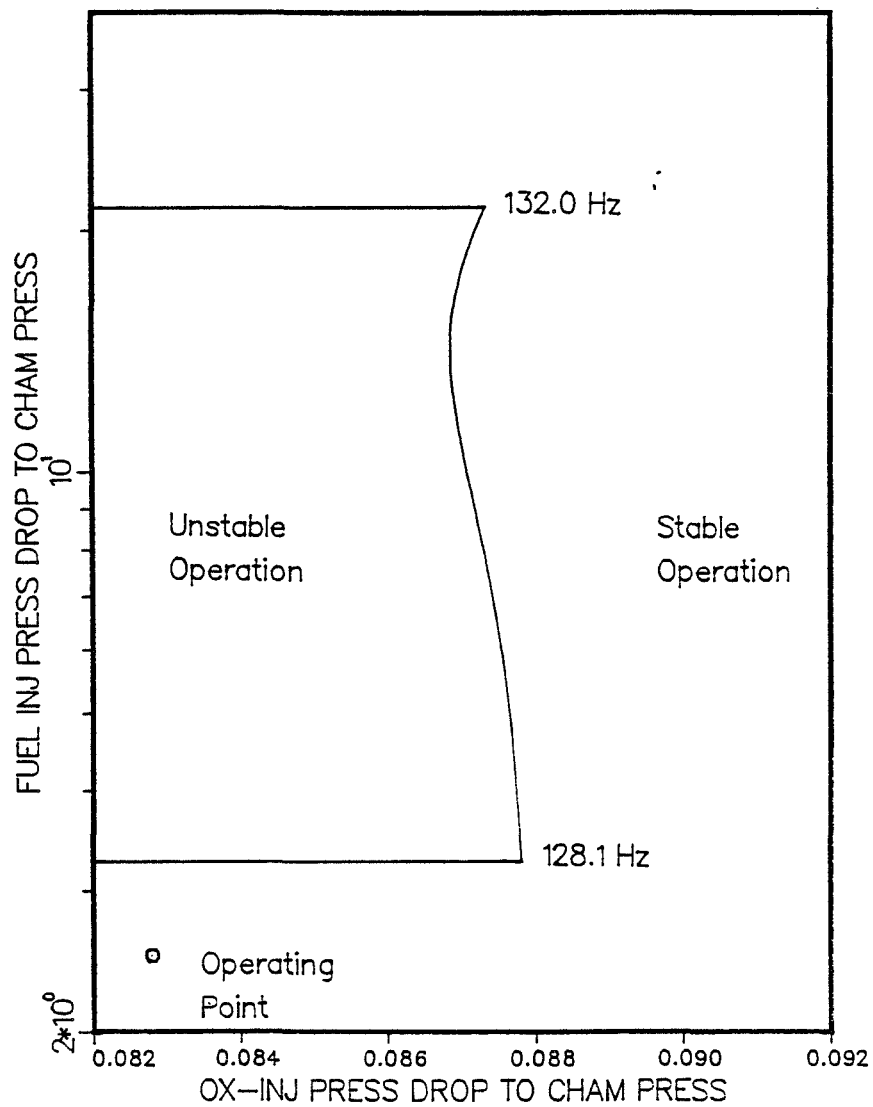


Figure 4.5 Stability of preburner with high oxidizer and fuel temperatures at maximum allowable pressure.  
 $P_c = 3.7902E6$  Pa,  $T_o = T_f = 120$  K



seconds after the shutdown command is issued and continues for about 0.5 seconds before stabilizing out.

The amplitude of the chug shown increases and then decreases with a pause at about 2.6 seconds before increasing again. This phenomenon experienced by the chug is still unclear and further investigation is needed in this area on amplitude prediction.

Since the chug was noted experimentally to stable out at approximately 3.0 seconds after the shutdown command is given, Fig. 4.3 shows the fuel preburner chamber pressure subsequently decreasing from  $4.4815\text{E}6$  Pa (650 psia) to about  $6.8945\text{E}5$  Pa (100 psia) after 3.9 seconds. Therefore, it may be inferred that stable operation in the fuel preburner is prevalent in the region where the chamber pressure is below the mean chugging pressure of  $4.4815\text{E}6$  Pa (650 psia).

The results obtained from the analytical solution, plotted in Figures 4.4 and 4.5, are in good agreement with the experimental results discussed above. The model was tested with a set of varying chamber pressures from  $3.4474\text{E}6$  Pa (500 psia) to  $5.8605\text{E}6$  Pa (850 psia). The other required input conditions during the shutdown phase of the SSME is presented in Table 4.2.

Figures 4.4 and 4.5 represent the nominal operating condition together with the critical pressure drop values  $(\Delta P_{fi}/P_c)'$  and  $(\Delta P_{oi}/P_c)'$  and the frequency. The only boundary point of interest is the critical value of the fuel injector pressure drop  $(\Delta P_{fi}/P_c)$ . At pressures greater than or equal to  $4.4815\text{E}6$  Pa (650 psia), shown in Fig 4.4, the calculated operating point  $\Delta P_{fi}/P_c = 1.98$  signifying

Table 4.2 Input values at shutdown condition

Parameters	Values
$P_c$ . . . . .	4.4815E6 Pa (650 psia)
$T_o$ . . . . .	120.0 K (216 R)
$T_f$ . . . . .	120.0 K (216 R)
$\dot{m}_o$ . . . . .	13.45 Kg/sec (25.59 lbm/sec)
$\dot{m}_f$ . . . . .	33.90 Kg/sec (74.58 lbm/sec)
$T_c$ . . . . .	1065.0 K (1917 R)

instability with a frequency of approximately 137 Hz. Fig 4.5 shows the marginal stability with an operating point,  $\Delta P_{fi}/P_c$  of 2.49, in the fuel preburner at a chamber pressure of 3.7902E6 Pa (550 psia). Because the operating point is just below the minimum point of the stability boundary where  $\Delta P_{fi}/P_c$  is 3.27, stable operation is indicated. Therefore, it can be concluded from these results that the model predictions are in agreement with experimental techniques.

#### Results of Sensitivity Study

The onset of the chugs due to chamber pressure variations were analyzed utilizing the computer program. The chamber pressure was varied from 3.4474E6 Pa (500 psia) to 5.8605E6 Pa (850 psia) as input into the program. Since the chugging frequency ranges between 75 to 200 Hz, the stability boundary computation is performed with the lower frequency bound and is incremented by 0.1 Hz to calculate the required

pressure drops. A stability boundary was therefore generated by computing the fuel injector pressure drop and the oxidizer injector pressure drop at the critical frequency of interest. The stability of the nominal operating point can thus be determined.

The model was used to generate stability curves for several parametric studies. These studies include chamber pressure variations, oxidizer and fuel temperature variations and oxidizer and fuel flow rate variations. The above parametric studies were also performed utilizing two different bulk moduli. The bulk moduli used in the model were for gaseous helium and liquid oxygen. Since helium is an inert gas the compressibility of helium may provide the necessary softness for the chug. Unless otherwise stated, the value of the helium bulk modulus was used in the model. These parametric studies were performed with a single variable parameter while others were held constant.

As indicated in Figures 4.4 and 4.5, instability exists at pressures greater than 3.7902E6 Pa (550 psia) while stable operation is prevalent at pressures below 3.7902E6 Pa (550 psia). At pressures greater than 4.4815E6 Pa (650 psia) instability exists, however, there is an upper bound to the instability since the preburner is stable at full power level.

When low oxidizer and fuel temperatures ( $T_o = 40$  K,  $T_f = 40$  K (72 R)) were utilized as inputs, with varying chamber pressure the system was inevitably unstable even at low pressures with a frequency of 115 Hz and 121 Hz, shown in Figures 4.6 and 4.7 respectively. The

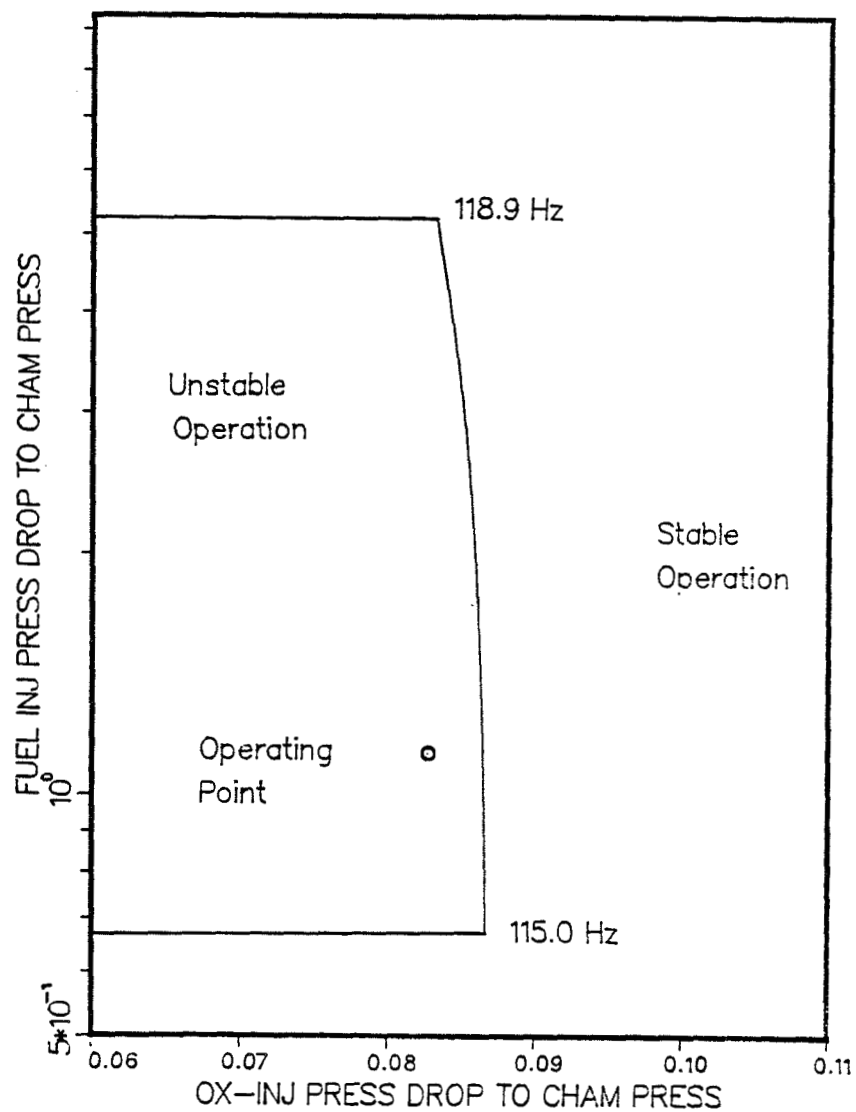


Figure 4.6 Unstable operation with low fuel and oxidizer temperatures at low chamber pressure.  
 $T_o = T_f = 40 \text{ K}$ ,  $P_c = 3.7902\text{E}6 \text{ Pa}$

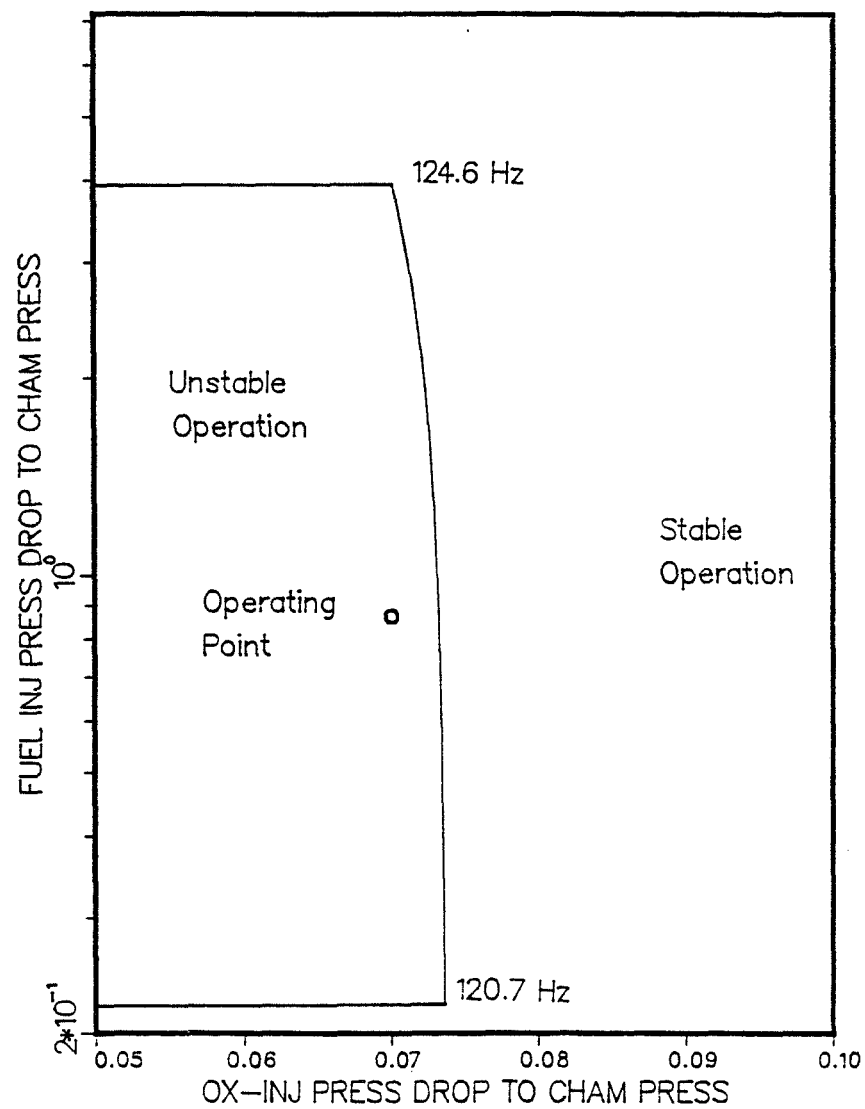


Figure 4.7 Unstable operation in preburner with low oxidizer and fuel temperatures at mean chugging pressure.  
 $T_o = T_f = 40$  K,  $P_c = 4.4815E6$  Pa

ratio of fuel injector pressure drop to chamber pressure ( $\Delta P_{fi}/P_c$ ) of the operating point was never below the minimum point of the stability boundary.

The effect of fuel and oxidizer temperatures on the stability of the system was also considered. At a chamber pressure of 4.4815E6 Pa (650 psia), which is the mean chugging pressure, the oxidizer temperature was subjected to a variation ranging from 40 K to 120 K while the fuel temperature was kept relatively low at 40 K. The variation of varying oxidizer temperature with low fuel temperature (Fig. 4.8) did not stabilize the fuel preburner system, however, it was noted that operation at high fuel and oxidizer temperatures (120 K and 100 K respectively) stabilized the system shown in Fig. 4.9. High oxidizer and fuel temperatures cause partial vaporization of the liquid oxidizer; hence smaller droplet radius. Vaporization and mixing times are thus decreased with the smaller droplet radius. The stability of the system, probably due to the proper mixing of the reactants, could be achieved by increasing propellant temperatures even at the mean pressure where chugging is prevalent.

Since it is undesirable to work with high oxidizer temperatures, several test cases were run to determine if oxidizer temperatures could be reduced and yet maintain stability. It was noted that stability was achieved with higher fuel temperatures while other parameters remained constant. This result presented in Fig. 4.10 shows the fuel temperature at 150 K while oxidizer temperature was lowered to 86 K.

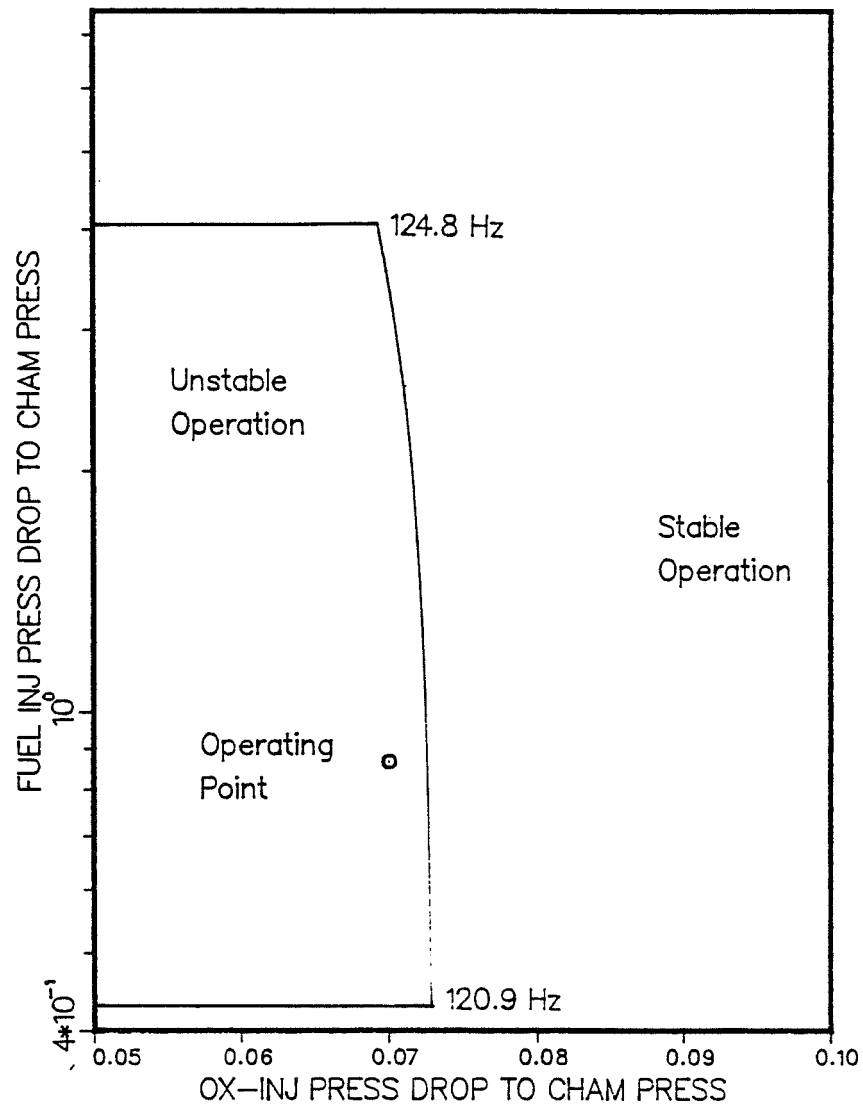


Figure 4.8 Unstable operation in preburner with low fuel and high oxidizer temperature at mean chugging pressure.  
 $T_o = 40 \text{ K}$ ,  $T_f = 120 \text{ K}$ ,  $P_c = 4.4815\text{E}6 \text{ Pa}$

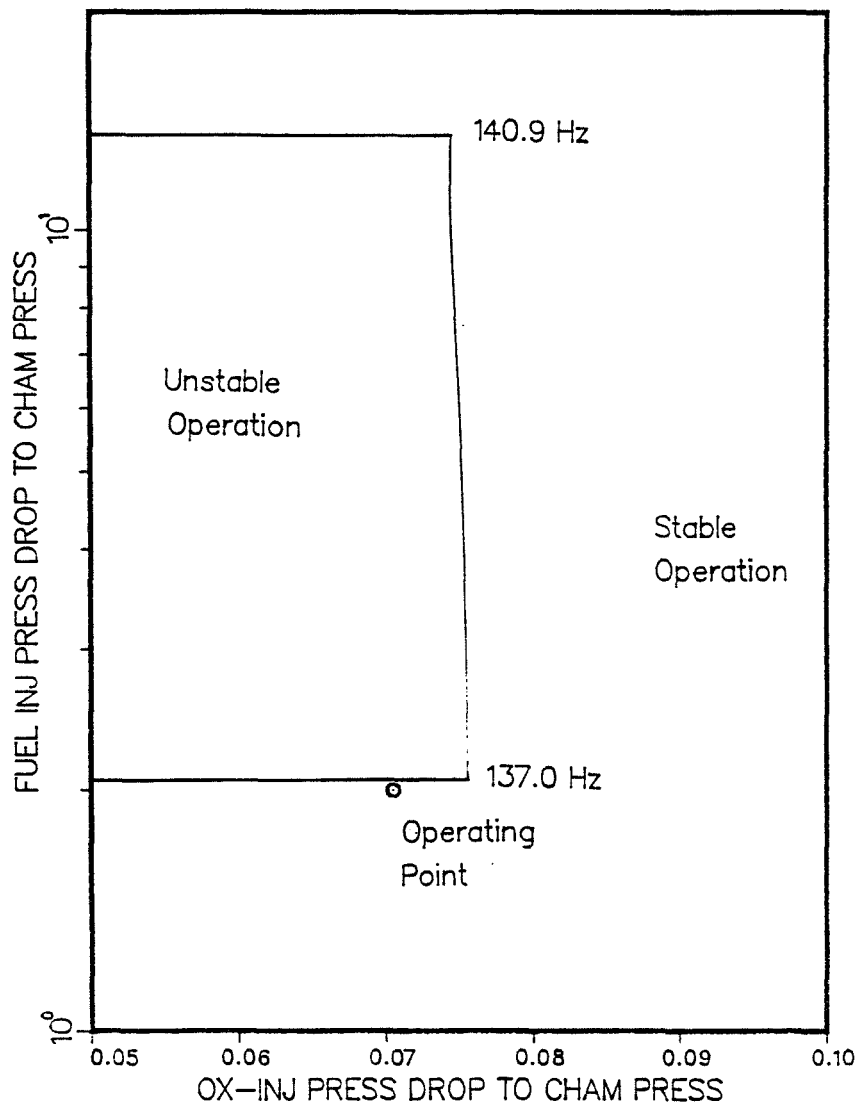


Figure 4.9 Stable operation in preburner with high fuel and high oxidizer temperatures at mean chugging pressure.  
 $T_o = 100 \text{ K}$ ,  $T_f = 120 \text{ K}$ ,  $P_c = 4.4815\text{E}6 \text{ Pa}$



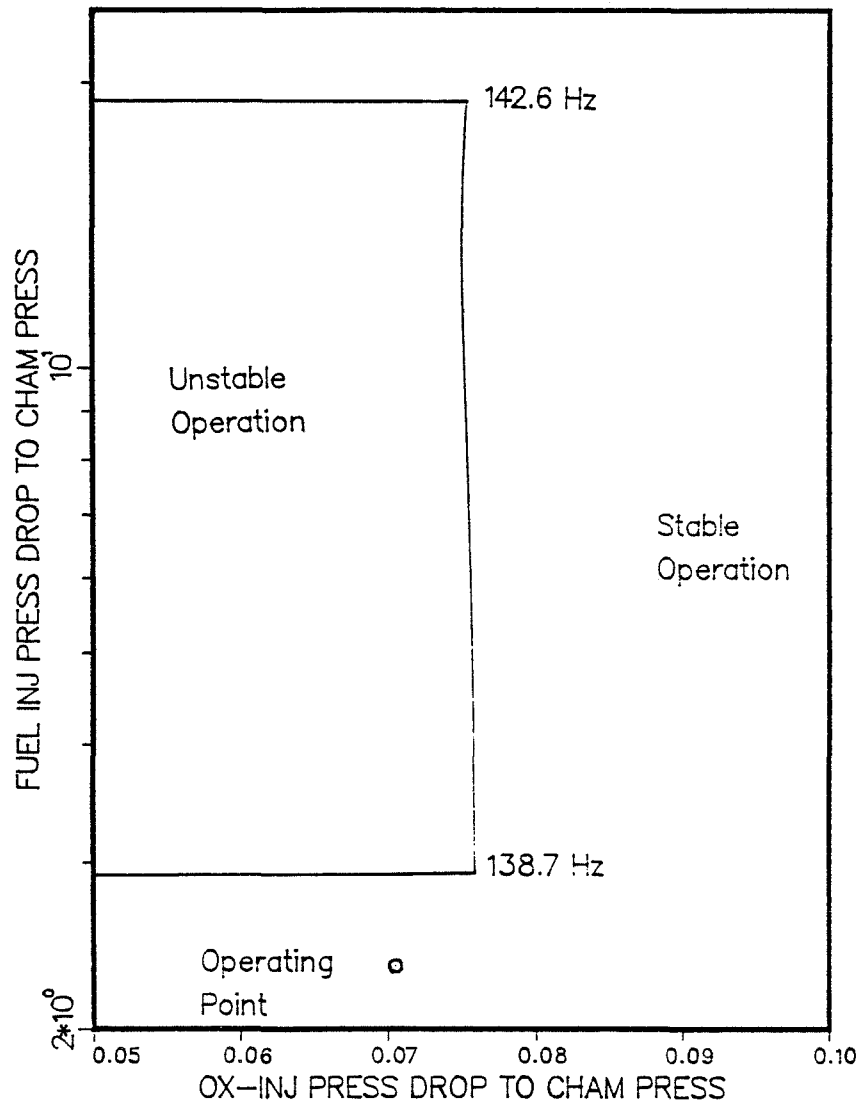


Figure 4.10 Stable operation in preburner with increasing fuel temperature and lower oxidizer temperature at mean chugging pressure.  
 $T_o = 85.7 \text{ K}$ ,  $T_f = 150 \text{ K}$ ,  $P_c = 4.4815\text{E}6 \text{ Pa}$

At the nominal operating point, reduction of fuel flow rate is unlikely to inhibit the chug, since chugging exists at relatively high fuel flow rate (equivalence ratio = 6.0). The mean droplet radius, being an inverse function of fuel flow rate, increases with fuel flow reduction. This causes an increase in vaporization and mixing time and hence increases the combustion instability. Figures 4.11 and 4.12 show the operating point in the unstable region with fuel flow reduction at a frequency of 129.2 Hz and 136.3 Hz respectively.

The influence of varying the oxidizer flow rate on the chug was studied. Although there is no oxidizer feed during shutdown, as the FPOV is already closed, the helium flow rate is considered as the oxidizer flow since it clears the residual oxidizer from the lines and manifold. This is possible because the residual oxidizer flow rate is equivalent to that of helium using the appropriate density value. The model predicted that stability was achieved at low pressures with increased flow rates.

The model was also tested with the bulk modulus of liquid oxygen at conditions where chugging exists. There were no stability boundaries generated for those conditions signifying stable operation. The frequency range of 75 to 200 Hz was tested with variations in the chamber pressure, oxidizer and fuel temperatures. The instability which was prevalent at previous operating conditions, with the bulk modulus of helium, was eliminated utilizing the bulk modulus of liquid oxygen. This shows that the chug depends not only on operating

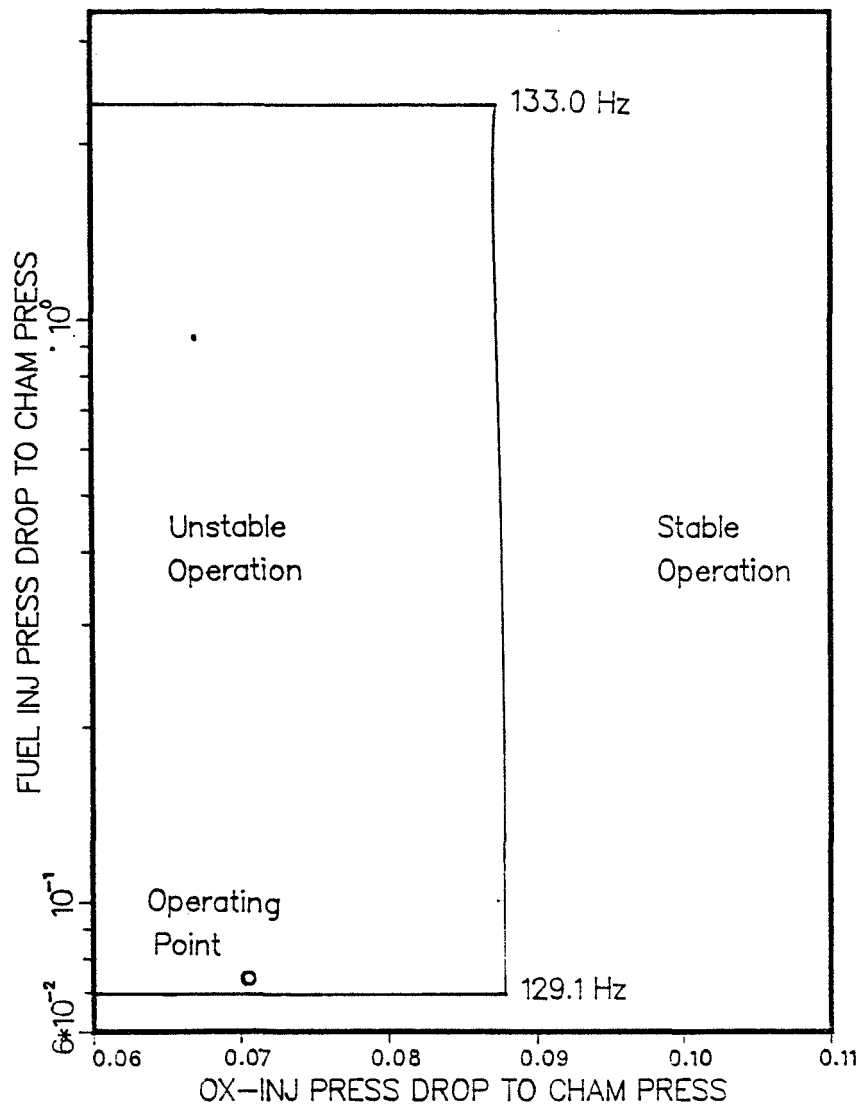


Figure 4.11 Unstable operation in preburner with low fuel flow rate at mean chugging pressure.  
 $\dot{m}_f = 5 \text{ Kg/sec}$ ,  $P_c = 4.4815\text{E}6 \text{ Pa}$

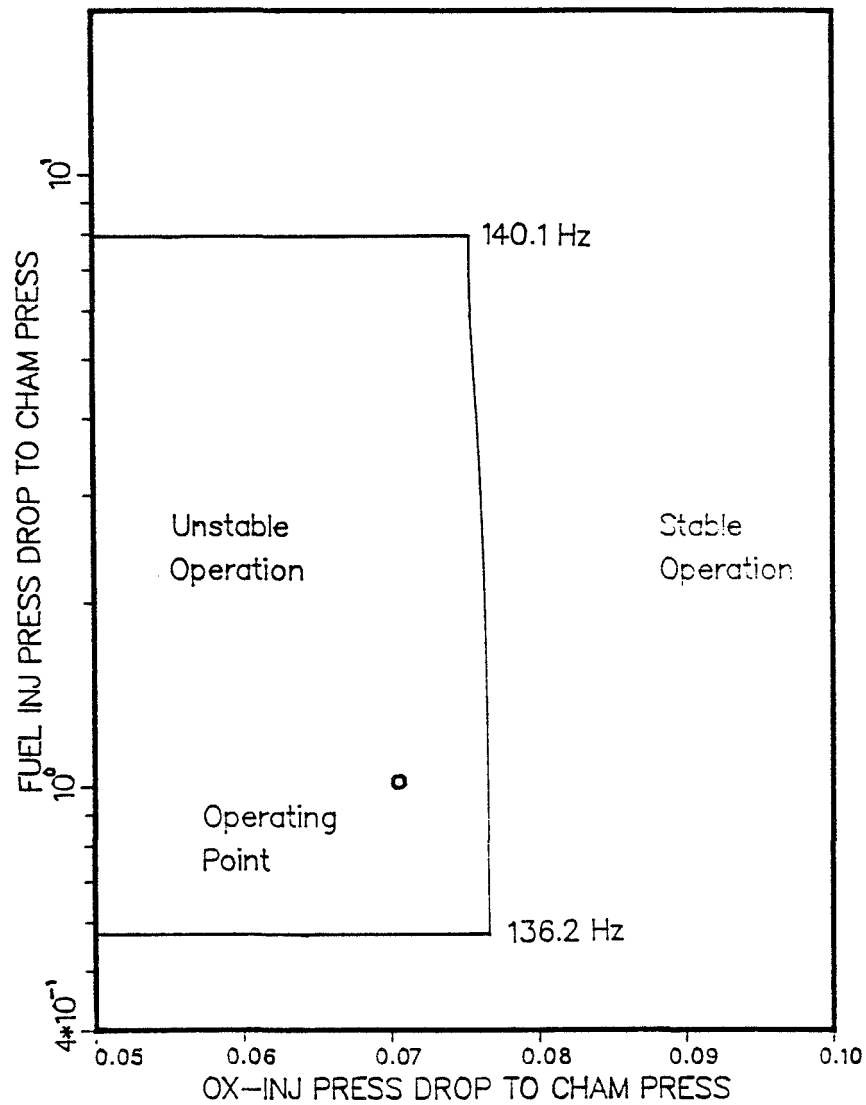


Figure 4.12 Unstable operation in preburner with low fuel flow rate at mean chugging pressure.  
 $\dot{m}_f = 21 \text{ Kg/sec}$ ,  $P_c = 4.4815\text{E}6 \text{ Pa}$

conditions but also on the helium purge conditions, specifically the compressibility of the helium.

The following figures (Figures 4.13, 4.14 and 4.15) show the variation of chugging frequency with oxidizer temperature, fuel flow rate and chamber pressure respectively. Fig. 4.13 shows that stable operation was achieved with oxidizer temperatures between 80 to 115 K. Temperatures below 80 K resulted in unstable operation at a frequency of 139 Hz. Fig. 4.14 shows that the system was unstable with fuel flow variation at a frequency of 138 Hz. The two endpoints of the curve were arbitrary selected for this parametric study. Fig. 4.15 shows that stable operation is permissible at low pressures. The chugging frequency increases somewhat linearly with increased chamber pressure up to 5.759E6 (830 psia).

The preceding parametric studies reflected several intriguing results. Although the analysis in this model was simplified, nevertheless, it provided the basic understanding to the occurrence of the SSME fuel preburner chug and the parameters to be investigated further for chug elimination.

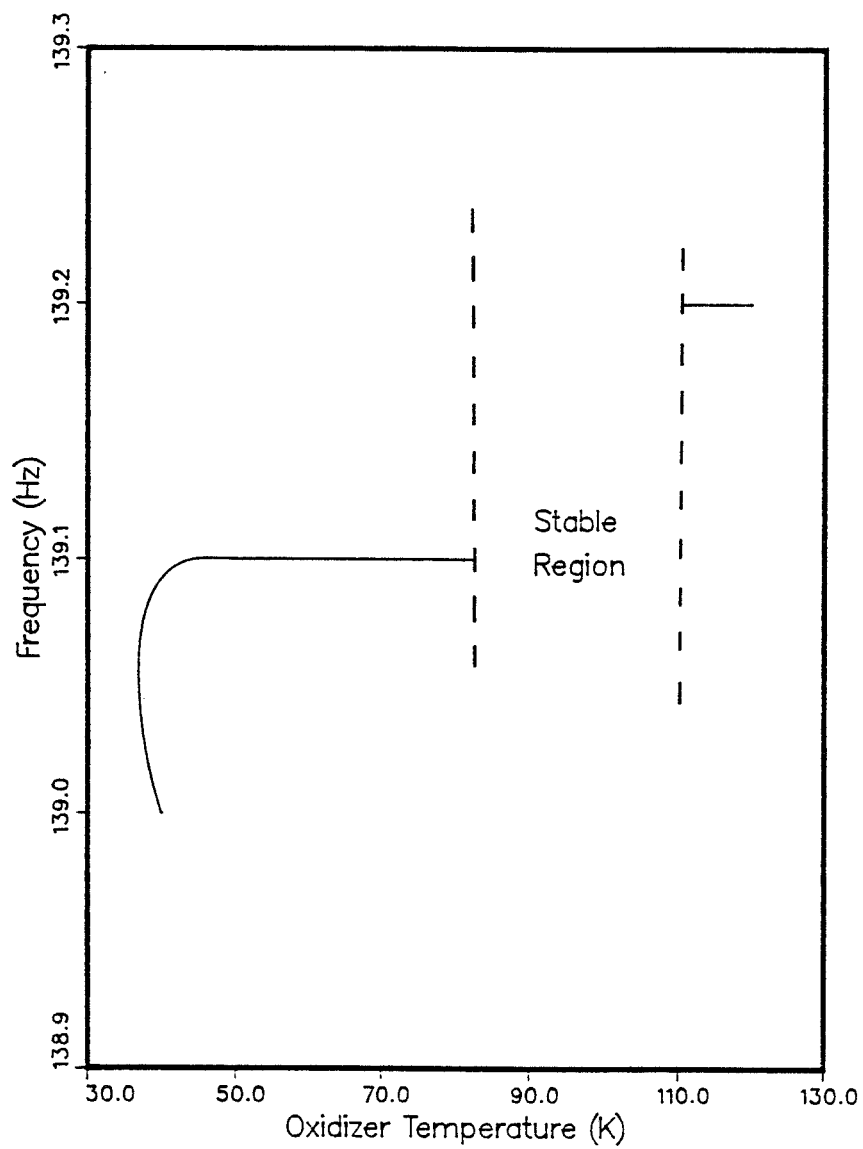


Figure 4.13 Variation of chugging frequency with oxidizer temperature.

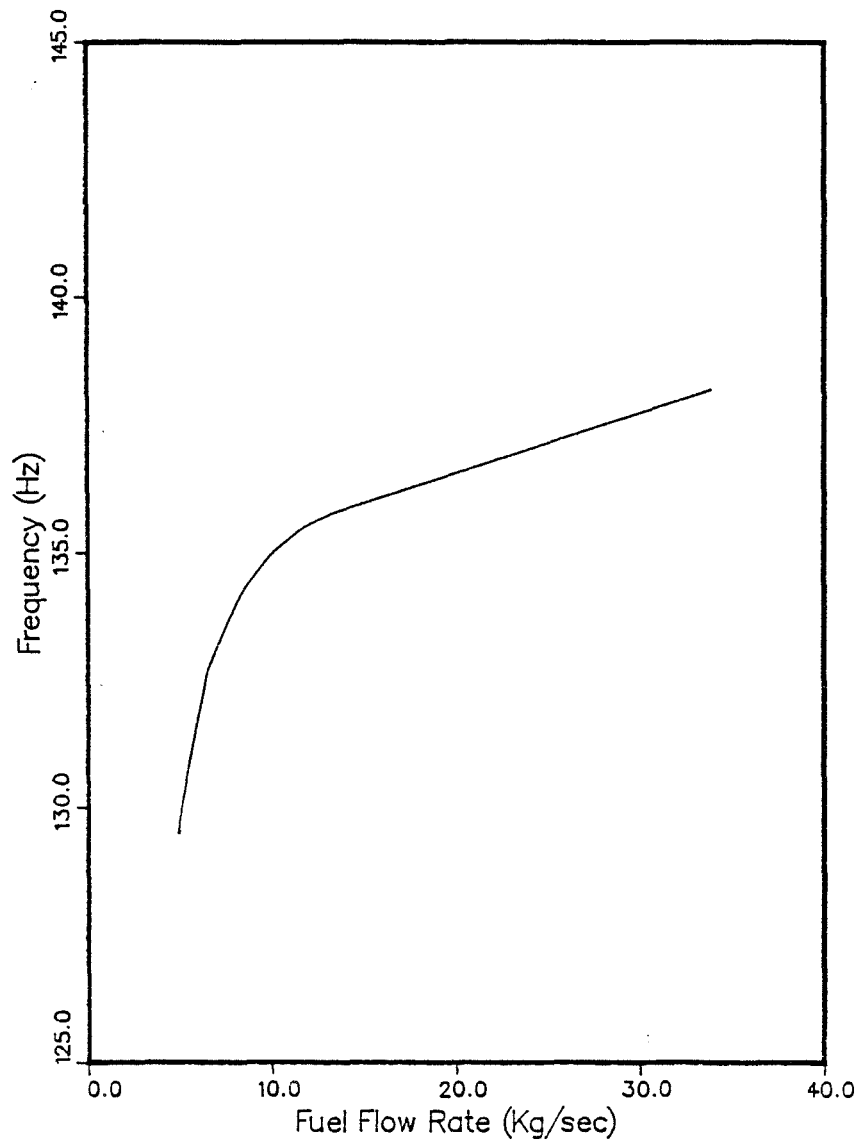


Figure 4.14 Variation of chugging frequency with fuel flow rate.

$T_o = 100$  K,  $T_f = 120$  K,  $P_c = 4.4815E6$  Pa

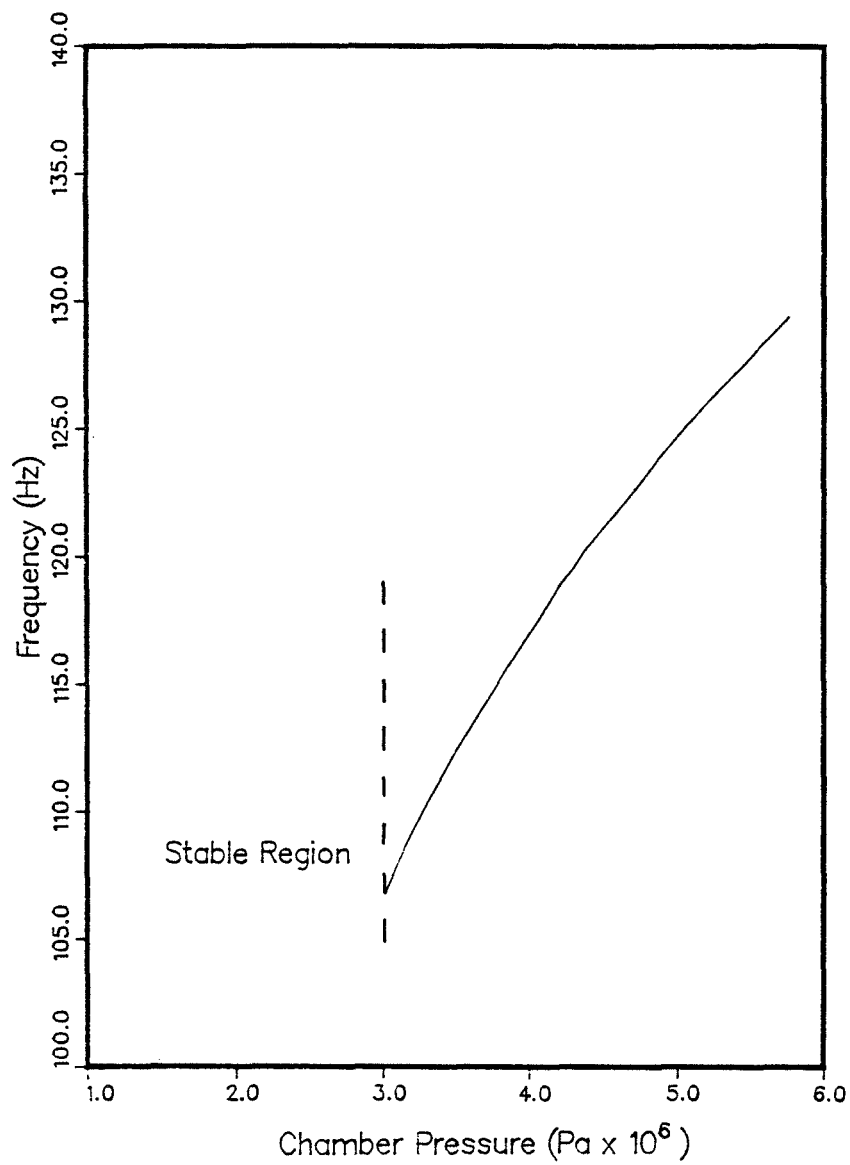


Figure 4.15 Variation of chugging frequency with chamber pressure.



## CHAPTER V

### CONCLUSIONS AND RECOMMENDATIONS

The objectives of this research were to identify the significant elements in triggering the onset of the chug and its' possible elimination. System variables such as chamber pressure, propellant temperatures and flow rates were varied and their effects on the stability of the SSME fuel preburner chug analyzed.

The first task was to review the literature in the area of low frequency instability as well as to solicit available computer models capable of analyzing the chug. The best available program was modified to analyze the fuel preburner chug. The model presented in this thesis is not restricted to SSME preburners but may also be applied to liquid propellant rocket engines. This model proved to be valuable in meeting the required objectives.

The model in this thesis assumes quasi-steady state conditions and was linearized to simplify the non-linear governing differential equation. The method of perturbations was used to linearize the governing differential equation. Chemical kinetics in the combustion process were assumed to be infinitely fast and were therefore neglected in the analysis.

Although the model has been simplified and linearized, it is nevertheless capable of chug predictions and is in excellent agreement with experimental results provided by Rocketdyne and NASA. The

predicted frequencies differing by less than ten percent of the measured value show that this model is effective in analyzing the SSME fuel preburner chug.

The VAX 11/780 CPU time required for each sensitivity study was approximately 5 seconds. This extraordinarily short CPU time is beneficial as several different test cases could be performed with limited cost compared to experimental runs.

Since the chug occurs during the helium purge of the oxidizer, the sensitivity studies were performed utilizing the bulk modulus of helium and repeated with the bulk modulus of the liquid oxidizer. The chugs did not exist when the relatively incompressible oxygen was considered.

The results of these sensitivity studies are presented and discussed in detail in the previous chapter. Table 5.1 summarizes the results. Several intriguing results were revealed by the model. The onset of the chugs were linked to a couple of significant parameters such as fuel temperatures and fuel flow rates. The predicted results show that the fuel preburner instability was suppressed at higher fuel temperatures. This explains why chugging is reduced at high cut-off power; hence high fuel temperature. It was also noted that at high fuel temperatures the oxidizer temperature could be reduced. Other parameters of interest such as oxidizer flow rates and bulk modulus have shown to influence the instability to some extent.

Table 5.1 Summary of parametric studies performed

Variation of System Variables	Comments
$P_c$	At low fuel and oxidizer temperatures approximately 40 K (72R) the system was inherently unstable. At the other extreme with high fuel and oxidizer temperature $T_o = T_f = 120$ K (216 R) stability is achieved with maximum pressure of 3.7902E6 Pa (550 psia)
$T_o$	At the mean chugging pressure of 4.4815E6 Pa (650 psia) low oxidizer temperature and high fuel temperature proved unsuitable for operation. However, with increased $T_o = 100$ K (180 R) stability is possible. Further increases in fuel temperature to 150 K (270 R) showed that stability was achieved with lower oxidizer temperatures.
$T_f$	At low fuel temperatures the chug was not inhibited at all with varying oxidizer temperatures even at low pressures where stability was prominent.
$\dot{m}_o$	High helium flow rates (analogous to oxidizer flow) showed that chugging was eliminated.
$\dot{m}_f$	Variation in fuel flow rate did not eliminate the chug. It was noted that since the MFV is not closed until after chugging ends, fuel variation would not eliminate the chug.
Bulk Modulus	When liquid oxygen bulk modulus value was used the system was inherently stable since no stability boundary was generated.

The modeling effort should be continued and supported in an attempt to understand the non-linear chugs. This model, being linearized is limited in the capability of predicting amplitude changes of the chug. The challenge now is to incorporate the NASA/Rocketdyne transient model into the analysis.

This research has laid the foundation for continuing study of the SSME shutdown chug. Although this model was developed to analyze the fuel preburner chug it may be applied to the oxidizer preburner or other liquid propellant rocket engine. This model will assist in the understanding of the chugging phenomenon as it was developed predominantly as a useful analysis tool for engine designs.

## REFERENCES

## REFERENCES

1. Summerfield, M., "A Theory of Unstable Combustion in Liquid Propellant," Journal of American Rocket Society, Vol. 21, Sept. 1951, pp. 108-114.
2. Crocco, L., "Aspects of Combustion Stability in Liquid Propellant Rocket Motors," Journal of American Rocket Society, Vol. 21, Nov. 1951, pp. 163-178.
3. Barrere, M., and Moutet, A., "Low Frequency Combustion Instability in Bipropellant Rocket Motors--Experimental Study," Journal of American Rocket Society, Vol. 26, Jan. 1956, pp. 9-19.
4. Weber, W. T., "Calculation of Low Frequency Unsteady Behavior of Liquid Rocket from Droplet Combustion Parameters," Journal of Spacecraft, Vol. 9, Apr. 1972, pp. 231-237.
5. Li, Y. T., "Stabilization of Low Frequency Oscillations of Liquid Propellant Rocket with Fuel Line Stabilizer," Journal of American Rocket Society, Vol. 26, Jan. 1956, pp. 26-39.
6. Gunder, D. F., and Friant, D. R., "Stability of Flow in Rocket Motor," Journal of Applied Mechanics, Vol. 17, (1950), pp. 327-333.
7. Harrje, D. T., and Reardon, F. H., Liquid Propellant Rocket Combustion Instability. NASA SP--194, 1972.
8. Wenzel, L. M., and Szuch, J., R., "Analysis of Chugging in Liquid Bipropellant Rocket Engines using Propellants with different Vaporization Rates," NASA TN--D--3080, 1965.
9. Nguyen, D. G., Engine Balance and Dynamic Model. Rockwell International Corporation, Rocketdyne Division, May 1981.

10. Gordon S., and McBride, B. J., A Computer Program for calculation of Complex Equilibrium compositions, rocket performance instant or reflected shocks and Chapman-Jouguet Detonations. NASA SP--273, 1971.
11. Van Wylen, G.J., and Sonntag, R. E., Fundamentals of Classical Thermodynamics. 2nd ed. New York: John Wiley and Sons Inc. 1973.
12. Szuch, J. R., "Digital Computer Program for Analysis of Chugging Instabilities," NASA TN--D--7026, Dec. 1970.
13. Priem, R. J., and Heidmann, M. F., "Propellant Vaporization as a Design Criterion for Rocket Engine Combustion Chambers," NASA TR--R--67, 1960.
14. Crocco, L., and Cheng, S., Theory of Combustion Instability in Liquid Propellant Rocket Motors. London: Butterworths Scientific Publications, 1956.
15. George II, P. E., "An Investigation of Space Shuttle Main Engine Shutdown Chugging Instability," Research Reports--1984 NASA/ASE Summer Faculty Fellowship Program, NASA CR--171317, Jan. 1985.

## APPENDIXES

»



APPENDIX A  
DERIVATION OF EQUATIONS

In this appendix the reduction process involved in acquiring eq. (3.5) from eq. (3.3) as well as the general reduction of the characteristic equation will be presented. The method of perturbations will be utilized to linearize any non-linear differential equations.

Eq. (3.3) is reproduced below:

$$\frac{\partial}{\partial t} \left[ \rho V_c \right] = \dot{m}_{fb}(t) + \dot{m}_{ob}(t) - \dot{m}_e(t) \quad (3.3)$$

Taking the perturbations of system variables and neglecting higher powers and products of perturbations results in the following equation.

$$V_c \frac{\partial}{\partial t} \left\{ \bar{\rho} + \tilde{\rho} \right\} = \bar{\dot{m}}_{fb}(t) + \tilde{\dot{m}}_{fb}(t) + \bar{\dot{m}}_{ob}(t) + \tilde{\dot{m}}_{ob}(t) - \bar{\dot{m}}_e(t) - \tilde{\dot{m}}_e(t) \quad (A1)$$

Dividing both sides by the total propellant flow rate gives:

$$\frac{V_c \bar{\rho}}{\dot{m}_t} \frac{\partial}{\partial t} \left\{ 1 + \frac{\tilde{\rho}}{\bar{\rho}} \right\} = \frac{\bar{\dot{m}}_{fb} + \bar{\dot{m}}_{ob} - \bar{\dot{m}}_e}{\dot{m}_t} + \frac{\tilde{\dot{m}}_{fb}(t) + \tilde{\dot{m}}_{ob}(t) - \tilde{\dot{m}}_e(t)}{\dot{m}_t} \quad (A2)$$

which can be reduced easily to:

$$\theta_s \frac{\partial}{\partial t} \left\{ \frac{\tilde{\rho}}{\bar{\rho}} \right\} + \frac{\tilde{\dot{m}}_e(t)}{\dot{m}_t} = \frac{\tilde{\dot{m}}_{fb}(t) + \tilde{\dot{m}}_{ob}(t)}{\dot{m}_t} \quad (3.5)$$

### Combination and reduction of characteristic equation

The characteristic equation, derived in chapter three, is presented below as:

$$-1 = \frac{\frac{P_c X K}{Z_o(s)} e^{-\tau_o s} + \frac{P_c Y K}{Z_f(s)} e^{-\tau_f s}}{\theta_g s + C1} \quad (3.24)$$

Letting  $s = j\omega'$ ,  $Z_o(s) = R_o' + jI_o$ ,  $Z_f(s) = R_f' + jI_f$  and noting that  $e^{-ix} = \cos(x) - j\sin(x)$ , eq. (3.24) thus becomes:

$$-C1 - j\omega'\theta_g = \left[ \frac{P_c X K \cos(\omega'\tau_o) - jP_c X K \sin(\omega'\tau_o)}{R_o' + jI_o} \right] + \left[ \frac{P_c Y K \cos(\omega'\tau_f) - jP_c Y K \sin(\omega'\tau_f)}{R_f' + jI_f} \right] \quad (A3)$$

Multiplying both sides of eq. (A3) by  $(R_o' + jI_o)$  and  $(R_f' + jI_f)$  and separating into the respective real and imaginary parts the following equations are obtained:

Real Part

$$R_o' R_f' C1 + \omega' \theta_g (I_o' R_f' + R_o' I_f') - I_o' I_f' C1 = P_c X K \left[ R_f' \cos(\omega' \tau_o) + I_f' \sin(\omega' \tau_o) \right] \\ + P_c Y K \left[ R_o' \cos(\omega' \tau_f) + I_o' \sin(\omega' \tau_f) \right] \quad (A4)$$

Imaginary Part

$$C1 \left[ R_o' I_f' + R_f' I_o' \right] + \omega' \theta_g \left[ I_o' I_f' - R_o' R_f' \right] = P_c X K \left[ I_f' \cos(\omega' \tau_o) - R_f' \sin(\omega' \tau_o) \right] \\ + P_c Y K \left[ I_o' \cos(\omega' \tau_f) - R_o' \sin(\omega' \tau_f) \right] \quad (A5)$$

Solving equations (A4 and A5) for  $R_f'$ :

Real Part

$$R_f' = \frac{P_c Y K \left[ R_o' \cos(\omega' \tau_f) + I_o' \sin(\omega' \tau_f) \right] + I_f' P_c X K \sin(\omega' \tau_o) - \omega' \theta_g R_o' I_f' + C1 I_o' I_f'}{R_o' C1 + \omega' \theta_g I_o' - P_c X K \cos(\omega' \tau_o)} \quad (A6)$$

Imaginary Part

$$R_f' = \frac{P_c Y K \left[ R_o' \sin(\omega' \tau_f) - I_o' \cos(\omega' \tau_f) \right] - I_f' P_c X K \cos(\omega' \tau_o) + \omega' \theta_g I_o' I_f' + C1 R_o' I_f'}{R_o' \omega' \theta_g - C1 I_o' - P_c X K \sin(\omega' \tau_o)} \quad (A7)$$

Equating equations (A6 and A7) and solving for  $R_o'$  yields the characteristic equation in quadratic form.

$$\begin{aligned}
& R_o'^2 \left[ F - \frac{I_f}{P_c Y K} \left\{ C1^2 + \omega'^2 \theta_g^2 \right\} \right] + \\
& R_o' \left[ \frac{2XI_f}{Y} \left\{ C1 \cos(\omega' \tau_o) + \omega' \theta_g \sin(\omega' \tau_o) \right\} - \right. \\
& \left. P_c X K \sin(\omega' \tau_o - \omega' \tau_f) \right] + \\
& \left[ I_o^2 F - I_o P_c X K \cos(\omega' \tau_o - \omega' \tau_f) - \frac{I_o^2 I_f}{P_c Y K} (C1^2 + \omega'^2 \theta_g^2) \right. \\
& \left. - \frac{I_f P_c X^2 K}{Y} - \frac{2XI_o I_f}{Y} \left\{ C1 \sin(\omega' \tau_o) - \omega' \theta_g \cos(\omega' \tau_o) \right\} \right] = 0
\end{aligned} \tag{3.29}$$

where

$$F = \omega' \theta_g \cos(\omega' \tau_f) - C1 \sin(\omega' \tau_f)$$

APPENDIX B

LISTING OF PROGRAM CHUGTEST

```

C #####
C #
C #
C #          PROGRAM CHUGTEST
C #          BY KAIR-CHUAN LIM
C #
C #####
C #
C #          THE PROGRAM BELOW WAS DEVELOPED TO ANALYSE THE
C #          COMBUSTION INSTABILITY (CHUGGING) IN THE FUEL PREBURNER
C #          OF THE SSME.
C #
C #####

```

```

* DIMENSION UPL(1000), ACRL(1000), UPH(100), ACRH(100), FL(1000),
*   FH(100)
* DIMENSION ACCL(10),UPPL(10), FFL(10), ACCH(10), UPPH(10),
*   FFH(10)

```

```

REAL NUMER
INTEGER ENO, ENF, PARAM
OPEN (UNIT=20,FILE='OUTCHUG.DAT',STATUS='OLD')
OPEN (UNIT=21,FILE='PLOT21.DAT',STATUS='OLD')
OPEN (UNIT=22,FILE='PLOT22.DAT',STATUS='OLD')
OPEN (UNIT=23,FILE='PLOT23.DAT',STATUS='OLD')
OPEN (UNIT=24,FILE='PLOT24.DAT',STATUS='OLD')
OPEN (UNIT=25,FILE='PLOT25.DAT',STATUS='OLD')
OPEN (UNIT=26,FILE='PLOT26.DAT',STATUS='OLD')
OPEN (UNIT=27,FILE='PLOT27.DAT',STATUS='OLD')
OPEN (UNIT=28,FILE='PLOT28.DAT',STATUS='OLD')

```

```

1 IOUT=20
  IO=21
  C1=-0.1072
  PI=4.*ATAN(1.)
  FORMAT (//)

```

```

C THE FOLLOWING DATA IS FOR HYDROGEN FUEL
  RF=4126.          ! FUEL GAS CONSTANT (J/kg C)
  RHOF=20.          ! FUEL DENSITY (kg/m3)

```

```

C THE FOLLOWING DATA IS FOR CYROGENIC OXYGEN OXIDIZER
  TCR=154.5         ! CRITICAL TEMP (K)
  WTO=32.           ! MOL. WT (kg/kg mole)
  HV=2.13E5         ! HT. OF VAPORIZATION (J/kg)
  RHO=1152.         ! DENSITY (kg/m3)
  ST=1.19E-2        ! SURF. TENSION (N/m)
  VIS=3.0348E-4     ! VISCOSITY (N s/m2)
  RSTVC=((1143./RHO)*(VIS/1.9E-4)*(ST/1.33E-2))**.25
  WTT=(WTO/100.)**.35 ! MOL. WT COEFF USED IN EL50

```

```

HVT=(HV/3.26E5)**.8      ! HT. OF VAP COEFF USED IN EL50
PHI=6.                    ! EQUIVALENCE RATIO
SWC=0.448                ! SWIRLING FACTOR

C  THE TYPE OF PARAMETRIC STUDY IS SELECTED AT THIS POINT
15 WRITE (5, 2)
2  FORMAT (1H , 'TYPE OF PARAMETRIC STUDY?', //, 3x, '1  CHAMBER
   @  'PRESSURE', //, 3x, '2  OXIDIZER FLOW RATE', //, 3x,
   @  '3  FUEL FLOW RATE', //, 3x, '4  OXIDIZER TEMPERATURE', //,
   @  '5  FUEL TEMPERATURE', //, 3x, 'ENTER SELECTION .....')
   READ (5, *) PARAM

C  THE FOLLOWING IS COMBUSTION CHAMBER GEOMETRY DATA OBTAINED
C  FROM NASA AND ROCKETDYNE
   CDIA=0.265             ! CHAMBER DIAMETER (m)
   ELC=0.108              ! CYL. CHAMBER LENGTH (m)
   AC=PI*CDIA**2/4.       ! COMB CHAMB. X-AREA (m2)
   VC=AC*ELC              ! CHAMBER VOL (m3)

C  THE FOLLOWING IS SPECIFIED INJECTOR GEOMETRY
   DO=2.8956E-3           ! OX INJECTOR ORIF. DIA (m)
   ENE=264.               ! NO. OF ELEMENTS
   ENO=ENE                ! NO OF OX ELEMENTS
   ENF=ENE                ! NO OF FUEL ELEMENTS
   ELO=0.0511            ! OX ELEMENT LENGTH

C  FOR SINGLE ORIFICE INJECTOR, VOM IS OXIDIZER INJECTOR MANIFOLD
C  VOLUME.  VOF IS FUEL MANIFOLD VOLUME

   CDO=.5                 ! FLOW COEFF OX INJ ELEMENT
   CDF=.5                 ! FLOW COEFF FUEL INJ ELEMENT
   SWC=.448               ! CORRECTION FOR SWIRLER
   VOF=6.55E-5            ! FUEL INJ MANIFOLD VOL (m3)
   ELLS=0.1061           ! SUCTION LINE LENGTH (m)
   DSU=0.0445            ! SUCTION LINE DIA (m)
   VOM=9.34E-4           ! OX MANIFOLD VOL (m3)
   APFO=1.329E-5         ! FUEL ANNULUS (m2)

C  AT THIS POINT A DECISION IS MADE WHETHER TO GENERATE BOUNDARIES
C  AT VARIOUS CHAMBER PRESSURES, USING OPERATING POINT DELAYS OR
C  TO GENERATE BOUNDARIES USING DELAY VALUES SENSITIVE TO FUEL
C  ANNULUS AREA JJ=0 DENOTES FORMER AND JJ=1 DENOTES LATTER

   J=1
   JJ=0                   ! TYPE OF STUDY
   MN=1                   ! LOWER THROTTLING LIMIT
   LI=0                   ! LOW FREQ SOLN INDEX
   IL=0                   ! HIGH FREQ SOLN INDEX
   IF (JJ .EQ. 0) MN=18

```



C THIS SECTION DIVIDES THE RANGE OF THE PARAMETRIC STUDY INTO  
C EIGHT EQUAL SEGMENTS

```

      IF (PARAM .EQ. 1) THEN
      WRITE (5, 3)
3      FORMAT (1H , 'WHAT IS THE MINIMUM AND MAXIMUM PRESSURE RANGE
@      FOR STUDY?')
      READ (5, *) PC1, PC2
      COUNT=(PC2-PC1)/(FLOAT(MN)-1.)
      WRITE (5, 4)
4      FORMAT (1H , 'INPUT OXIDIZER AND FUEL FLOW RATE AND
@      TEMPERATURE RESPECTIVELY')
      READ (5, *) WO, WF, TO, TF
      GO TO 13
      ELSE IF (PARAM .EQ. 2) THEN
      WRITE (5, 5)
5      FORMAT (1H , 'WHAT IS THE MINIMUM AND MAXIMUM OXIDIZER FLOW
@      RATE RANGE FOR STUDY')
      READ (5, *) WO1, WO2
      COUNT=(WO2-WO1)/(FLOAT(MN)-1.)
      WRITE (5, 6)
6      FORMAT (1H , 'INPUT CHAMBER PRESSURE, OXIDIZER AND FUEL
@      TEMPERATURE FUEL FLOW RATE RESPECTIVELY')
      READ (5, *) PC, TO, TF, WF
      GO TO 13
      ELSE IF (PARAM .EQ. 3) THEN
      WRITE (5, 7)
7      FORMAT (1H , 'WHAT IS THE MINIMUM AND MAXIMUM FUEL FLOW RATE
@      RANGE FOR STUDY')
      READ (5, *) WF1, WF2
      COUNT=(WF2-WF1)/(FLOAT(MN)-1.)
      WRITE (5, 8)
8      FORMAT (1H , 'INPUT CHAMBER PRESSURE, OXIDIZER AND FUEL
@      TEMPERATURE AND OXIDIZER FLOW RATE')
      READ (5, *) PC, TO, TF, WO
      GO TO 13
      ELSE IF (PARAM .EQ. 4) THEN
      WRITE (5, 9)
9      FORMAT (1H , 'WHAT IS THE MINIMUM AND MAXIMUM OXIDIZER
@      TEMPERATURE RANGE FOR STUDY')
      READ (5, *) TO1, TO2
      COUNT=(TO2-TO1)/(FLOAT(MN)-1.)
      WRITE (5, 10)
10     FORMAT (1H , 'INPUT CHAMBER PRESSURE, OXIDIZER AND FUEL FLOW
@      RATE AND FUEL TEMPERATURE')
      READ (5, *) PC, WO, WF, TF
      GO TO 13
      ELSE IF (PARAM .EQ. 5) THEN
      WRITE (5, 11)
11     FORMAT (1H , 'WHAT IS THE MINIMUM AND MAXIMUM FUEL

```

```

@ TEMPERATURE RANGE FOR STUDY')
  READ (5, *)TF1, TF2
  COUNT=(TF2-TF1)/(FLOAT(MN)-1.)
  WRITE (5, 12)
12  FORMAT (1H, 'INPUT CHAMBER PRESSURE, OXIDIZER AND FUEL
@ FLOW RATE AND OXIDIZER TEMPERATURE')
  READ (5, *)PC, WO, WF, TO
13  END IF
  DO 90 I=1,MN
  INDEX=I-1
  IF (PARAM .EQ. 1)PC=PC1+COUNT*FLOAT(INDEX)
  IF (PARAM .EQ. 2)WO=WO1+COUNT*FLOAT(INDEX)
  IF (PARAM .EQ. 3)WF=WF1+COUNT*FLOAT(INDEX)
  IF (PARAM .EQ. 4)TO=TO1+COUNT*FLOAT(INDEX)
  IF (PARAM .EQ. 5)TF=TF1+COUNT*FLOAT(INDEX)
  OF=WO/WF ! MIXTURE RATIO
  BO=PC ! BULK MODULUS (Pa)
  K=0 ! VARIABLE FUEL AREA INDEX
  APF=APFO ! FUEL ANNULUS AREA (m2)
  AOV=PI*0.0279**2/4. ! CTRL VAL AREA (m2)

C COMPUTE SLOPE OF X AND Y FROM EQUATIONS .....

  SLOPE=1.3644*PHI**3-38.7501*PHI**2+376.18*PHI-1340.08

C THE SPECIFIC HEAT RATIO IS USED TO CALCULATE CHAMBER PRESSURE
C AT THE INJECTOR FACE

  TC=1065. ! COMBUSTION TEMP
  RC=122.3 ! COMB PROD GAS CONST (J/Kg K)
  GAMMA=0. ! SPECIFIC HEAT RATIO OF PRODUCTS
  CALL GAM (TC, GAMMA)
  ACOUS=SQRT(GAMMA*RC*TC) ! ACOUSTIC VEL EXIT
  WTOT= WO + WF
  RHOH2=PC*1.E-6*2./(82.06E-3*TC*101325*1.03)
  RHOH2O=(1./1.834)/(2.2*2.54E-2**3*12.**3)
  RHO1=(5./20.)*RHOH2 + (1./20.)*RHOH2O
  AE=4.92E-2
  EMC=WTOT/(ACOUS*RHO1*AE) !MACH NO AT EXIT

  VELC=EMC*ACOUS ! GAS VEL EXIT
  EXP1=GAMMA/(GAMMA - 1.)
  PCI=PC*(1.+GAMMA*EMC**2)/(1.+(GAMMA-1.)/2.*EMC**2)
@ **EXP1 ! INJ. PRESS

C COMPUTE VELOCITIES AND PRESSURE DROPS.

14  VF=WF/ENF/PCI*RF*TF/APF ! FUEL INJECTION VEL
  PF=PCI*SQRT(1.+VF**2/CDF**2/RF/TF) ! FUEL INJ MANIFOLD PRESS
  VO=WO/ENO/RHO/PI/DO**2*4. ! INJ VEL OF DROPLET

```

```

      EMR=OF*VO/VF                                ! INJ MOMENTUM RATIO
      DPJ=(WO/ENO/CDO/PI/DO**2*4.)**2/RHO/2. ! OX INJ-ORI PRESS
C      DROP
      DPS=(WO/AOV)**2/RHO/2. ! PRESS DROP SUCTION LINE
      DPP=DPJ+DPS            ! PRESS DROP VALVE TO INJ FACE
      PO=PCI+DPP             ! OX MAN PRESSURE

C  THE FOLLOWING SECTION COMPUTES DROP SIZE, BURNING LENGTH,
C  DELAY TIMES.

17  RMCTN=0.118*DO*SWC*RSTVC*SQRT(EMR)           ! MEAN OX DROP RAD
      TT=(1.-TO/TCR)**.4                         ! TEMPERATURE COEFF.
      EL50=0.0699*TT*(RMCTN/7.62E-5)**1.45*(VO/30.5)**.75*
      @  WTT*HVT/(PC/2.07E6)**.66                ! LENGTH FOR 50% PROPELLANT
C      VAPROIZED (m)
      TAUUV=EL50/VO                             ! OX VAP TIME DELAY (sec)
      WTOT=WF+WO                                ! TOTAL PROPELLANT FLOW
C      RATE (kg/sec)

C  COMPUTE GAS RESIDENCE TIME, GAS PHASE DELAY COEFF AND OPERATING
C  POINT PRESSURE DROP RATIOS.

20  THETAG=RHOF*VC/WTOT ! GAS RESIDENCE TIME (sec)
      DPO=(PO-PCI)/PC    ! OX-INJ ORI PRESS DROP TO CHAMB PRESS
      DPF=(PF-PCI)/PC    ! FUEL-INJ PRESS DROP TO CHAMB PRESS
      COEFF=1.E3*(ELC-EL50)/VELC ! GAS PHASE DELAY COEFF
      TAUM=TM(COEFF)      ! GAS PHASE MIXING AND RX TIME DELAY
      TAUT=TAUM+TAUV      ! TOTAL OX TIME DELAY

C  THE FOLLOWING SECTION COMPUTES LINEARIZED RESISTANCES,
C  INDUCTANCES, CAPACITANCES AND GAINS

      XG=((1.+(0.5*(1.+PHI)/TC)*SLOPE)/WTOT)*(PCI/PC)
      FG=(1.-(0.5*(PHI*(1.+PHI)/TC)*SLOPE)/WTOT)*(PCI/PC)
      RESF=(PF**2-PCI**2)/(PCI*WF) ! LINEARIZED FUEL
      ELJ=ELO*4./ENO/PI/DO**2 ! OX-INJ ELEM INDUCTANCE (1/m)
      ELSU=ELLS*4./PI/DSU**2 ! SUCTION LINE INDUCTANCE (1/m)
      COM=-BO/(RHO*VOM)      ! OX INJ MAN. CAP. (1/sec m2)
      COF=VOF/RF/TF          ! FUEL INJ MAN. CAP (1/sec m2)

C  PARAMETERS OF INTEREST ARE WRITTEN OUT

      WRITE (IOUT, 21)
21  FORMAT (1H ,4X,'PC',10X,'PO',10X,'PF',7X,'MO',6X,'MF',3X,
      @  'FTEMP',2X,'OXTEMP',3X,'TETAG',5X,'TAUM',5X,'RADIUS',6X,
      @  'DPO',9X,'DPF')
      WRITE (IOUT, 22)
22  FORMAT (1H ,3X,'(Pa)',8X,'(Pa)',8X,'(Pa)',4X,'(Kg/s)',2X,
      @  '(Kg/s)',2X,'(K)',4X,'(K)',5X,'(sec)',5X,'(sec)',6X,'(m)',
      @  7X,'(Pa)',8X,'(Pa)',/)

```

```

        WRITE (IOUT, 23) PC, PO, PF, WO, WF, TF, TO, THETAG, TAUM,
@      RMCTN, DPO, DPF
23      FORMAT (1H ,E10.4,2X,E10.4,2X,E10.4,2X,F5.2,2X,F5.2,2X,F5.1,
@      2X,F5.1,2X,E8.2,2X,E8.2,2X,E8.2,2X,E10.4,2X,E10.4,/)

C      THE FREQUENCY BANDS AND INCREMENT ARE SELECTED
C      AND THE SOLUTION OF THE CHARACTERISTIC EQUATION IS INITIATED

        FREQ=74.9
        JN=0
        N=0
        NN=0
27      FREQ=FREQ + .1
        IF ((FREQ .GT. 200.) .AND. (FREQ .LT. 300.)) GO TO 28
        GO TO 29
28      IF (N .EQ. 0) JN=1
        N1=N
        FREQ=300.
        JM=0
        N=0
        NN=1
        GO TO 30
29      IF (FREQ .GT. 300.) GO TO 50
30      W=6.2832*FREQ      ! ANGULAR FREQUENCY
        II=1              ! MULTIPLE OX SOLN INDEX
        RX=0.              ! CRIT. REAL PART OF OX IMPEDANCE
        RX1=0.
        RX2=0.
        RRF=0.             ! CRIT. REAL PART FUEL IMPEDANCE
        RRF1=0.
        RRF2=0.
        DPOC2=0.           ! RATIO OF OX-INJ PRESS DROP TO CHAMB PRESS
        DPOC5=0.
        DPOC8=0.
        DPFC=0.            ! CRIT VAL OF FUEL-INJ PRESS DROP TO CHAMB PRESS
        DPF1=0.
        DPF2=0.

```

```

C      TERMS IN THE CHARACTERISTIC EQUATION ARE EVALUATED AT THE
C      SPECIFIED FREQUENCY

```

```

        EMAGF=-1./W/COF*PF/PCI      ! IMAG PART OF FUEL IMPEDENCE
        THETAT=TAUT*W
        THETAM=TAUM*W
        THETAV=TAUV*W
        THETAL=ELJ*W
        ALPHAG=THETAG*W
        A1=COS(THETAM)
        B1=SIN(THETAM)
        A2=COS(THETAV)

```

```

      B2=SIN(THETAV)
      A3=COS(THETAT)
      B3=SIN(THETAT)
      F=ALPHAG*A1-C1*B1

C   THE SECOND AND FIRST ORDER COEFF OF THE CHARACTERISTIC
C   QUADRATIC EQUATION FOR CRITICAL OX REAL PART
C   ARE EVALUATED

      AG=F-EMAGF/(PC*FG)*(C1**2+ALPHAG**2)
      BG=-PC*XG*B2+2.*XG*EMAGF/FG*(C1*A3+ALPHAG*B3)

C   THE FOLLOWING SECTION COMPUTES REAL AND IMAGINARY PARTS OF THE
C   IMPEDANCES LOOKING UPSTREAM FOR A SINGLE ORIFICE CONFIG.

      AXA=2.*(PCI-PO)/WO      ! REAL PART OX-IMP (N s/m2 kg)
      NUMER=((COM/W)*(ELSU*W)**2 + (ELSU*W)*(COM/W)**2)
      DENOM=(ELSU*W + COM/W)**2
      BXA=NUMER/DENOM
32    EMAGO=THETAL+BXA      ! IMAG PART OF OX IMPEDANCE

C   THE ZEROth ORDER COEFFICIENT IN THE QUADRATIC EQUATION FOR
C   CRITICAL OX REAL PART IS EVALUATED.  THE FOLLOWING SECTION
C   SOLVES THE QUADRATIC AND RELATES SOLUTION TO THE PRESSURE
C   DROP RATIO.

      CG=EMAGO**2*F-EMAGO*PC*XG*A2-2.*XG*EMAGF*EMAGO/FG*
      @ (C1*B3-ALPHAG*A3)-EMAGF*EMAGO**2/(PC*FG)*(C1**2+ALPHAG**2)
      @ -XG**2*PC*EMAGF/FG

C   THIS SECTION STARTS THE COMPUTATION OF THE CRITICAL
C   REAL VALUES OF THE OXIDIZER IMPEDANCE (Ro)

      IF (AG .NE. 0.) GO TO 33
      RX= -CG/BG
      RPC=RX-AXA      ! CRIT REAL PART OF OX-INJ IMP
      IF (RPC .LE. 0.) GO TO 27
      DPOC2=RPC*WO/PC/2.
      GO TO 38
33    ALPHA=(BG**2-4.*AG*CG)      ! SQRT FACT IN QUADRATIC EQ.
      IF (ALPHA) 27, 34, 35
34    RX=-BG/2./AG
      RPC=RX-AXA
      IF (RPC .LE. 0.) GO TO 27
      DPOC2=RPC*WO/PC/2.
      GO TO 38
35    RX1=(-BG+SQRT(ALPHA))/2./AG      ! CRIT VAL REAL PART OX-INJ
      RX2=(-BG-SQRT(ALPHA))/2./AG
      RPC1=RX1-AXA
      RPC2=RX2-AXA

```

```

      IF ((RPC1 .LE. 0.) .AND. (RPC2 .LE. 0.)) GO TO 27
      IF (RPC1 .LE. 0.) GO TO 36
      IF (RPC2 .LE. 0.) GO TO 37
      II=2
      DPOC5=RPC1*WO/PC/2.
      DPOC8=RPC2*WO/PC/2.
      GO TO 39
36    RPC=RPC2
      DPOC2=RPC*WO/PC/2.
      RX=RX2
      GO TO 38
37    RPC=RPC1
      DPOC2=RPC*WO/PC/2.
      RX=RX1
      GO TO 38

C    THE CRITICAL FUEL REAL PART IS DETERMINED USING OX SOLUTIONS.
C    THE RESULTS IS RELATED TO THE PRESSURE DROP
C    RATIO

38    RRF=(FG*RX*B1*PC-FG*EMAGO*A1*PC-XG*EMAGF*A3*PC+ALPHAG*EMAGO*
      @ EMAGF+EMAGF*RX*C1)/(RX*ALPHAG-EMAGO*C1-XG*B3*PC)
      IF (RRF) 27, 27, 43
39    RRF1=(FG*RX1*B1*PC-FG*EMAGO*A1*PC-XG*EMAGF*A3*PC+ALPHAG*EMAGO*
      @ EMAGF+EMAGF*RX1*C1)/(RX1*ALPHAG-EMAGO*C1-XG*B3*PC)
      RRF2=(FG*RX2*B1*PC-FG*EMAGO*A1*PC-XG*EMAGF*A3*PC+ALPHAG*EMAGO*
      @ EMAGF+EMAGF*RX2*C1)/(RX2*ALPHAG-EMAGO*C1-XG*B3*PC)
      IF (RRF1 .GT. 0.) GO TO 40
      RRF1=0.
      DPOC5=0.
      IF (RRF2 .LE. 0.) GO TO 41
      GO TO 42
40    IF (RRF2 .GT. 0.) GO TO 42
41    RRF2=0.
      DPOC8=0.
42    DPF1=(SQRT(PCI**2+WF*PCI*RRF1)-PCI)/PC
      DPF2=(SQRT(PCI**2+WF*PCI*RRF2)-PCI)/PC
      GO TO 44
43    DPF3=(SQRT(PCI**2+WF*PCI*RRF)-PCI)/PC
44    IF ((DPOC2 .EQ. 0.) .AND. (DPF3 .EQ. 0.) .AND. (DPOC5 .EQ. 0.)
      @ .AND. (DPF1 .EQ. 0.) .AND. (DPOC8 .EQ. 0.) .AND. (DPF2
      @ .EQ. 0.)) GO TO 27

C    THE LOW AND HIGH FREQUENCY SOLUTIONS ARE SORTED IN
C    ORDER OF INCREASING FUEL PRESSURE DROP RATIO

      IF (NN.EQ. 1) GO TO 47
      IF (DPF1 .EQ. 0.) GO TO 45
      IF (DPF2 .EQ. 0.) GO TO 46
      N=N+1

```

```

      UPL(N)=DPF1
      FL(N)=FREQ
      ACRL(N)=DPOC5
      N=N+1
      UPL(N)=DPF2
      FL(N)=FREQ
      ACRL(N)=DPOC8
      GO TO 27
45    N=N+1
      UPL(N)=DPF2
      FL(N)=FREQ
      ACRL(N)=DPOC8
      GO TO 27
46    N=N+1
      UPL(N)=DPF1
      FL(N)=FREQ
      ACRL(N)=DPOC5
      GO TO 27
47    IF (DPF1 .EQ. 0.) GO TO 48
      IF (DPF2 .EQ. 0.) GO TO 49
      N=N+1
      UPH(N)=DPF1
      FH(N)=FREQ
      ACRH(N)=DPOC5
      N=N+1
      UPH(N)=DPF2
      FH(N)=FREQ
      ACRH(N)=DPOC8
      GO TO 27
48    N=N+1
      UPH(N)=DPF2
      FH(N)=FREQ
      ACRH(N)=DPOC8
      GO TO 27
49    N=N+1
      UPH(N)=DPF1
      FH(N)=FREQ
      ACRH(N)=DPOC5
      GO TO 27
50    IF ((FREQ .GT. 300.) .AND. (N .EQ. 0)) JM=1
      N2=N
      IF ((JN .EQ. 1) .AND. (JM .EQ. 1)) GO TO 78
      IF (JM .EQ. 1) GO TO 51
      IF (JN .EQ. 1) GO TO 52
      IM=3
      GO TO 53
51    IM=1
      GO TO 53
52    IM=2
      GO TO 56

```

```

53      N11=N1-1
        DO 55 IX=1, N11
          IX1=IX+1
          DO 55 JX=IX1, N1
            IF (UPL(IX)-UPL(JX)) 55,55,54
54      TEMP=UPL(IX)
          UPL(IX)=UPL(JX)
          UPL(JX)=TEMP
          TEMP=ACRL(IX)
          ACRL(IX)=ACRL(JX)
          ACRL(JX)=TEMP
          TEMP=FL(IX)
          FL(IX)=FL(JX)
          FL(JX)=TEMP
55      CONTINUE
          IF (IM .EQ. 1) GO TO 59
56      N22=N2-1
          DO 58 KX=1, N22
            KX1=KX+1
            DO 58 LX=KX1, N2
              IF (UPH(KX)-UPH(LX)) 58, 58, 57
57      TEMP=UPH(KX)
            UPH(KX)=UPH(LX)
            UPH(LX)=TEMP
            TEMP=ACRH(KX)
            ACRH(KX)=ACRH(LX)
            ACRH(LX)=TEMP
            TEMP=FH(KX)
            FH(KX)=FH(LX)
            FH(LX)=TEMP
58      CONTINUE

C      THE VARIABLE AREA CASE (JJ=1) CALLS INTERPOLATION TO FIND
C      CRITICAL OX REAL PART AND FREQUENCY AT THE OPERATING FUEL
C      PRESSURE DROP RATIO.  THE RESULT IS STORED.
C      THE THROTTLING CASE (JJ=0) CALLS FOR WRITING OUT SOLUTION

59      IF ((JJ .EQ. 1) .AND. (IM .EQ. 1)) GO TO 60
          IF ((JJ .EQ. 1) .AND. (IM .EQ. 2)) GO TO 62
          IF ((JJ .EQ. 1) .AND. (IM .EQ. 3)) GO TO 64
          GO TO 68
60      IF ((DPF .LT. UPL(1)) .OR. (DPF .GT. UPL(N1))) GO TO 79
          LI=LI+1
          NS=N1-1
          DO 61 L=1, NS
            IF (DPF .GT. UPL(L+1)) GO TO 61
            ACCL(LI)=ACRL(L)+(DPF-UPL(L))*(ACRL(L+1)-ACRL(L))/(UPL(L+1)-
@      UPL(L))
            FFL(LI)=FL(L)+(DPF-UPL(L))*(FL(L+1)-FL(L))/(UPL(L+1)-UPL(L))
            UPPL(LI)=DPF

```



```

        GO TO 79
61      CONTINUE
        LI=LI-1
        GO TO 79
62      IF ((DPF .LT. UPH(1)) .OR. (DPF .GT. UPH(N2))) GO TO 79
        IL=IL+1
        NS=N2-1
        DO 63 L=1, NS
        IF (DPF .GT. UPH(L+1)) GO TO 63
        ACCH(IL)=ACRH(L)+(DPF-UPH(L))*(ACRH(L+1)-ACRH(L))/(UPH(L+1)
@      -UPH(L))
        FFH(IL)=FH(L)+(DPF-UPH(L))*(FH(L+1)-FH(L))/(UPH(L+1)-UPH(L))
        UPPH(IL)=DPF
        GO TO 79
63      CONTINUE
        IL=IL-1
        GO TO 79
64      IF ((DPF .LT. UPL(1)) .OR. (DPF .GT. UPL(N1))) GO TO 66
        LI=LI+1
        NS=N1-1
        DO 65 L=1, NS
        IF (DPF .GT. UPL(L+1)) GO TO 65
        ACCL(LI)=ACRL(L)+(DPF-UPL(L))*(ACRL(L+1)-ACRL(L))/(UPL(L+1)
@      -UPL(L))
        FFL(LI)=FL(L)+(DPF-UPL(L))*(FL(L+1)-FL(L))/(UPL(L+1)-UPL(L))
        UPPL(LI)=DPF
        GO TO 66
65      CONTINUE
        LI=LI-1
66      IF ((DPF .LT. UPH(1)) .OR. (DPF .GT. UPH(N2))) GO TO 79
        IL=IL+1
        NS=N2-1
        DO 67 LJ=1, NS
        IF (DPF .GT. UPH(LJ+1)) GO TO 67
        ACCH(IL)=ACRH(LJ)+(DPF-UPH(LJ))*(ACRH(LJ+1)-ACRH(LJ))/
@      (UPH(LJ+1)-UPH(LJ))
        FFH(IL)=FH(LJ)+(DPF-UPH(LJ))*(FH(LJ+1)-FH(LJ))/(UPH(LJ+1)
@      -UPH(LJ))
        UPPH(IL)=DPF
        GO TO 79
67      CONTINUE
        IL=IL-1
        GO TO 79

```

# C WRITE OUT ORDERED SOLUTIONS

```

68      WRITE (IOUT, 69)
69      FORMAT (6X,'FREQUENCY',9X,'DELTAP FUEL/PC',6X,'DELTAP OX/PC',
@      6X,'FREQUENCY',9X,'DELTAP FUEL/PC';9X,'DELTAP OX/PC',/)
        IF (N1 .GT. 40 .OR. N1 .EQ. 40) ISTEP=40/2

```

```

        IF (N1 .LT. 40) ISTEP=N1
        WRITE (IOUT, 70) (FL(KL), UPL(KL), ACRL(KL), FL(KL+ISTEP),
@      UPL(KL+ISTEP), ACRL(KL+ISTEP), KL=1, ISTEP)
70      FORMAT (2(8X,F5.1,2X,E20.3,2X,E20.3))
        WRITE (IOUT, 1)
        WRITE (IO, 71) (FL(IND), ACRL(IND), UPL(IND), DPO, DPF,
@      IND=1, 40)
71      FORMAT (1H ,4X,F5.1,2X,E10.4,2X,E10.4,2X,E10.4,2X,E10.4)

```

C VARIABLE AREA IS SPECIFIED

```

78      IF (JJ .EQ.0) GO TO 89
79      J=2
        K=K+1
        YY=K
        IF (YY .GT. 8.) GO TO 80
        IF (YY .EQ. 1.) GO TO 87
        APF=APF*YY/(YY-1.)
        GO TO 14

```

C THE VARIABLE AREA VALUES OF CRITICAL OX REAL PART  
C AND FREQUENCY AT OPERATING FUEL PRESSURE DROP RATIOS ARE  
C CONVERTED TO PROPER VARIABLES FOR ORDERING AND WRITING

```

80      IF ((IL .EQ. 0) .AND. (LI .EQ. 0)) GO TO 89
        IF (IL .EQ. 0) GO TO 83
        IF (LI .EQ. 0) GO TO 85
        DO 81 IZ=1, LI
        UPL(IZ)=UPPL(IZ)
        ACRL(IZ)=ACCL(IZ)
        FL(IZ)=FFL(IZ)
81      CONTINUE
        N1=LI
        IM=3
        JJ=0
        DO 82 IZ=1, IL
        UPH(IZ)=UPPH(IZ)
        ACRH(IZ)=ACCH(IZ)
        FH(IZ)=FFH(IZ)
82      CONTINUE
        N2=IL
        GO TO 53
83      DO 84 IZ=1, LI
        UPL(IZ)=UPPL(IZ)
        ACRL(IZ)=ACCL(IZ)
        FL(IZ)=FFL(IZ)
84      CONTINUE
        N1=LI
        IM=1
        JJ=0

```

```

      GO TO 53
85    DO 86 IZ=1, IL
      UPH(IZ)=UPPH(IZ)
      ACRH(IZ)=ACCH(IZ)
      FH(IZ)=FFH(IZ)
86    CONTINUE
      N2=IL
      IM=2
      JJ=0
      GO TO 56
87    APF=.25*APF
      GO TO 14
88    J=1
89    IO=IO+1
90    CONTINUE
      WRITE (5, 92)
92    FORMAT (1H , 'ANOTHER STUDY?', //, 3x, '1   YES', //, 3x, '2   NO')
      READ (5, *) INPUT
      IF (INPUT .EQ. 1) THEN
94    FORMAT (1H1)
      GO TO 15
      END IF
      STOP
      END

```

```

      FUNCTION TM(COEFF)
C    THIS MAPS THE EMPIRICAL MIXING CURVE
      DIMENSION S(7), V(7)
      DATA S(1)/.5/, S(2)/1./, S(3)/1.5/, S(4)/1.8/, S(5)/2./, S(6)
@    /2.2/
      DATA V(1)/.15/, V(2)/.35/, V(3)/.7/, V(4)/1.075/, V(5)/1.4/,
@    V(6)/1.9/
      DO 1 I=1, 5
      IF ((S(I) .LE. COEFF) .AND. (COEFF .LT. S(I+1))) GO TO 2
1    CONTINUE
2    TM=1.E-3*(V(I)+(COEFF-S(I))*(V(I+1)-V(I))/(S(I+1)-S(I)))
      RETURN
      END

```

```

      SUBROUTINE GAM (TC, GAMMA)
C   THIS SUBROUTINE COMPUTES THE AVERAGE SPECIFIC HEAT RATIO OF THE
C   PRODUCTS USING THE EQUATIONS FOUND IN VAN WYLEN.
      THETA=TC/100.
      R=1.987
      CPH2=13.505-167.96*THETA**(-0.75)+278.44*THETA**(-1)-134.01
@   *THETA**(-1.5)
      CPH20=34.19-43.868*THETA**(0.25)+19.778*THETA**(0.5)-0.88407
@   *THETA
      CPAVG=(5./20.)*CPH2 + (1./20.)*CPH20
      GAMMA=1./(1.-R/CPAVG)
      RETURN
      END

```

## VITA

Kair Chuan Lim was born in [REDACTED] on [REDACTED]. He attended primary and secondary schools in Singapore and obtained his G.C.E. 'O' Levels certificate in 1974 from St. Patrick's Secondary School. The following year he entered Catholic Junior College and obtained his G.C.E. 'A' Levels in 1977.

After a two and one-half years of mandatory duty in the Singapore Armed Forces, he was accepted into the undergraduate program at the University of Tennessee. In June 1984 he received his Bachelor of Science in Mechanical Engineering and subsequently accepted a teaching assistantship to pursue his Master's degree in Aerospace Engineering. The degree was conferred in August 1986.

The author is a member of Pi Tau Sigma, American Institute of Aeronautics and Astronautics, American Society of Mechanical Engineers, Royal Life Saving Society and The Boy Scouts of Singapore.